Supporting Information

for

Metalation of a gold(I) metalloligand with P,C-bridging phosphino-ferrocenyl groups enables construction of defined multimetallic arrays

Jiří Schulz, Ivana Císařová, Róbert Gyepes and Petr Štěpnička*

Contents

EXPERIMENTAL

Materials and Methods

All syntheses were performed under argon or nitrogen using standard Schlenk techniques. Anhydrous tetrahydrofuran, dichloromethane and methanol were obtained from an in-house PureSolv MD5 Solvent Purification System (Innovative Technology, Inc., USA). Anhydrous acetonitrile was obtained by distillation from calcium hydride and stored under nitrogen. Gold(I) complexes $[Au(tht)_2][SbF_6]$ (tht = tetrahydrothiophene; the perchlorate salt was obtained analogously),[1] $[AuCl(FcPPh_2)]$[2] (Fc = ferrocenyl), $[AuCl(PCy_3)]$[3] and 1-bromo-1′-(diphenylphosphino)ferrocene[4] were prepared according to literature procedures (complex $[AuCl(PPh_3)]$ was obtained similarly to $[AuCl(FcPPh_2)]$). The remaining reagents were purchased from commercial suppliers (Sigma-Aldrich and TCI) and used as received.

NMR spectra were recorded at 25°C on a Bruker AVANCE III 600 spectrometer (^{1}H, 600.17 MHz, ^{13}C, 150.93 MHz) or on a Varian UNITY Inova 400 spectrometer (^{1}H, 399.95 MHz, ^{13}C{^{1}H}, 100.58 MHz, ^{19}F, 376.29 MHz, ^{31}P{^{1}H}, 161.90 MHz). Chemical shifts (δ/ppm) are given relative to internal tetramethylsilane (^{1}H and ^{13}C NMR), to external 85% aqueous H_3PO_4 (^{31}P NMR) and to neat trichlorofluoromethane (^{19}F NMR). Electrospray-ionisation mass spectra were recorded in positive-ion mode. Low resolution spectra were recorded on an Esquire 3000 spectrometer (Bruker), while high resolution spectra were obtained using either a Compact QTOF-MS spectrometer (Bruker) or a LTQ Orbitrap XL instrument (Thermo Scientific). The identity of the ionic species was confirmed by comparing theoretical and experimentally determined isotopic patterns. Elemental analyses were performed on a Perkin-Elmer PE 2400 CHN analyser.

Syntheses

Synthesis of $[(Ph_2PfcAu)_2]$ (1, fc = ferrocene-1,1'-diyl). 1-Bromo-1′-(diphenylphosphino)-ferrocene (898 mg, 2.0 mmol) was introduced to a flame-dried three-necked flask (250 mL) equipped with a magnetic stirring bar, an argon inlet and a solid addition tube charged with $[AuCl(SMe_2)]$ (589 mg, 2.0 mmol). The reaction vessel was thoroughly purged with argon, and the ferrocene precursor was dissolved in anhydrous tetrahydrofuran (20 mL). The solution was cooled to –78 °C in a dry ice/ethanol bath and treated with *n*-BuLi in hexane (0.8 mL of 2.5 M solution, 2.0 mmol). After stirring for 1 hour at –78 °C, $[AuCl(SMe_2)]$ was added to the solution from the solid addition tube, and the reaction mixture was stirred for another 30 min at –78 °C and then allowed to warm to room temperature overnight. The solvents were evaporated on a

rotary evaporator, and the solid residue was extracted with two portions of dichloromethane (50 mL in total). The organic extracts were filtered through a short Celite pad, and the filtrate was concentrated to ca. 10 mL. The solution was transferred to a test tube and layered with acetonitrile. The crystalline material obtained overnight was isolated by decantation, washed with CH_2Cl_2 and diethyl ether and dried under vacuum. Yield 945 mg (83%), orange crystals.

^{1}H NMR ($CDCl_3$, 399.95 MHz): δ = 4.17 (vq, *J* = 1.4 Hz, 4 H, CH of fc), 4.38 (d of vt, *J* = 2.7, 1.8 Hz, 4 H, CH of fc), 4.43 (vt of d, *J* = 1.9, 0.9 Hz, 4 H, CH of fc), 4.45 (vq, *J* = 1.5 Hz, 4 H, CH of fc), 7.28-7.39 (m, 12 H, PPh_2), 7.66-7.74 (m, 8 H, PPh_2) ppm. ^{13}C{^{1}H} NMR ($CDCl_3$, 100.58 MHz): δ = 69.92 (d, J_{PC} = 6 Hz, CH of fc), 70.32 (d, $^1J_{PC}$ = 62 Hz, C^{ipso}–P of fc), 71.05 (d, J_{PC} = 8 Hz, CH of fc), 72.41 (d, J_{PC} = 13 Hz, CH of fc), 79.16 (d, J_{PC} = 5 Hz, CH of fc), 103.94 (d, $^2J_{PC}$ = 125 Hz, C^{ipso}–Au of fc), 128.21 (d, J_{PC} = 10 Hz, CH of PPh_2), 130.11 (d, $^4J_{PC}$ = 2 Hz, CH^{para} of PPh_2), 133.78 (d, $^1J_{PC}$ = 50 Hz, C^{ipso}–P of PPh_2), 133.80 (d, J_{PC} = 13 Hz, CH of PPh_2) ppm. ^{31}P{^{1}H} NMR ($CDCl_3$, 161.90 MHz): δ = 40.5 (s) ppm. HR ESI+ MS: *m/z* = 1132.032 (M^+). Anal. Calc. for $C_{44}H_{36}Au_2Fe_2P_2$ (1132.3): C 46.67, H 3.20%. Found: C 46.42, H 3.04%.

Preparation of $[(Ph_2PfcAu)_2\{Au(FcPPh_2)\}_2][SbF_6]_2$ (2). A solution of [AuCl($FcPPh_2$)] (60.2 mg, 0.10 mmol) in dichloromethane (5 mL) was combined with an acetonitrile solution of Ag[SbF_6] (34.3 mg, 0.10 mmol in 2 mL of the solvent), whereupon a white precipitate (AgCl) separated. The reaction mixture was stirred for 15 minutes, filtered through a PTFE syringe filter (0.45 μm pore size), and the filtrate was evaporated to dryness. The solid residue was taken up with dichloromethane (3 mL) and filtered again through syringe filter to remove residual AgCl. The filtrate was mixed with a solution of **1** (56.6 mg, 0.050 mmol) in dichloromethane (10 mL) whereupon the reaction mixture turned from orange to red. After stirring for 1 hour, the mixture was filtered through Celite and evaporated to dryness to give **2**. Yield: 129 mg (94%), pale red powdery solid. Crystals suitable for structure determination were obtained by slow diffusion of diethyl ether into a dichloromethane solution of the complex.

^{1}H NMR (CD_2Cl_2+CD_3OD, 399.95 MHz): δ = 3.77-3.90 (m, 2 H, CH of fc), 4.01 (s, 10 H, CH of fc), 4.09-4.63 (m, 14 H, CH of fc), 4.82-5.09 (m, 6 H, CH of fc), 6.17-6.35 (m, 2 H, CH of fc), 6.85-7.09 (m, 4 H, PPh_2), 7.16-7.81 (m, 36 H, PPh_2) ppm. ^{31}P{^{1}H} NMR (CD_2Cl_2+CD_3OD, 161.90 MHz): δ = 31.9 (d, J_{PP} = 4 Hz, $fcPPh_2$), 35.5 (d, J_{PP} = 4 Hz, $FcPPh_2$) ppm. HR ESI+ MS: *m/z* = 1133.039 ([M – $2SbF_6$]$^{2+}$). Anal. Calc. for $C_{88}H_{74}Au_4F_{12}Fe_4P_4Sb_2$ (2738.2): C 38.60, H 2.72%. Found: C 38.69, H 2.76%.

Preparation of $[\{(Ph_2PfcAu)_2\{Au(PCy_3)\}_2][SbF_6]_2$ (3). A solution of [AuCl(PCy_3)] (51.3 mg, 0.10 mmol) in dichloromethane (5 mL) was combined with an acetonitrile solution of Ag[SbF_6] (34.3 mg, 0.10 mmol in 3 mL). The reaction mixture was stirred for 30 minutes to complete AgCl precipitation and filtered through a PTFE syringe filter, and the filtrate was evaporated to dryness. The white solid residue was redissolved in dichloromethane (5 mL) and

the solution filtered through a syringe filter to completely remove AgCl. The resulting clear solution was added to an orange solution of **1** (56.6 mg, 0.050 mmol) in dichloromethane (10 mL), yielding a red reaction mixture. After stirring for 1 hour, the clear mixture was filtered through Celite and evaporated thoroughly to dryness, resulting in **3**. Yield: 126 mg (98%), pale red solid. Crystals suitable for structure determination were grown by liquid-phase diffusion of fluorobenzene to a dichloromethane solution of the complex.

^{1}H NMR (CD_2Cl_2+CD_3NO_2, 399.95 MHz): δ = 1.09-1.22 (m, 6 H, PCy_3), 1.23-1.52 (m, 20 H, PCy_3), 1.65-1.84 (m, 26 H, PCy_3), 1.94-2.05 (m, 10 H, PCy_3), 2.14-2.26 (m, 4 H, PCy_3), 5.20-5.27 (br s, 2 H, CH of fc), 7.47-7.75 (m, 20 H, PPh_2) ppm. Signals due to remaining ferrocene protons were not observed due to extensive broadening. ^{31}P{^{1}H} NMR (CD_2Cl_2+CD_3NO_2, 161.90 MHz): δ = 31.5 (d, $^{3}J_{PP}$ = 3 Hz, PPh_2), 61.4 (d, $^{3}J_{PP}$ = 3 Hz, PCy_3) ppm. HR ESI+ MS: *m/z* = 1043.216 ([M – 2SbF_6]$^{2+}$). Anal. Calc. for $C_{80}H_{102}Au_4F_{12}Fe_2P_4Sb_2$ (2558.6): C 37.55, H 4.02%. Found: C 37.98, H 4.04%.

Preparation of [{(Ph_2PfcAu)$_2${$Au(PPh_3)$}$_2$][SbF_6]$_2$ (4). A solution of [$AuCl(PPh_3)$] (49.5 mg, 0.10 mmol) in dichloromethane (5 mL) was mixed with an acetonitrile solution of Ag[SbF_6] (34.3 mg, 0.10 mmol in 3 mL), whereupon AgCl separated as an off-white solid. The reaction mixture was stirred for 30 minutes and then filtered through PTFE syringe filter. The solvents were removed under reduced pressure, and the solid residue was redissolved in dichloromethane (5 mL). The resulting cloudy solution was filtered once again and then mixed with a solution of **1** (56.6 mg, 0.050 mmol) in dichloromethane (10 mL). After stirring for 1 hour, the reaction mixture was filtered through Celite and carefully evaporated to give **4**. Yield: 119 mg (94%), red powdery solid. The purity of this sample exceeded 90%. The major contaminants, present inherently and inevitably, are the hexagold cluster **5** and the side product of the **4** → **5** conversion, complex [$Au(PPh_3)_2$][SbF_6].[5]

^{1}H NMR (CD_2Cl_2, 399.95 MHz): δ = 4.07 (br s, 2 H, CH of fc), 4.20 (br s, 2 H, CH of fc), 4.30 (br s, 2 H, CH of fc), 4.62-4.75 (m, 4 H, CH of fc), 4.86 (br s, 2 H, CH of fc), 5.26 (br s, 2 H, CH of fc), 6.18 (br s, 2 H, CH of fc), 6.96-7.10 (m, 4 H, PPh_2), 6.25-7.70 (m, 46 H, PPh_2) ppm. ^{31}P{^{1}H} NMR (CD_2Cl_2, 161.90 MHz): δ = 31.9 (d, $^{3}J_{PP}$ = 4 Hz, PPh_2), 39.0 (d, $^{3}J_{PP}$ = 4 Hz, PPh_3) ppm. ESI+ MS: *m/z* = 1025.3 ([M – 2SbF_6]$^{2+}$). Anal. Calc. for $C_{80}H_{66}Au_4F_{12}Fe_2P_4Sb_2$ (2522.3): C 38.09, H 2.64%. Found: C 37.99, H 2.55%.

Preparation of [{(Ph_2PfcAu)$_2$Au}$_2$][SbF_6]$_2$ (5). Solid [$Au(tht)_2$][SbF_6] (30.5 mg, 0.050 mmol) was added to a solution of **1** (56.6 mg, 0.050 mmol) in dichloromethane (10 mL). The reaction mixture turned red and became turbid. After stirring for 1 hour, the solvents were removed under reduced pressure. The solid residue was taken up with dichloromethane (5 mL) and filtered through short Celite pad, and the filtrate was added slowly to diethyl ether (20 mL). The precipitate was isolated by decantation, washed with diethyl ether and dried under vacuum.

Yield of **5**: 66 mg (85%), red microcrystalline compound. Note: the same compound was obtained during attempted crystalisation of **4** from CH_2Cl_2-acetonitrile/diethyl ether or CH_2Cl_2-THF/diethyl ether mixtures.

^{1}H NMR (CD_2Cl_2+CD_3OD, 399.95 MHz): δ = 3.93 (t of vt, *J* = 2.7 Hz, 1.4 Hz, 4 H, CH of fc), 4.25 (d of vt, *J* = 2.6, 1.0 Hz, 4 H, CH of fc), 4.34 (t of vt, *J* = 2.6 Hz, 1.4 Hz, 4 H, CH of fc), 4.87 (vt of d, *J* = 2.6, 1.2 Hz, 4 H, CH of fc), 5.13-5.17 (m, 8 H, CH of fc), 5.31-5.33 (m, 4 H, CH of fc), 6.11 (t of vt, *J* = 2.7 Hz, 1.4 Hz, 4 H, CH of fc), 7.39-7.62 (m, 40 H, PPh_2) ppm. ^{13}C{^{1}H} NMR (CD_2Cl_2+CD_3OD, 100.58 MHz): δ = 66.55 (d, $^1J_{PC}$ = 64 Hz, C^{ipso}–P of fc), 66.82 (dd, J_{PC} = 18, 7 Hz, CH of fc), 73.94 (d, J_{PC} = 9 Hz, CH of fc), 74.30 (d, J_{PC} = 6 Hz, CH of fc), 76.34 (d, $^1J_{PC}$ = 57 Hz, C^{ipso}–Au of fc), 77.53 (d, J_{PC} = 3 Hz, CH of fc), 77.98 (d, J_{PC} = 4 Hz, CH of fc), 78.36 (d, J_{PC} = 5 Hz, CH of fc), 85.22 (s, CH of fc), 91.06 (t, J_{PC} = 3 Hz, CH of fc), 128.53 (d, $^1J_{PC}$ = 56 Hz, C^{ipso}–P of PPh_2), 130.08 (d, J_{PC} = 11 Hz, CH of PPh_2), 130.12 (d, J_{PC} = 12 Hz, CH of PPh_2), 132.35 (d, $^4J_{PC}$ = 3 Hz, CH^{para} of PPh_2), 132.40 (d, J_{PC} = 14 Hz, CH of PPh_2), 132.96 (d, $^4J_{PC}$ = 2 Hz, CH^{para} of PPh_2), 133.06 (d, $^1J_{PC}$ = 51 Hz, C^{ipso}–P of PPh_2), 135.40 (d, J_{PC} = 15 Hz, CH of PPh_2) ppm. ^{31}P{^{1}H} NMR (CD_2Cl_2+CD_3OD, 161.90 MHz): δ = 31.8 (s) ppm. HR ESI+ MS: *m/z* = 1329.000 ($[M - 2SbF_6]^{2+}$). Anal. Calc. for $C_{88}H_{72}Au_6F_{12}Fe_4P_4Sb_2$ (3130.1): C 33.77, H 2.32%. Found: C 33.73, H 2.18%.

Preparation of $[\{(Ph_2PfcAu)_2Au\}_2](ClO_4)_2$ (5a). ***Method A:*** Compound **1** (56.6 mg, 0.050 mmol) and [$AuCl(PPh_3)$] (49.4 mg, 0.10 mmol) were dissolved in dichloromethane (5 mL). $AgClO_4$ (20.7 mg, 0.10 mmol) dissolved in the same solvent (2 mL) was added and the reaction mixture was stirred for 1 hour, during which time it deposited a dark solid and changed colour from orange to red. The precipitated AgCl was removed by filtration through a PTFE syringe filter, and the filtrate was evaporated to dryness under vacuum. Subsequent recrystallisation of the crude product by liquid-phase diffusion of *tert*-butyl methyl ether into a dichloromethane-acetonitrile solution (3:1, v/v) produced red crystals, which were isolated by decantation, washed with diethyl ether and dried under vacuum. Yield of **5a**: 55 mg (77%), red crystals.

Method B: A solution of **1** (56.6 mg, 0.050 mmol) in dichloromethane (10 mL) was combined with a solution of $[Au(tht)_2][ClO_4]$ (23.6 mg, 0.050 mmol) in the same solvent (5 mL). The colour of the reaction mixture changed immediately from orange to red. The mixture was stirred for 1 hour and evaporated under reduced pressure. The crude product was dissolved in dichloromethane (5 mL), and the solution was filtered through a short Celite pad. The filtrate was evaporated to dryness, and the resulting solid was suspended in diethyl ether (20 mL) and briefly sonicated to remove residual tetrahydrothiophene. The product was then isolated by decantation and dried under vacuum. Yield of **5a**: 70 mg (98%), red powder.

^{1}H NMR (CD_2Cl_2+CD_3OD, 399.95 MHz): δ = 3.94 (t of vt, *J* = 2.5, 1.4 Hz, 4 H, CH of fc), 4.25 (d of vt, *J* = 2.6, 1.4 Hz, 4 H, CH of fc), 4.35 (t of vt, *J* = 2.6 1.2 Hz, 4 H, CH of fc), 4.88 (vt of d, *J* = 2.6, 1.2 Hz, 4 H, CH of fc), 5.14-5.18 (m, 8 H, CH of fc), 5.35 (m, 4 H, CH of fc), 6.13 (t of vt, *J* = 2.3, 1.2

Hz, 4 H, CH of fc), 7.40-7.63 (m, 40 H, PPh_2) ppm. $^{13}C\{^1H\}$ NMR (CD_2Cl_2+CD_3OD, 100.58 MHz): δ = 66.54 (d, $^1J_{PC}$ = 64 Hz, C^{ipso}–P of fc), 66.83 (dd, J_{PC} = 18, 7 Hz, CH of fc), 73.96 (d, J_{PC} = 9 Hz, CH of fc), 74.34 (d, J_{PC} = 6 Hz, CH of fc), 76.36 (d, $^1J_{PC}$ = 57 Hz, C^{ipso}–Au of fc), 77.57 (d, J_{PC} = 3 Hz, CH of fc), 78.00 (d, J_{PC} = 5 Hz, CH of fc), 78.37 (d, J_{PC} = 5 Hz, CH of fc), 85.24 (CH of fc), 92.06 (t, J_{PC} = 3 Hz, CH of fc), 128.55 (d, $^1J_{PC}$ = 56 Hz, C^{ipso}–P of PPh_2), 130.08 (d, J_{PC} = 11 Hz, CH of PPh_2), 130.13 (d, J_{PC} = 12 Hz, CH of PPh_2), 132.35 (d, $^4J_{PC}$ = 2 Hz, CH^{para} of PPh_2), 132.42 (d, J_{PC} = 14 Hz, CH of PPh_2), 132.96 (d, $^4J_{PC}$ = 2 Hz, CH^{para} of PPh_2), 133.08 (d, $^1J_{PC}$ = 51 Hz, C^{ipso}–P of PPh_2), 135.41 (d, J_{PC} = 15 Hz, CH of PPh_2) ppm. $^{31}P\{^1H\}$ NMR (CD_2Cl_2+CD_3OD, 161.90 MHz): δ = 31.8 (s) ppm. HR ESI+ MS: *m/z* = 1329.000 ($[M - 2ClO_4]^{2+}$). Anal. Calc. for $C_{88}H_{72}Au_6Cl_2Fe_4O_8P_4$ (2857.5): C 36.99, H 2.54%. Found: C 37.17, H 2.56%.

Preparation of $[\{(Ph_2PfcAu)_2Ag\}_2][SbF_6]_2$ (6). A solution of **1** (56.6 mg, 0.05 mmol) in dichloromethane (10 mL) was mixed with a solution of $Ag[SbF_6]$ (17.2 mg, 0.05 mmol) in anhydrous acetonitrile (2 mL). The initially orange solution turned instantly red. After being stirred for 1 hour, the reaction mixture was concentrated under reduced pressure to approximately half the volume and precipitated by adding diethyl ether (30 mL). The precipitate was isolated by decantation, washed with cold dichloromethane (2 mL) and diethyl ether (10 mL) and dried under vacuum. Yield of **6**: 68 mg (92%), red microcrystalline solid.

^1H NMR (CD_2Cl_2, 399.95 MHz): δ = 4.08-4.13 (m, 8 H, CH of fc), 4.38 (br d, *J* = 2.5 Hz, 4 H, CH of fc), 4.76 (vt of d, *J* = 2.6, 1.2 Hz, 4 H, CH of fc), 5.11 (t of vt, *J* = 2.4, 1.1 Hz, 4 H, CH of fc), 5.18-5.23 (m, 8 H, CH of fc), 5.72 (t of vt, *J* = 2.4, 1.0 Hz, 4 H, CH of fc), 7.32-7.39 (m, 8 H, PPh_2), 7.41-7.55 (m, 28 H, PPh_2), 7.56-7.62 (m, 4 H, PPh_2) ppm. $^{13}C\{^1H\}$ NMR (CD_2Cl_2, 100.58 MHz): δ = 63.35 (d, J_{PC} = 18 Hz, CH of fc), 67.16 (d, $^1J_{PC}$ = 65 Hz, C^{ipso}–P of fc), 72.69 (ddd, *J* = 87, 81, 6 Hz, C^{ipso}–Au of fc), 73.96 (d, J_{PC} = 9 Hz, CH of fc), 74.00 (d, J_{PC} = 6 Hz, CH of fc), 76.71 (d, J_{PC} = 3 Hz, CH of fc), 77.21 (d, J_{PC} = 5 Hz, CH of fc), 77.32 (d, J_{PC} = 4 Hz, CH of fc), 84.97 (s, CH of fc), 92.08 (t, J_{PC} = 5 Hz, CH of fc), 128.19 (d, $^1J_{PC}$ = 57 Hz, C^{ipso}–P of PPh_2), 129.92 (d, J_{PC} = 11 Hz, CH of PPh_2), 130.02 (d, J_{PC} = 11 Hz, CH of PPh_2), 132.25 (d, $^4J_{PC}$ = 2 Hz, CH^{para} of PPh_2), 132.40 (d, $^1J_{PC}$ = 51 Hz, C^{ipso}–P of PPh_2), 132.80 (d, J_{PC} = 14 Hz, CH of PPh_2), 132.86 (d, $^4J_{PC}$ = 2 Hz, CH^{para} of PPh_2), 135.21 (d, J_{PC} = 14 Hz, CH of PPh_2) ppm. $^{31}P\{^1H\}$ NMR (CD_2Cl_2, 161.90 MHz): δ = 37.2 (d, $^3J_{AgP}$ = 10 Hz) ppm. HR ESI+ MS: *m/z* = 1239.940 ($[M - 2SbF_6]^{2+}$). Anal. Calc. for $C_{88}H_{72}Ag_2Au_4F_{12}Fe_4P_4Sb_2$ (2951.9): C 35.80, H 2.46%. Found: C 35.91, H 2.35%.

Preparation of $[(\mu_4\text{-}O)\{(Ph_2PfcAu)_2Cu_2\}_2][BF_4]_2$ (8). Solid $[Cu(MeCN)_4][BF_4]$ (63 mg, 0.20 mmol) was added to a solution of **1** (114 mg, 0.10 mmol) in dichloromethane (20 mL). Anhydrous methanol (2 mL) was added to dissolve the copper complex completely, and the reaction mixture was mixed with a methanolic potassium hydroxide (0.5 mL, 200 mM solution), changing the colour from orange to red-orange. The resulting mixture was stirred for 1 h and then evaporated to dryness. The solid residue was taken up with dichloromethane (8 mL) and

precipitated by diethyl ether addition (2 mL). The precipitate was filtered off, and the mother liquor was concentrated to approximately half volume. Slow diffusion of diethyl ether into the solution afforded complex **8**. Yield 51 mg (37%), orange crystals. Crystals suitable for structure determination were selected from the preparatory batch.

^{1}H NMR (CD_2Cl_2, 399.95 MHz): δ = 3.10 (t of vt, *J* = 2.5 Hz, 1.3 Hz, 4 H, CH of fc), 3.35 (d of vq, *J* = 2.5 Hz, 1.0 Hz, 4 H, CH of fc), 4.16 (d of vq, *J* = 2.5 Hz, 1.0 Hz, 4 H, CH of fc), 4.30 (t of vt, *J* = 2.3 Hz, 1.2 Hz, 4 H, CH of fc), 4.51 (vt of d, *J* = 2.6 Hz, 1.1 Hz, 4 H, CH of fc), 4.73-4.78 (m, 8 H, CH of fc), 7.33-7.41 (m, 8 H, PPh_2), 7.48-7.54 (m, 8 H, PPh_2), 7.56-7.69 (m, 24 H, PPh_2), 7.72 (t of vt, *J* = 2.7 Hz, 1.1 Hz, 4 H, CH of fc) ppm. ^{13}C{^{1}H} NMR (CD_2Cl_2, 100.58 MHz): δ = 66.72 (d, $^{1}J_{PC}$ = 66 Hz, C^{ipso}–P of fc), 67.61 (d, J_{PC} = 21 Hz, CH of fc), 68.24 (d, $^{2}J_{PC}$ = 93 Hz, C^{ipso}–Au of fc), 72.37 (d, J_{PC} = 9 Hz, CH of fc), 74.80 (d, J_{PC} = 5 Hz, CH of fc), 76.25 (d, J_{PC} = 5 Hz, CH of fc), 76.60 (d, J_{PC} = 3 Hz, CH of fc), 77.68 (d, J_{PC} = 2 Hz, CH of fc), 81.57 (d, J_{PC} = 3 Hz, CH of fc), 86.59 (d, J_{PC} = 2 Hz, CH of fc), 127.96 (d, $^{1}J_{PC}$ = 58 Hz, C^{ipso}–P of PPh_2), 129.99 (d, J_{PC} = 12 Hz, CH of PPh_2), 130.05 (d, J_{PC} = 11 Hz, CH of PPh_2), 132.23 (d, $^{4}J_{PC}$ = 2 Hz, CH^{para} of PPh_2), 132.32 (d, $^{1}J_{PC}$ = 53 Hz, C^{ipso}–P of PPh_2), 132.52 (d, J_{PC} = 13 Hz, CH of PPh_2), 133.31 (d, $^{4}J_{PC}$ = 2 Hz, CH^{para} of PPh_2), 135.23 (d, J_{PC} = 15 Hz, CH of PPh_2) ppm. ^{19}F{^{1}H} NMR (CD_2Cl_2, 376.29 MHz): δ = –151.30 (s, $^{11}BF_4$), –151.24 (s, $^{10}BF_4$) ppm. ^{31}P{^{1}H} NMR (CD_2Cl_2, 161.90 MHz): δ = 41.6 (s) ppm. ESI+ MS: *m/z* = 1267.61 ([M – $2BF_4$]$^{+}$). Anal. Calc. for $C_{88}H_{72}Au_4B_2Cu_4F_8Fe_4P_4O{\cdot}CH_2Cl_2$ (2793.4): C 38.27, H 2.67%. Found: C 38.04, H 2.80%.

Preparation of [(μ-Cl){($Ph_2PfcAu)_2Cu_2$}][BF_4] (9). Solid $[CuCl(cod)]_2$ (21 mg, 0.050 mmol) was added to a solution of **1** (56.6 mg, 0.050 mmol) in 1,2-dichloroethane (10 mL). The reaction mixture changed colour from orange to red-orange. A solution of Ag[BF_4] (9.7 mg, 0.050 mmol) in tetrahydrofuran (2 mL) was introduced. Immediately after the addition, AgCl separated and the colour of the reaction mixture turned back to orange. After the reaction mixture was stirred for 1 hour, the precipitated AgCl was removed by filtration through a PTFE syringe filter, and the filtrate evaporated under reduced pressure. The solid residue was dissolved in dichloromethane (3 mL) and added into diethyl ether. The orange precipitate was isolated by decantation and dried under vacuum. Yield of **9**: 64 mg (92%), pale orange powder. Crystals suitable for structure determination were obtained by slow diffusion of diethyl ether into a dichloromethane solution of the complex. *Note:* The same product has been obtained when using 19.4 mg of Ag[BF_4] (0.10 mmol).

^{1}H NMR (CD_2Cl_2, 399.95 MHz): δ = 3.92 (d of vq, *J* = 2.5, 1.0 Hz, 1 H, CH of fc), 4.18 (d of vq, *J* = 2.4, 1.0 Hz, 1 H, CH of fc), 4.41 (t of vt, *J* = 2.6, 1.4 Hz, 1 H, CH of fc), 4.46 (t of vt, *J* = 2.3, 1.2 Hz, 1 H, 1 H, CH of fc), 4.87 (vt of d, *J* = 2.5, 1.0 Hz, 1 H, CH of fc), 5.00 (t of vt, *J* = 2.6, 0.8 Hz, 1 H, CH of fc), 5.04 (vt of d, *J* = 2.6, 1.2 Hz, 1 H, CH of fc), 7.05 (t of vt, *J* = 2.5, 1.0 Hz, 1 H, CH of fc), 7.40-7.68 (m, 40 H, PPh_2) ppm. ^{13}C{^{1}H} NMR (CD_2Cl_2, 100.58 MHz): δ = 63.97 (d, J_{PC} = 20 Hz, CH of fc), 67.90 (d, $^{1}J_{PC}$ = 65 Hz, C^{ipso}–P of fc), 71.21 (d, $^{1}J_{PC}$ = 96 Hz, C^{ipso}–Au of fc), 73.48 (d, J_{PC} = 9 Hz,

CH of fc), 75.32 (d, J_{PC} = 6 Hz, CH of fc), 76.79 (d, J_{PC} = 5 Hz, CH of fc), 77.05 (d, J_{PC} = 3 Hz, CH of fc), 77.80 (d, J_{PC} = 3 Hz, CH of fc), 80.84 (d, J_{PC} = 3 Hz, CH of fc), 87.39 (d, J_{PC} = 2 Hz, CH of fc), 128.22 (d, $^{1}J_{PC}$ = 58 Hz, C^{ipso}–P of PPh_2), 129.76 (d, J_{PC} = 11 Hz, CH of PPh_2), 129.91 (d, J_{PC} = 12 Hz, CH of PPh_2), 131.50 (d, $^{1}J_{PC}$ = 53 Hz, C^{ipso}–P of PPh_2), 132.20 (d, $^{4}J_{PC}$ = 2 Hz, CH^{para} of PPh_2), 132.85 (d, J_{PC} = 13 Hz, CH of PPh_2), 133.10 (d, $^{4}J_{PC}$ = 2 Hz, CH^{para} of PPh_2), 134.96 (d, J_{PC} = 15 Hz, CH of PPh_2) ppm. $^{31}P\{^{1}H\}$ NMR (CD_2Cl_2, 161.90 MHz): δ = 42.1 (s) ppm. HR ESI+ MS: *m/z* = 1294.858 ([M – BF_4]$^+$). Anal. Calc. for $C_{44}H_{36}Au_2BCu_2ClF_4Fe_2P_2$ (1381.7): C 38.25, H 2.63%. Found: C 37.99, H 2.66%.

Preparation of [(Ph_2PfcAu)$_2${(Cu(MeCN-κ*N*)}$_2$][BF_4]$_2$ (10). A solution of **1** (56.6 mg, 0.050 mmol) in dichloromethane (10 mL) was mixed with a solution of [$Cu(MeCN)_4$][BF_4] (31.4 mg, 0.10 mmol) in anhydrous acetonitrile (5 mL). The reaction mixture was stirred for 15 minutes and then evaporated to dryness under vacuum. The solid residue was dissolved in boiling dichloromethane (10 mL), and the solution was allowed to cool down slowly. Small crystals of the product appeared instantly. The crystallisation was completed at 4 °C overnight. The separated crystalline product was isolated by decantation, washed with cold dichloromethane (2 mL) and diethyl ether (10 mL), and dried under vacuum. Yield of **10**: 60 mg (75%), orange crystalline compound. Crystals used for X-ray diffraction analysis were selected from the preparative batch.

^{1}H NMR (CD_2Cl_2+CD_3NO_2, 399.95 MHz): δ = 2.43 (s, 6 H, MeCN), 4.84 (br s, 4 H, CH of fc), 5.09 (br s, 4 H, CH of fc), 7.34-7.74 (m, 20 H, PPh_2) ppm. $^{31}P\{^{1}H\}$ NMR (CD_2Cl_2+CD_3NO_2, 161.90 MHz): δ = 43.0 (s) ppm. HR ESI+ MS: *m/z* = 1194.962 ([M – Cu – 2MeCN – 2BF_4]$^+$). Anal. Calc. for $C_{48}H_{42}Au_2B_2Cu_2F_8Fe_2P_2{\cdot}CH_2Cl_2$ (1600.1): C 36.78, H 2.77, N 1.75%. Found: C 36.39, H 2.78, 1.32%.

DFT COMPUTATIONS

Density Functional Theory computations were performed using Gaussian16, Revision C.01.[6] All cationic species were first symmetrized to point group D_2 and subsequently optimised by imposing no geometry constraints during the optimisation stage. All computations utilised the M06 functional,[7] the Stuttgart-Dresden core potentials[8] for the Au, Ag, Cu and Fe atoms and the 6-311G(d,p) basis set for all remaining atoms. Empirical dispersion was accounted for by including the Grimme D3 damping function.[9] The Hessians needed for geometry optimisations were estimated before the initial optimisation steps. Natural Bonding Orbital studies were performed using the standalone version of NBO6.[10] Nuclear Independent Chemical Shifts (NICS) were computed for dummy atoms placed at the centroids of the consituted by the group 11 atoms using the Gauge Independent Atomic Orbital (GIAO) approach.[11] Molar volumes were computed using 0.001 e bohr^{-3} density envelopes for the Monte-Carlo integrations.

Description of the bonding situation in 5

The DFT-optimised complex cation in **5** has a symmetry of the D_2 point group (Figure S1), whose origin is located at the centroid of the hexagold ring. Hence, the six atoms of this ring can be subdivided into two symmetrically inequivalent groups – the first incorporating four Au atoms with a coordinated phosphine moiety (Au1, Au3, Au4 and Au6) and the second group including the two remaining atoms with no bonded phosphine (Au2 and Au5). The cyclic structure formed by the Au atoms suggests two main types of aurophilic interactions, one between any two neighbouring atoms belonging to the first group and the other between two proximal atoms, an atom from the first and another from the second groups. Any other atomic combinations involve significant interatomic separations and, with the exception of the Au2–Au5 atom pair, do not result in substantial aurophilic interactions.

The strongest aurophilic interaction in the cation occurred between atoms belonging to the first group and the nearest neighbouring atoms from the second group (*i.e.*, in the Au1–Au2 pair and all symmetry equivalents). The respective Mayer Bond Order (MBO) was 0.290, and Natural Bond Orbital (NBO) decomposition described this interaction as a mixture of numerous orbital delocalisations. These delocalisations occurred mostly into Rydberg orbitals on the acceptor sides. Among all possible NBO donor–acceptor interactions, only the lone-pair → Rydberg (LP → RY) delocalisations were prevailing. The Au1(LP) → Au2(RY) delocalisations occurred from five donor hybrids on Au1, but the principal contribution occurred with the Au1 donor hybrid, primarily of $5d_{xy}$-character. The total LP → RY delocalisation energy was 206.7 kJ mol^{-1}, and the contribution of the $5d_{xy}$ donor was 154.3 kJ mol^{-1}, while its most effective

delocalisation occurred into a hybrid with 84.7% d-character and 14.4% p-character on Au2. The reversed Au2(LP) → Au1(RY) delocalisations summed even to a higher total energy, although they were generated from three donor lone pairs only. The overall sum of the latter delocalisation energies was 376.4 kJ mol^{-1}, with the markedly dominant contribution (268.5 kJ mol^{-1}) from the 5d$_{xy}$ hybrid donor on Au2.

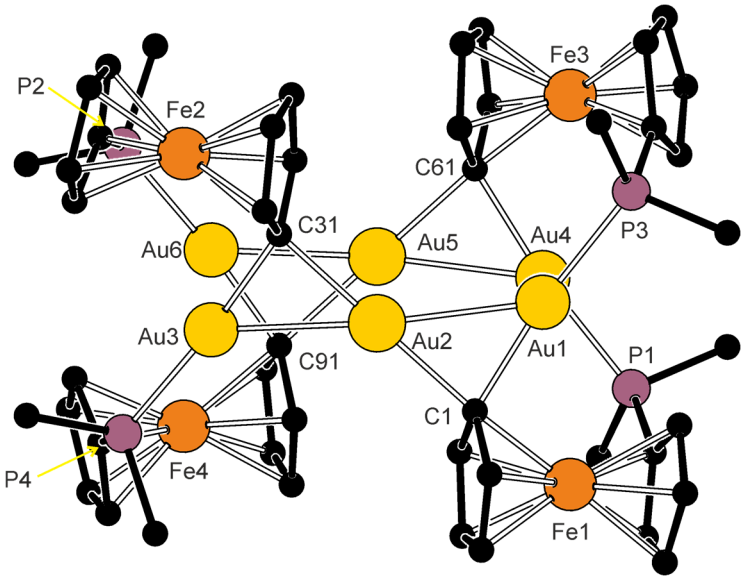

Figure S1. Simplified structure diagram of the complex cation in **5**/**5a** derived from DFT optimised coordinates. Hydrogen atoms are omitted and only the pivotal carbon atoms from the phenyl rings are shown.

The second strongest aurophilic interaction occurred in the pairs of neighbouring atoms from the first group (*i.e.*, in the Au1–Au4 and Au3–Au6 pairs), with the respective MBO reaching 0.172. Even this interaction was generated mostly by Au(LP) → Au(RY) delocalisations, with the 5d$_{xy}$ donor prevailing again, accounting for 44.1 kJ mol^{-1} of the total delocalisation energy (80.7 kJ mol^{-1}). The most effective delocalisation of 5d$_{xy}$ was observed into a hybrid with 81.1% d-character, 16.6% p-character and 2.3% s-character on the acceptor side. Because the atoms involved in this particular aurophilic interaction are symmetrically equivalent, all donor-acceptor interactions occur in equal extents in both donor-acceptor schemes.

The third and weakest aurophilic interaction was observed between Au2 and Au5, with a reported MBO of 0.144, despite an interatomic separation of 3.942 Å. This interaction was primarily generated by Au(LP) → Au(RY) delocalisations which used four lone pairs on the donor side. The predominant donor hybrid mostly consisted of 5d$_{xy}$ character, albeit with a significant portion of 5d$_{x^2-y^2}$ mixed in. This particular hybrid accounted for 38.2 kJ mol^{-1} of the overall delocalisation energy (43.8 kJ mol^{-1}). This donor hybrid exhibited its most effective delocalisation into an acceptor hybrid of 13.8% s character, 26.4% p character and 59.8% d-

character, while the second most effective delocalisation occurred into an acceptor of 95% d-character. The most important orbital contributions to the first acceptor hybrid were the $6d_{z^2}$, $7p_z$, $7d_{xy}$, $8p_z$ and 8s orbitals, while the $6d_{x^2-y^2}$ orbital contributed predominantly to the second hybrid. The acceptor orbitals used to generate aurophilic interactions were already considerably diffuse and thus allowed generation of long-range interaction(s) in the cation of **5**. Since the last aurophilic interactions were generated between symmetrically equivalent atoms, all respective donor-acceptor interactions occurred symmetrically in both donor-acceptor directions.

Comparison of compounds 5, 6 and 7

The correlation of the computed molar volumes of the cations present in compounds **5**, **6** and **7** (Table S1) with the atomic radii of M2/M5 within their metallic rings suggested that their overall geometry is controlled by factors other than these radii. After optimising the geometry of these cations, we observed that they all became isostructural and adopted the D_2 symmetry (Figure S2). The largest computed molar volume was determined for **6**, while the hexagold cation in **5**, containing the most voluminous metals, showed the most compact arrangement. The loose correlation between the computed molar volumes and the atomic radii of M2/M5 (Cu: 1.45 Å, Ag 1.65 Å, Au 1.74 Å)[12], suggests that electronic effects of the auxiliary ligands play an important role. The largest molar volume of **6** is not only the consequence of more voluminous central ring, but also of the weakest Au–P overlaps present among all cations (Table S1). By contrast, the Au–M overlaps of **5** are considerably more effective than those of other cations and coupled with long-range interaction between M2 and M5 (see below), which also explains why **5** has the lowest molar volume since such an interaction could even counterbalance the effect of weakened Au–P overlaps, which became the strongest in the Cu-Ag complex **7**.

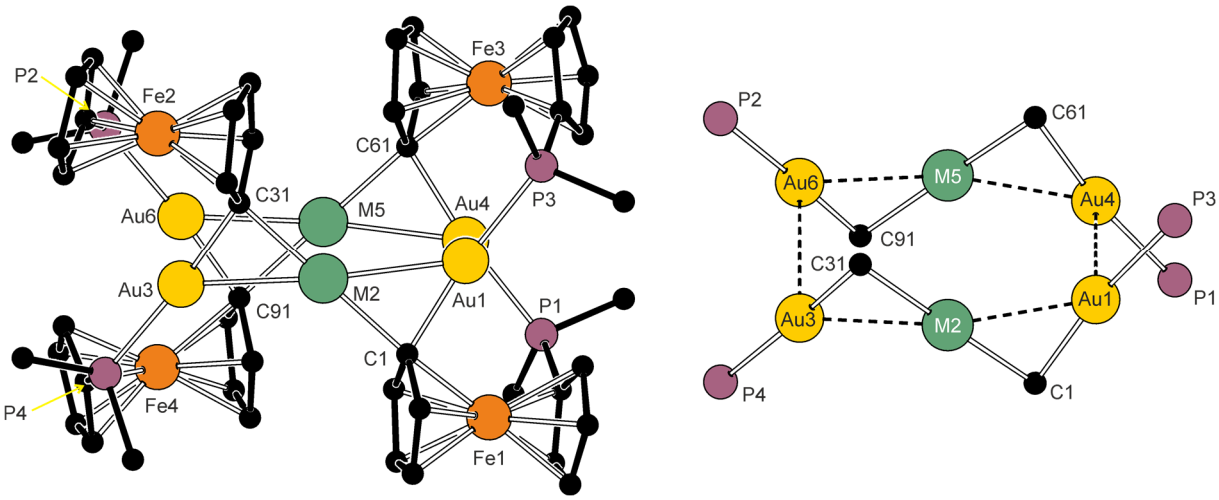

Figure S2. (left) Simplified structure diagram of the complex cations in **5**-**7** and (right) detailed view of the central six-membered ring.

Table S1. Summary of the DFT computed parameters of the cations in **5**-**7**

Cation (M)	Molar volume [au³ mol⁻¹]	Au–M		Au1–Au4/ Au3–Au6		Au–P		M2–M5		Au1–Au6 [Å]	Au–M–Au [°]	Au–Au–M [°]	NICS(0) [ppm][a]
		d [Å]	MBO	d [Å]	MBO	d [Å]	MBO	d [Å]	MBO				
5 (Au)	11450.5	2.837	0.290	3.180	0.172	2.381	0.568	3.942	0.144	6.435	164.11	97.44	−2.75
6 (Ag)	11973.9	2.809	0.215	3.194	0.192	2.385	0.554	4.032	0.061	6.367	162.11	98.11	−1.82
7 (Cu)	11592.9	2.651	0.168	3.203	0.195	2.387	0.671	4.015	0.047	6.039	160.49	97.64	−0.83

[a] Nuclear Independent Chemical Shift value at the Au1–M2–Au3–Au6–M5–Au4 ring centroid.

Although the molar volume of both **6** and **7** could be decreased by decreasing M2–M5 separations, such a geometry change is prevented by the existing strain within the central ring, as shown by the Au–Au–M (e.g., Au4–Au1–M2) angles. Among the three cations, only in **5** does this strain become partly compensated by the direct interaction between M2 and M5. The direct interaction between M2 and M5 allows the most advantageous electron distribution across the central ring of **5**, which is also the least antiaromatic ring among the three cations.

All Au–P bonds within the cations were decomposed into concurrent contributions from P → Au coordination and Au → P back-donation. The most effective P → Au interaction was identified in **5**, while the weakest Au → P back-donation occurred in **7**. A more precise bonding description, however, suggested that all Au–P bonds are effected by *3c4e* hyperbonds, generated between the neighbouring Au and P atoms and the closest ferrocenyl carbon atom (C1/C31/C61/C91) coordinated midway between one Au atom and its neighbouring M. The generation of such hyperbonds accounts for the significant influence of the phosphine moieties on the M atoms, despite substantial P–M interatomic separations. Since the P, Au, and C^{Fc} atoms are nearly collinear, any hyperbonds generated between them can stabilise the M atoms through long-range interactions with the phosphine moieties. Together with direct M–Au overlaps, these factors explain the stabilisation of the central rings (Table S2).

Table S2. Delocalisation energies (kJ mol⁻¹) between the P–Au, P–M and Au–M atom pairs of cations **5**-**7**[a]

Cation (M)	P–Au			Au→P	P→M	Au–M		
	LP(P)→LV(Au)	LP(P)→RY(Au)	Σ_{en}(P–Au)	LP→BD*	LP→RY	Au→M	M→Au	Σ_{en}(Au–M)
5 (Au)	811.2	489.6	1300.8	28.2	661.2	208.4	352.4	560.8
6 (Ag)	613.0	566.7	1179.7	28.3	557.8	215.3	271.5	486.8
7 (Cu)	620.7	642.0	1262.7	18.4	537.7	165.4	287.3	452.7

[a] LP – lone pair, LV – Lewis valence, RY – Rydberg, BD* – antibonding orbitals.

Among the three cations, the overall phosphine to M contributions were the weakest in **7**; in conjunction with the least effective direct Au–Cu overlap, these factors explain why this cation has the Cu atoms bonded least stably. These phosphine contributions occurred as lone-pair delocalisations into the metallic Rydberg acceptors.

The direct Au–M interactions were decomposed into two complementary contributions by NBO—into delocalisations from Au to M and backwards (Table S3). The most effective delocalisation was identified in **5**, namely the delocalisation of M into Au. This delocalisation occurred from three donor lone-pair hybrids on Au, while the most effective was of predominantly $5d_{xy}$ character, accounting for 268.5 kJ mol^{-1} of the total M → Au delocalisation energy (347.1 kJ mol^{-1}). Although this donor hybrid is delocalised into as many as 20 acceptor orbitals, only three prevailing contributions are detected, with energies of 47.5, 38.0 and 35.4 kJ mol^{-1}. The most effective delocalisation occurs into a hybrid acceptor with 84% p-character and is generated by mixing mostly the $6p_x$, $6p_y$ and $7p_x$ orbitals. The second acceptor hybrid is of 57.5% p-character, 21.5% s-character and 21% d-character and is generated by mixing $6p_x$, $6p_y$ and 8s. The third hybrid consists of 65.6% d-character, 21% d-character and 13.4% s-character, mixed mostly from $6d_{xy}$.

Table S3. Delocalisation energies from M into Au and Au into M of **5**-**7** and their sum (kJ mol^{-1})

Cation (M)	M → Au	Au → M	Σ_{deloc}
5 (Au)	347.1	206.7	553.8
6 (Ag)	271.5	215.3	486.8
7 (Cu)	287.1	165.1	452.2

In **5**, where this type of interaction is the most impaired, the donor hybrid has 97% d-character, with a predominant contribution from $4d_{xy}$. The delocalisation from this hybrid is again the most effective, accounting for 231.3 kJ mol^{-1} of the overall energy (271.5 kJ mol^{-1}). On the acceptor side, however, no terms prevail, and the most effective overlap, with an energy of 27.6 kJ mol^{-1}, is achieved by a hybrid with 61.4% p-character and with contributions from the $6p_x$, $7p_x$, $8p_x$ orbitals. These results suggest that orbitals involved in this delocalisation become more separated in energy within the heterobimetallic cations, causing a less efficient metal-metal interaction. In the least stable complex **7**, the Au → M delocalisation becomes particularly impaired; the donor hybrid on its Au mostly consists of $5d_{xy}$, while the most effective acceptor hybrid consists of a mixture of $4d_{xy}$, $4d_{z^2}$ and 5s.

X-RAY CRYSTALLOGRAPHY

Diffraction data were collected on a Bruker Apex II (**1**·$CHCl_3$) or a Bruker D8 VENTURE Kappa Duo diffractometer (all other compounds) equipped with a Cryostream Cooler (Oxford Cryosystems), using Mo Kα radiation (λ = 0.71073 Å). The structures were solved using direct methods (SHELXT-2014[13]) and refined using full-matrix least-squares minimisation on F^2 (SHELXL-2014/2017[14]). Non-hydrogen atoms were refined with anisotropic displacement parameters. Hydrogens were placed in their theoretical positions and refined as riding atoms with U_{iso}(H) set to a multiple of U_{eq}(C) of their bonding carbon atoms. Structure-specific details are provided below.

Because of inefficient packing of the relatively large and irregularly shaped complex cations, the complexes typically contained structural voids, which accommodated the counter anions and disordered solvent molecules. If no reliable structure model could be found for the solvent molecules, their contribution to the overall scattering was eliminated using PLATON SQUEEZE.[15] This approach was applied to the solvent molecules in **5a**·MeCN·$4CH_2Cl_2$, where 748 electrons were removed from the unit cell (space group $P2_1/c$, Z = 4), matching the expected value (760 electrons), and to 1.5 acetonitrile molecule in **6**·3.5MeCN·$C_2H_4Cl_2$ (64 electrons removed, 64 electrons expected; space group P–1, Z = 2). For **9**·$C_2H_4Cl_2$, one 1,2-dichloroethane molecule was refined over two positions, and the other was treated as diffuse scattering. In total, 214 electrons were eliminated from the unit cell ($C2/c$, Z = 4), also corresponding to the expected value (200 electrons).

The data on the crystals of **10**·1.5CH_2Cl_2 had to be collected at 230 K because the crystals disintegrated upon cooling below this temperature, most likely due to phase transition. Even in this case, the solvent molecules were treated by PLATON SQUEEZE (280 electrons removed, 252 electrons expected). In addition, one phenyl ring and one fluorine atom had to be refined over two positions. For **1**·$CHCl_3$, PLATON SQUEEZE was used to eliminate diffuse electron density near the solvent molecule (likely another orientation of the solvent molecule; 39 electrons per the unit cell). Lastly, the crystal of **3**·2C_6H_5F was a two-component non-merohedral twin. The twin matrix and the ratio of the two contributing domains were [1 0 0; 0 –1 0; –0.735 0 –1] and 88:12, respectively.

Crystallographic data and refinement parameters are outlined in Table S4. The geometric data and structural diagrams were obtained using the PLATON program.[16] Complete crystallographic data were deposited at the Cambridge Crystallographic Data Centre and are available from www.ccdc.cam.ac.uk/data_request/cif, by email at data_request@ccdc.cam.ac.uk or by contacting The Cambridge Crystallographic Data Centre, 12 Union Road, Cambridge CB2 1EZ, UK; fax: +44 1223 336033. The deposition numbers are outlined in Table S4.

Table S4. Selected crystallographic data and structure refinement parameters[a]

Compound	**1**·$CHCl_3$	**2**·2.5$C_2H_4Cl_2$	**3**·2C_6H_5F
Formula	$C_{45}H_{37}Au_2Cl_3Fe_2P_2$	$C_{93}H_{84}Au_4Cl_5F_{12}Fe_4P_4Sb_2$	$C_{92}H_{112}Au_4F_{14}Fe_2P_4Sb_2$
M	1251.67	2985.49	2750.76
Crystal system	monoclinic	triclinic	monoclinic
Space group	$P2_1/c$ (no. 14)	$P\bar{1}$ (no. 2)	$P2_1/c$ (no. 14)
a [Å]	10.1146(2)	14.2855(9)	15.3175(6)
b [Å]	18.5309(4)	14.827(1)	16.1547(6)
c [Å]	22.2454(4)	23.602(2)	37.867(1)
α [°]	90	71.730(2)	90
β [°]	98.335(1)	83.076(3)	98.533(1)
γ [°]	90	89.182(2)	90
V [Å]^3	4125.5(1)	4711.2(6)	9266.3(6)
Z	4	2	4
μ(Mo Kα) [mm^{-1}]	8.084	7.640	7.326
Diffrns collected	72720	152889	21734
Independent diffrns	9486	21676	21734
Observed[a] diffrns	8441	19326	20412
R_{int}[b] [%]	2.73	3.39	5.14
No. of parameters	487	1117	1064
R[b] obsd diffrns [%]	2.52	2.14	3.21
R, *wR*[b] all data [%]	3.02, 6.02	2.76, 4.97	3.66, 6.95
Δρ [e Å^{-3}]	1.92, –2.29	2.18, –1.58	1.32, –1.17
CCDC deposition no.	2124923	2124924	2124925

[a] Diffractions with $I > 2\sigma(I)$. [b] Definitions: $R_{int} = \Sigma\left|F_o^2 - F_o^2(\text{mean})\right|/\Sigma F_o^2$, where F_o^2(mean) is the average intensity of symmetry-equivalent diffractions. $R = \Sigma\left|\left|F_o\right| - \left|F_c\right|\right|/\Sigma\left|F_o\right|$ and $wR = [\Sigma\{w(F_o^2 - F_c^2)^2\}/\Sigma w(F_o^2)^2]^{1/2}$.

Table S4 continued

Compound	**5a**·MeCN·4CH_2Cl_2	**6**·3.5MeCN·$C_2H_4Cl_2$	**8**·3CH_2Cl_2
Formula	$C_{94}H_{83}Au_6Cl_{10}Fe_4NO_8P_4$	$C_{97}H_{86.5}Ag_2Au_4Cl_2F_{12}Fe_4N_{3.5}P_4Sb_2$	$C_{91}H_{78}Au_4B_2Cl_6Cu_4F_8Fe_4OP_4$
M	3238.19	3194.48	2963.16
Crystal system	monoclinic	triclinic	monoclinic
Space group	$P2_1/c$ (no. 14)	$P\bar{1}$ (no. 2)	$P2_1/c$ (no. 14)
a [Å]	13.2872(7)	16.6460(8)	19.4460(7)
b [Å]	22.755(1)	18.333(1)	17.9881(6)
c [Å]	33.741(2)	18.500(1)	26.4218(9)
α [°]	90	110.924(2)	90
β [°]	96.291(2)	110.250(2)	103.181(1)
γ [°]	90	95.271(2)	90
V [Å]^3	10140.0(1)	4795.3(4)	8998.8(5)
Z	4	2	4
μ(Mo Kα) [mm^{-1}]	9.578	7.823	8.354
Diffrns collected	181788	336904	221386
Indep diffrns	23310	22004	20630
Observed[a] diffrns	19479	21044	19570
R_{int}[b] [%]	5.89	3.41	3.69
No. of parameters	1009	1137	1117
R[b] obsd diffrns [%]	2.96	1.52	1.70
R, wR[b] all data [%]	4.10, 7.45	1.66, 3.70	1.89, 3.71
Δρ [e Å^{-3}]	1.65, –1.95	2.52, –1.00	0.77, –0.99
CCDC no.	2124926	2124927	2124928

Table S4 continued

Compound	**9**·2$C_2H_4Cl_2$	**10**·1.5CH_2Cl_2
Formula	$C_{48}H_{44}Au_2BCl_5Cu_2F_4Fe_2P_2$	$C_{49.5}H_{45}Au_2B_2Cl_3Cu_2F_8Fe_2N_2P_2$
M	1579.54	1642.50
Crystal system	monoclinic	monoclinic
Space group	*Cc* (no. 9)[c]	$P2_1/c$ (no. 14)
a [Å]	21.478(2)	20.4517(8)
b [Å]	17.976(1)	17.3088(6)
c [Å]	15.735(1)	15.9032(6)
α [°]	90	90
β [°]	125.385(2)	102.174(1)
γ [°]	90	90
V [Å]^3	4952.9(6)	5503.0(4)
Z	4	4
μ(Mo Kα) [mm^{-1}]	7.700	6.851
Diffrns collected	66207	57601
Independent diffrns	11214	6322
Observed[a] diffrns	11159	5908
R_{int}[b] [%]	2.22	2.30
No. of parameters	569	348
R[b] obsd diffrns [%]	1.32	2.16
R, *wR*[b] all data [%]	1.33, 3.25	2.40, 5.86
Δρ [e Å^{-3}]	0.75, –0.40	0.68, –0.72
CCDC deposition no.	2124929	2124930

[c] Flack's enantiomorph parameter: –0.010(1).

Crystal structure of 1·$CHCl_3$

The compound crystallizes in the monoclinic space group $P2_1/n$ as a monochloroform solvate. A view of the molecular structure is shown in Figure S3, and the geometric parameters are outlined in Table S5. Both structurally independent gold atoms in **1** are linearly coordinated, and their distance excludes any intramolecular aurophilic interaction (Au1···Au2 = 4.2516(3) Å). The Au-C and Au-P distances are similar to those in [FcAu(PPh_3)].[17] The ferrocene units are negligibly tilted and adopt an approximately 1,2′ conformation (ideal value: 72°).

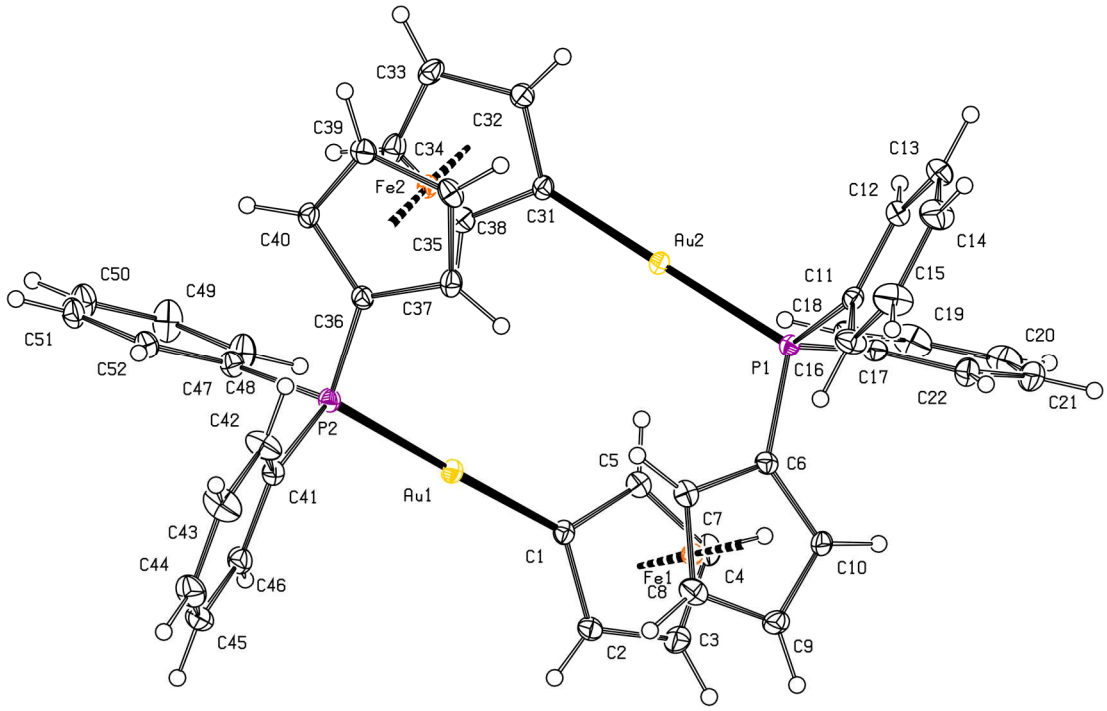

Figure S3. PLATON plot of the complex molecule in the structure of **1**·$CHCl_3$ showing displacement ellipsoids at the 30% probability level.

Table S5. Selected geometric parameters for **1**·$CHCl_3$ (in Å and deg)[a]

Au1-C1	2.033(4)	Au2-C31	2.040(4)
Au1-P2	2.290(1)	Au2-P1	2.278(1)
C1-Au1-P1	177.9(1)	C31-Au2-P1	179.4(1)
Fe1-C(1-10)	2.028(4)-2.107(4)	Fe2-C(31-40)	2.033(4)- 2.074(4)
tilt(Fe1)	2.3(2)	tilt(Fe2)	1.2(2)
τ(Fe1)	–83.9(3)	τ(Fe2)	–84.8(3)

[a] Definitions: tilt is the dihedral angle of the least-squares cyclopentadienyl planes and τ stands for the torsion angle C1-Cg1-Cg2-C6 for Fe1 (C31-Cg3-Cg4-C36 for Fe2), where Cg denotes the respective cyclopentadienyl ring centroid.

Crystal structure of 2·2.5$C_2H_4Cl_2$

The structure of compound **2**·2.5$C_2H_4Cl_2$ and a view of the tetragold core in its complex cation are shown in Figures S4 and S5, respectively. Relevant structural parameters are presented in Table S6.

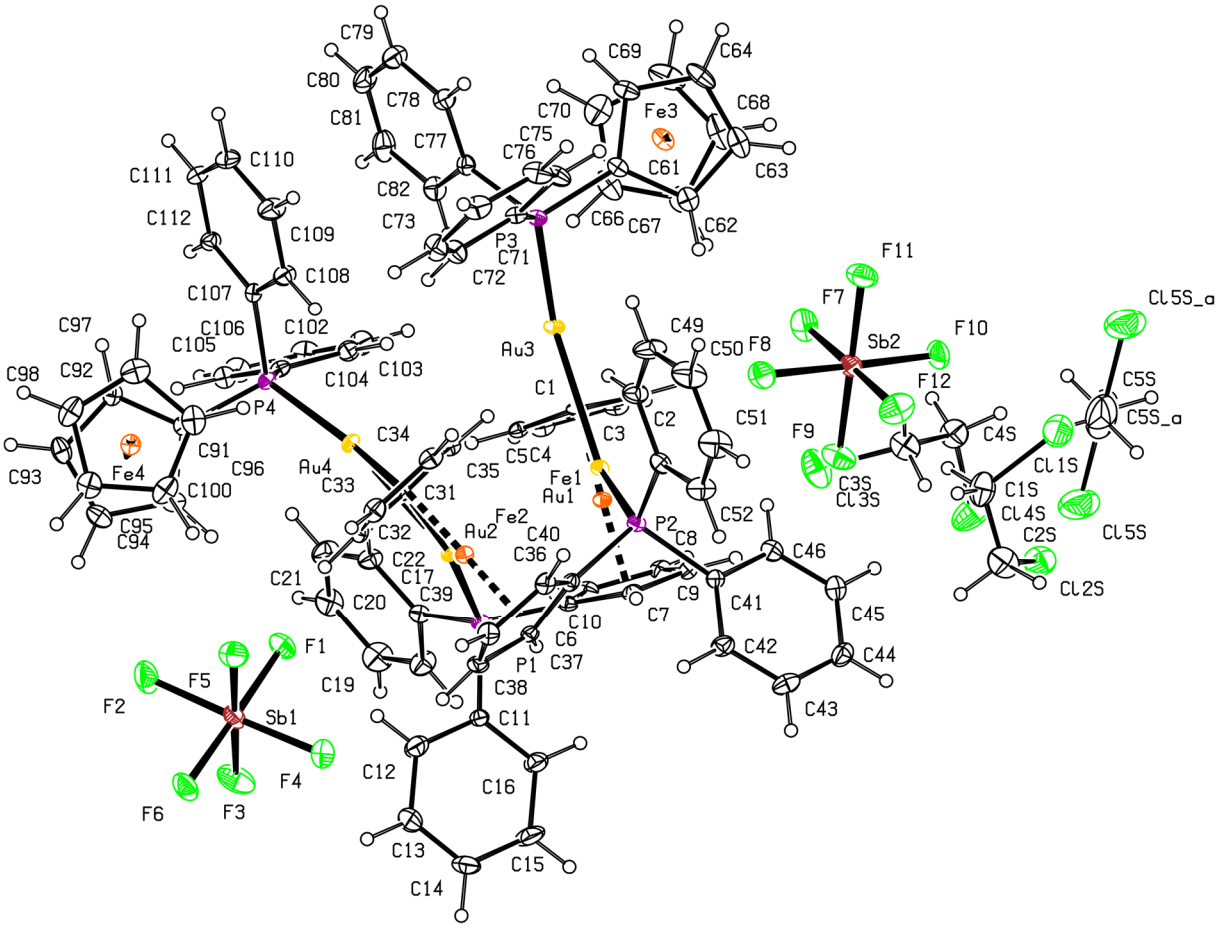

Figure S4. A complete structural diagram for **2**·2.5$C_2H_4Cl_2$ with 30% displacement ellipsoids.

The geometry of the complex cation is generally similar to that of a tetrafluoroborate salt reported previously.[18] Unlike this reference compound, however, the cation in **2** lacks any imposed symmetry. Formally, the cation can be described as metalloligand **1** with two additional LAu^+ fragments (L = $FcPPh_2$), forming a tetragold complex cation. This notion is consistent with the nearly linear C1-Au1-P2 (173.26(8)°) and C31-Au2-P1 (171.88(9)°) angles and more bent C1-Au3-P3 (161.90(0)°) and C31-Au4-P4 (160.40(9)°) angles. The Au1···Au2 (3.2201(6) Å) and, mainly, the Au3···Au4 (4.3624(6) Å) distance in **2**·2.5$C_2H_4Cl_2$ are significantly longer than the Au···Au distances within the geminally diaurated fragments (Au1···Au3 2.7813(6) Å, Au2···Au4 2.7572(5); *cf.* 2.768(3) Å in [Fc{Au(PPh_3)}$_2$][BF_4][19]). The corresponding Au-C distances (Au1-C1 2.134(3) Å, Au3-C1 2.136(3) Å, Au2-C31 2.131(4) Å, and Au3···C31 2.136(3) Å) are identical

within the margins of experimental error, and all {AuC_2} fragments are oriented perpendicularly to the planes of their parent cyclopentadienyl rings (*cf*. {Au1,Au3,C1} *vs*. C(1-5) 88.0(2)°, {Au2,Au4,C31} *vs*. C(31-35) 89.3(2)°). The ferrocene units are tilted by 10.3(2)° (Fe1) and 9.5(2)° (Fe2), which is also reflected by the larger variation in Fe-C bonds (compare the Fe1-C(1-10) 2.037(3)-2.098(3) Å and Fe2-C(31-40) 2.035(4)-2.094(3) Å distances in the aurated ferrocene units with the Fe3-C(61-10) 2.031(3)-2.056(4) Å and Fe4-C(91-100) 2.036(3)-2.054(4) Å distances in the terminal phosphine ligands). The Au-P bonds of the aurated ferrocene ligand (Au1-P2 2.291(1) Å and Au2-P1 2.284(1) Å) are slightly elongated with respect to the Au-P distances of the non-aurated ligands (Au3-P3 2.269(1) Å, Au4-P4 2.262(1) Å).

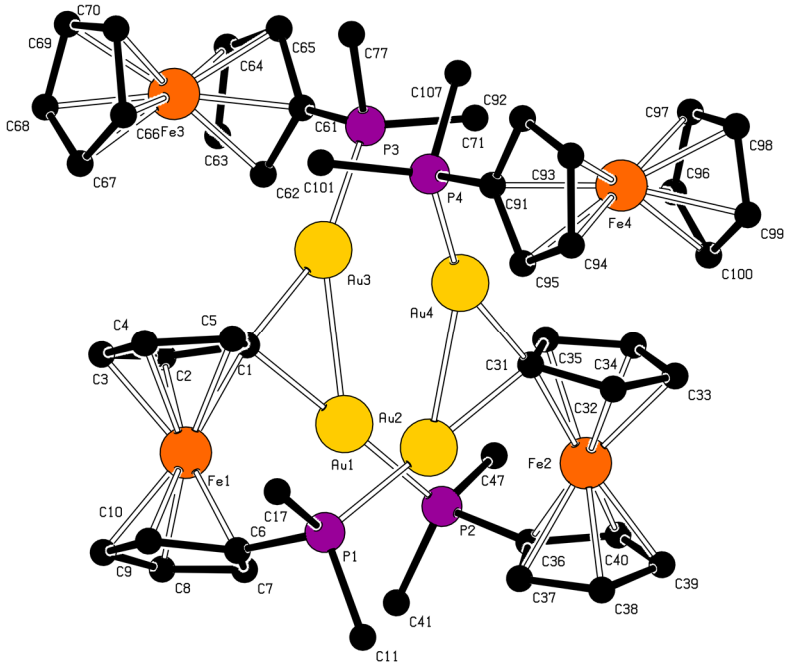

Figure S5. Simplified view of the tetragold core in the complex cation of **2**·2.5$C_2H_4Cl_2$. All hydrogens and phenyl ring carbons except for pivotal ones are omitted.

Table S6. Selected distances and angles for **2**·2.5$C_2H_4Cl_2$ (in Å and deg)

Au1···Au3	2.7813(6)	Au2···Au4	2.7572(5)
Au1-C1	2.134(3)	Au2-C31	2.131(3)
Au3-C1	2.136(3)	Au4-C31	2.133(3)
Au1-C1-Au3	81.3(1)	Au2-C31-Au4	80.6(1)
Au1-P2	2.291(1)	Au2-P1	2.284(1)
Au3-P3	2.269(1)	Au4-P4	2.262(1)
P2-Au-C1	173.26(8)	P1-Au2-C31	171.88(8)
P3-Au3-C1	161.90(9)	P4-Au4-C31	160.40(9)

Crystal structure of $3 \cdot 2C_6H_5F$

The complex cation in the structure of $\mathbf{3} \cdot 2C_6H_5F$ is structurally analogous to that of $\mathbf{2} \cdot 2.5C_2H_4Cl_2$ discussed above, bearing two tricyclohexylphosphine (PCy_3) molecules as terminal ligands (Figure S6 and S7, parameters in Table S7). Replacing $FcPPh_2$ with the bulkier PCy_3 ligands increases the twisting of the U-shaped array of the four gold atom, as illustrated by the torsion angles Au3-Au1-Au2-Au4 –8.37(2)° in $\mathbf{2} \cdot 2.5C_2H_4Cl_2$, and 14.76(2)° in $\mathbf{3} \cdot 2C_6H_5F$. Accordingly, the variation in the Au-C distances of $\mathbf{3} \cdot 2C_6H_5F$ is larger (the outer gold atoms Au2 and Au4 form longer Au-C bonds than the internal ones, Au1 and Au3), and the Au3-P3 and Au4-P4 bonds are elongated with respect to those in $\mathbf{2} \cdot 2.5C_2H_4Cl_2$.

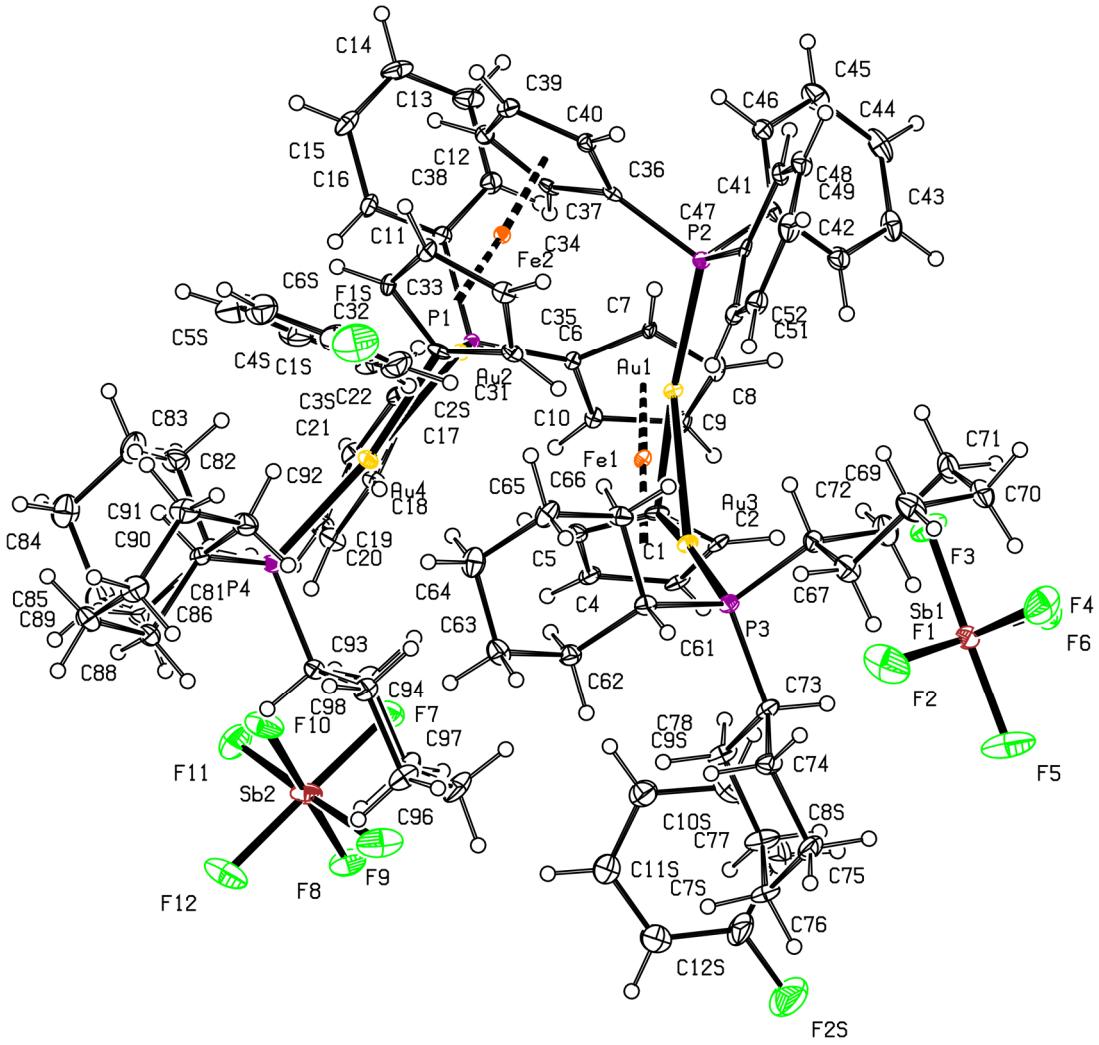

Figure S6. Complete structural diagram of $\mathbf{3} \cdot 2C_6H_5F$ with displacement ellipsoids scaled to the 30% probability level

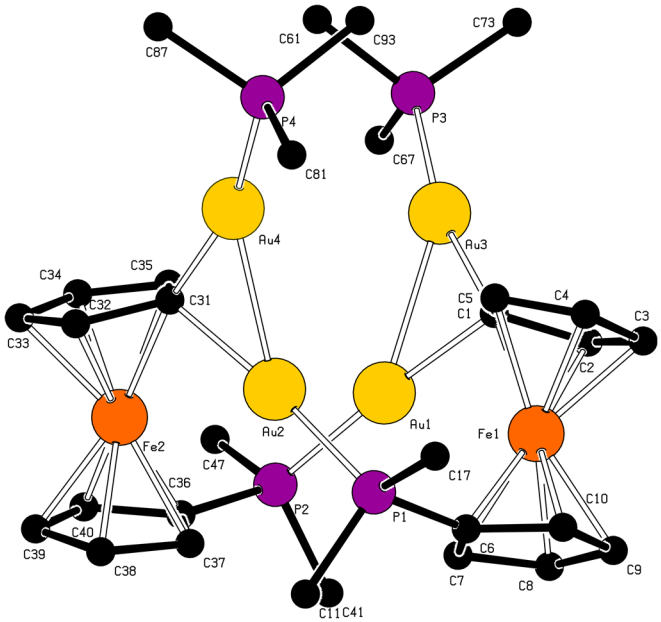

Figure S7. Simplified view of the tetragold core in the complex cation of **3**·2C_6H_5F. All hydrogens and phenyl ring carbons except for pivotal ones are omitted.

Table S7. Selected distances and angles of **5**·2C_6H_5F (in Å and deg)

Au1···Au3	2.782(1)	Au2···Au4	2.771(1)
Au1-C1	2.122(6)	Au2-C31	2.124(6)
Au3-C1	2.150(6)	Au4-C31	2.154(6)
Au1-C1-Au3	81.3(2)	Au2-C31-Au4	80.7(2)
Au1-P2	2.280(2)	Au2-P1	2.276(2)
Au3-P3	2.288(2)	Au4-P4	2.290(2)
P2-Au1-C1	175.1(2)	P1-Au2-C31	173.4(2)
P3-Au1-C1	167.6(2)	P4-Au4-C31	165.2(2)

Crystal structures of 5a·MeCN·4CH_2Cl_2 and 6·3.5MeCN·$C_2H_4Cl_2$

Compounds **5a·MeCN·4CH_2Cl_2** and **6·3.5MeCN·$C_2H_4Cl_2$** are analogous, differing by the "central" atoms within the linear trimetallic assemblies (Au_3 *vs.* Au_2Ag; Figure S8 and Table S8). Key geometric parameters are discussed in the main text.

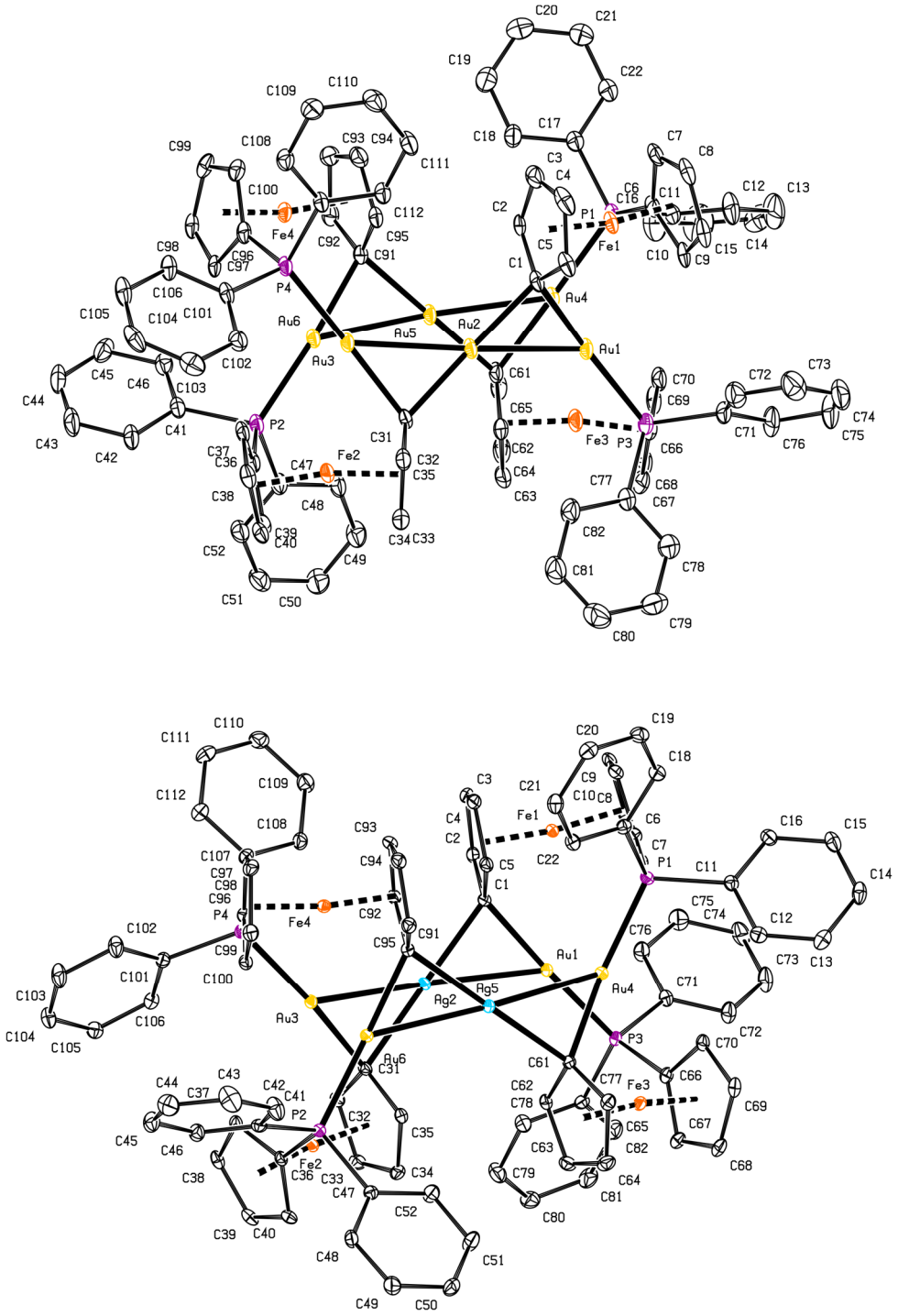

Figure S8. PLATON plots of the complex cations in the structure of **5a**·MeCN·4CH_2Cl_2 (top) and **6**·3.5MeCN·$C_2H_4Cl_2$ (bottom) showing 30% displacement ellipsoids. H-atoms are omitted.

Table S8. Distances and angles for **5a**·MeCN·4CH_2Cl_2 (M = Au) and **6**·3.5MeCN·$C_2H_4Cl_2$ (M = Ag) (in Å and deg)

Distance	**5a**·MeCN·4CH_2Cl_2	**6**·3.5MeCN·$C_2H_4Cl_2$	Angle	**5a**·MeCN·4CH_2Cl_2	**6**·3.5MeCN·$C_2H_4Cl_2$
Au1-M2	2.761(1)	2.7356(5)	Au1-M2-Au3	166.57(2)	167.90(2)
Au3-M2	2.7670(9)	2.7441(5)	Au4-M5-Au6	167.11(2)	167.44(2)
Au4-M5	2.765(1)	2.7759(5)	Au1-C1-M2	80.8(2)	78.29(8)
Au6-M5	2.764(1)	2.7653(5)	M2-C31-Au3	80.7(2)	78.47(9)
Au1-C1	2.151(5)	2.086(3)	Au4-C61-M5	80.5(2)	79.20(9)
M2-C1	2.110(5)	2.244(2)	M5-C91-Au6	80.6(2)	78.77(9)
M2-C31	2.123(5)	2.248(2)	C1-Au1-P3	171.2(1)	170.60(7)
Au3-C31	2.149(5)	2.086(3)	C1-M2-C31	175.1(2)	177.9(1)
Au4-C61	2.159(5)	2.077(2)	C31-Au3-P4	171.7(1)	171.17(8)
M5-C61	2.119(5)	2.272(3)	C61-Au4-P1	171.4(1)	171.79(8)
M5-C91	2.114(5)	2.268(3)	C61-M5-C91	175.2(2)	177.9(1)
Au6-C91	2.160(5)	2.085(2)	C91-Au6-P2	172.8(1)	169.90(8)
Au1-P3	2.290(2)	2.2845(8)	tilt(Fe1)	12.2(3)	9.5(1)
Au3-P4	2.288(1)	2.2879(8)	tilt(Fe2)	14.0(3)	8.3(1)
Au4-P1	2.290(1)	2.2868(8)	tilt(Fe3)	13.0(3)	10.0(2)
Au6-P2	2.292(1)	2.2891(8)	tilt(Fe4)	13.1(3)	10.1(2)
Au1···Au4	3.1246(5)	3.2404(6)	τ(Fe1)	64.9(4)	–67.2(2)
M2···M5	3.7596(6)	3.7878(6)	τ(Fe2)	66.1(4)	–62.5(2)
Au3···Au6	3.2262(6)	3.1889(6)	τ(Fe3)	64.1(4)	–64.9(2)
φ	11.64(1)	7.11(1)	τ(Fe4)	68.8(4)	–65.6(2)

[a] Tilt and τ are defined as for **1**·$CHCl_3$; φ is the angle between the (Au1···Au3)/(Au4···Au6) lines.

Crystal structures of 8·3CH_2Cl_2 and 9·2$C_2H_4Cl_2$

The Cu-Au complexes [(μ_4-O){($Ph_2PfcAu)_2Cu_2$}$_2$][BF_4]$_2$ (**8**) and [(μ-Cl){($Ph_2PfcAu)_2Cu_2$}$_2$][BF_4] (**9**) are closely structurally related; therefore, their structures will be discussed jointly. In fact, the compounds differ only in their bridging ligand, whose nature dictates whether it will act as a bridge within one dicuprated metalloligand **1** (*viz.*, {Ph_2PfcAu}$_2Cu_2$) or interconnect two such moieties. Structures of the complex cations are shown in Figures S9 and S10; selected geometric data are outlined in Table S9.

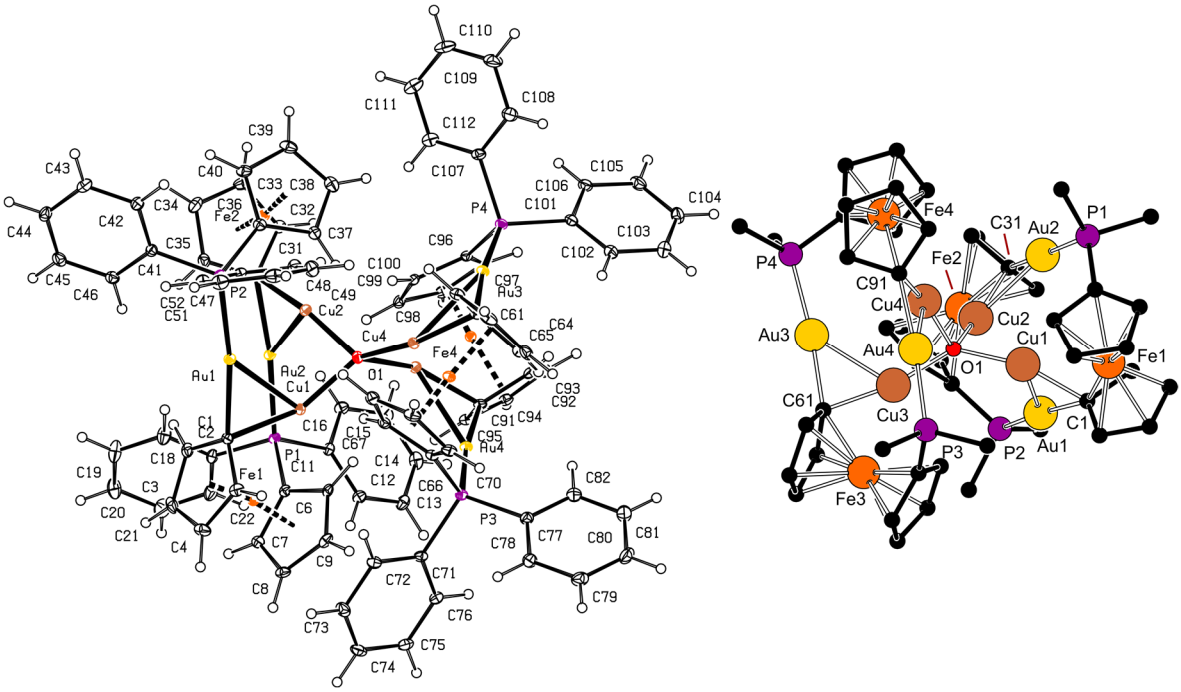

Figure S9. Full (left) and partial (right) structure diagram for the cation in **8**·3CH_2Cl_2.

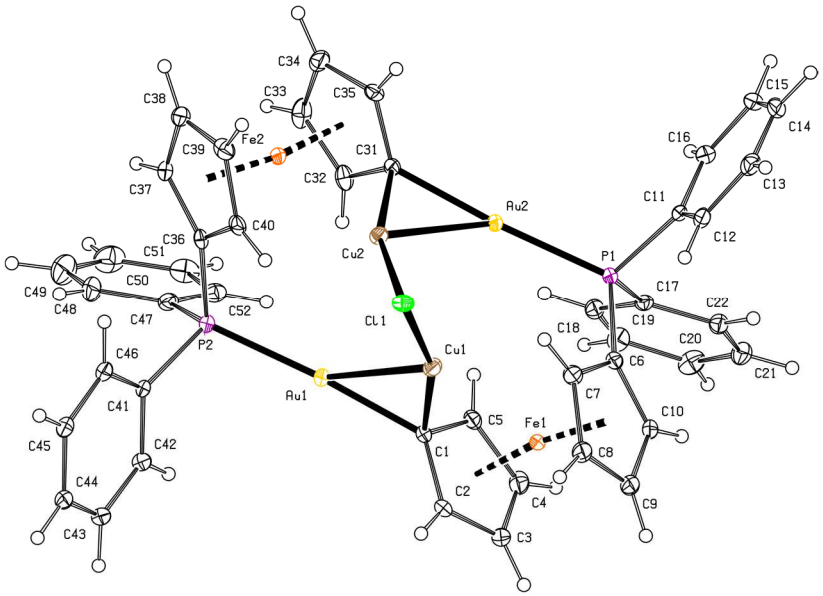

Figure S10. PLATON plot of the complex cation in the structure of **9**·2$C_2H_4Cl_2$ showing displacement ellipsoids at the 30% probability level.

The complex cation in **9** consists of two equivalent parts, which are are mutually tilted, as illustrated by the dihedral angles of the {Au1,Cu1,C1} and {Au2,Cu2,C31} planes (72.1(2)°) or by the angle between the metalated cyclopentadienyl planes C(1-5) and C(31-35) (74.2(3)°). Compound **9** has longer Au-C bonds (by 0.06-0.07 Å) and narrower C-Au-P angles (by 3-4°) than the parent **1**, in line with the presence of an additional metal atom (Cu) bonding to the aurated cyclopentadienyl carbon (C1/C31) in **9**. Similarly to the structure of **2** and **3**, the {Au1,Cu1,C1} and {Au2,Cu2,C31} planes in **9** are oriented nearly perpendicularly to the plane of their parent cyclopentadienyl rings (C(1-5) and C(31-35); the respective dihedral angles are 78.4(2)° and 80.2(3)°). The Au-Cu distances (≈2.58 Å) are shorter than the sum of the respective covalent radii (2.68 Å)[20] and match the Au-Cu separation observed in polymeric complexes $[\{(C_6F_5)_2Au\}\{Cu(MeCN)\}]_n$ featuring bridging pentafluorophenyl ligands (2.57 and 2.59 Å).[21] The ferrocene cyclopentadienyls are tilted by approximately 10-12° and mutually rotated into an approximately 1,2' conformation.

As stated already above, compound **8** contains two $\{Ph_2PfcAg\}_2Cu_2$ units connected by a quadruply bridging oxide ligand. The geometry of the two structurally independent $\{Ph_2PfcAg\}_2Cu_2$ moieties is similar to that of **9** (see Table S8), but the distances of the Cu(I) ions towards the bridging ligand are shorter (Cu-O < Cu-Cl), which brings the two $\{Ph_2PfcAg\}_2Cu_2$ fragments closer, thereby distorting the sterically crowded environment of the bridging oxygen atom from ideally tetrahedral (Cu1-O1-Cu4 117.67(9)°, Cu2-O1-Cu3 129.1(1)°, Cu2-O1-Cu4 109.84(8)°, and Cu3-O1-Cu4 84.20(8)°).

Table S9. Selected distances and angles for **8**·3CH_2Cl_2 and **9**·2$C_2H_4Cl_2$ (in Å and deg)

Parameter	**8**·3CH_2Cl_2 (X = O1)		**9**·2$C_2H_4Cl_2$ (X = Cl1)
	Au1/Au2/Cu1/Cu2	Au3/Au4/Cu3/Cu4[a]	
Au1-Cu1	2.5558(7)	2.6007(6)	2.5771(7)
Au1-C1	2.110(3)	2.112(2)	2.094(4)
Cu1-C1	2.030(3)	1.990(3)	2.027(4)
Au1-C1-Cu1	76.23(9)	78.62(9)	77.4(2)
Au1-P2	2.2777(7)	2.2864(7)	2.279(1)
C1-Au1-P2	172.19(8)	173.37(8)	175.0(1)
Au2-Cu2	2.5454(6)	2.5491(6)	2.5891(9)
Au2-C31	2.122(3)	2.124(2)	2.101(4)
Cu2-C31	2.007(3)	1.998(3)	2.011(5)
Au2-C31-Cu2	76.05(9)	76.33(8)	78.0(1)
Au2-P1	2.2830(7)	2.2835(7)	2.282(1)
C31-Au2-P1	172.37(7)	173.37(8)	173.7(1)
Cu1-X	1.917(2)	1.902(2)	2.226(1)
Cu2-X	1.907(2)	1.890(2)	2.230(1)
C1-Cu1-X	152.63(9)	166.93(9)	161.5(1)
C31-Cu2-X	159.45(9)	156.04(9)	161.5(1)
Cu1-X-Cu2	84.73(8)	84.20(8)	70.23(4)
tilt(Fe1/Fe2)	10.8(2)/9.7(2)	12.1(2)/10.7(2)	11.5(2)/10.6(3)
τ(Fe/Fe2)	−64.3(2)/−68.0(2)	68.8(2)/75.0(2)	−71.7(3)/−68.9(3)

[a] Given are the analogous parameters for the "second", chemically equivalent half of the complex cation.

Crystal structure of 10·1.5CH_2Cl_2

The cation in the structure of **10**·1.5CH_2Cl_2 resides over the crystallographic centre. As a result, only half of this cation is structurally independent (Figure S11, parameters in Table S10). The structure of the cation can be regarded as metalloligand **1** capped by two {Cu(MeCN)}$^+$ fragments on both sides of the central {$Au_2C_2P_2$} ring: the pairs of Au1, C1 and P1 atoms that form a six-membered ring are coplanar within approximately 0.03 Å, and the Cu1/Cu1' atom are displaced 1.5164(4) Å above and below the mean ring plane (see alternative view in Figure S11).

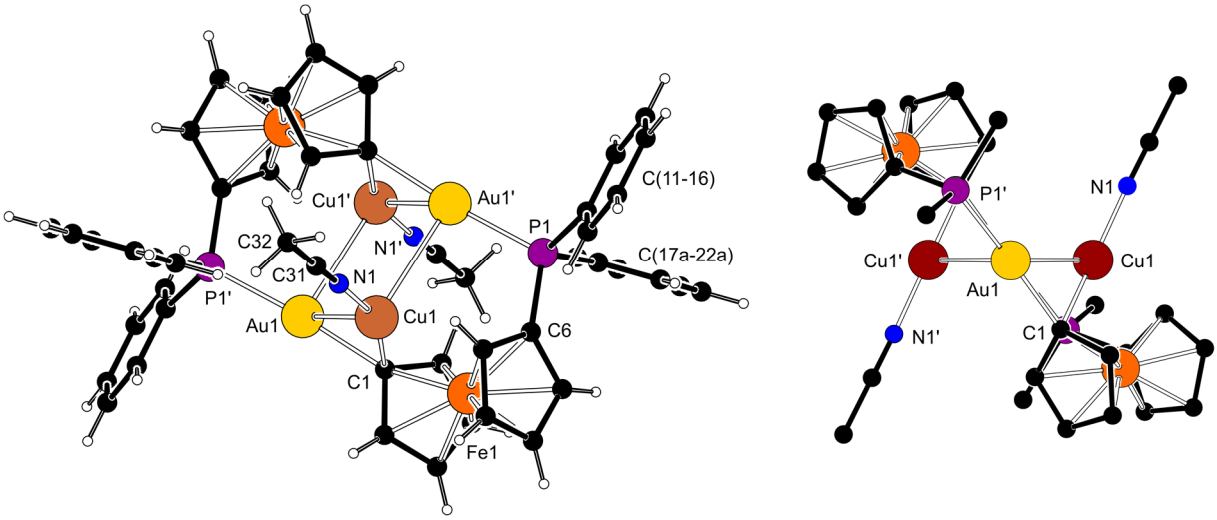

Figure S11. Complete diagram (left) and simplified side view (right) of the complex cation in the structure of **10**·1.5CH_2Cl_2. Only one position of the disordered phenyl ring C(17-22) is shown for clarity. The prime-labelled atoms are generated by crystallographic inversion.

Table S10. Selected distances and angles of **10**·1.5CH_2Cl_2 (in Å and deg)

Distance		Angle	
Au1-Cu1	2.5897(6)	Cu1-Au1-Cu1'	85.71(2)
Au1-Cu1'	2.9953(6)	Au1-Cu1-Au1'	94.29(2)
Au1-C1	2.104(3)	Au1-C1-Cu1	78.0(1)
Au1-P1'	2.2940(9)	C1-Au1-P1'	174.61(8)
Cu1-C1	2.011(3)	C1-Cu1-Au1'	98.67(8)
Cu1-N1	1.888(3)	Au1-Cu1-N1	113.4(1)
Fe1-C(1-10)	2.042(4)-2.070(3)	Au1'-Cu1-N1	98.86(9)
Au1···Au1'	4.1035(5)	tilt	11.2(2)
Cu1···Cu1'	3.8101(6)	τ	−62.5(2)

The central {Au_2Cu_2} ring is compressed along the Cu···Cu diagonal, as evidenced by the Au1···Au1' and Cu1···Cu1' distances and the interring angle (86 and 94°). The copper(I) ions are further coordinated by terminal acetonitrile ligands (Cu1-N1 1.888(3) Å, C31-N1 1.123(6) Å), which extend away from the centre of the molecule (the angle between the plane of the {$Au_2C_2P_2$} ring and the C31-N1 bond is 62.5(3)°). Otherwise, the geometric parameters of the {$(Ph_2PfcAu)_2Cu_2$} motif in **10** are generally similar to those of **8** and **9**. The {Au1,Cu1,C1} plane is oriented nearly perpendicularly to the cyclopentadienyl plane involving C1 (dihedral angle 82.3(2)°), and the ferrocene cyclopentadienyls are tilted (11°) and mutually rotated by ≈63°.

COPIES OF THE NMR AND MS SPECTRA

(Note: residual solvent signals in the NMR spectra are denoted by an asterisk.)

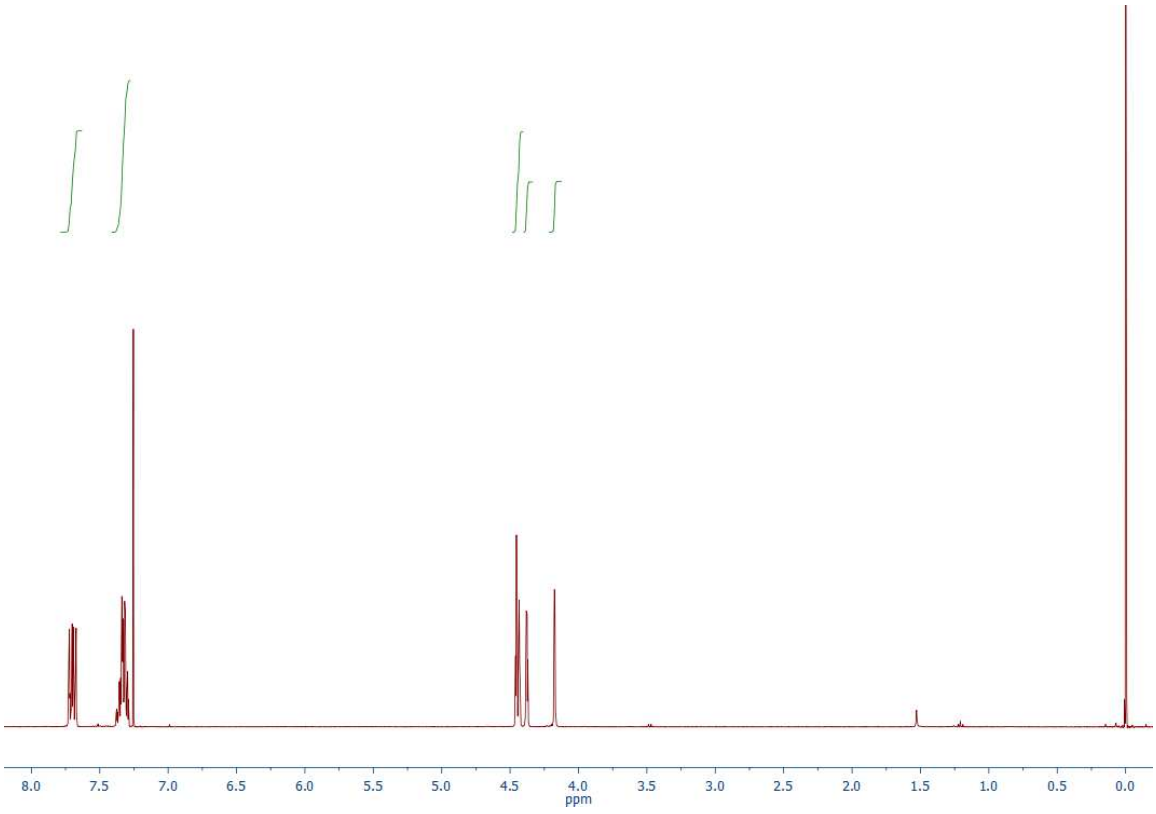

Figure S12. ^{1}H NMR spectrum (399.95 MHz, $CDCl_3$) of **1**.

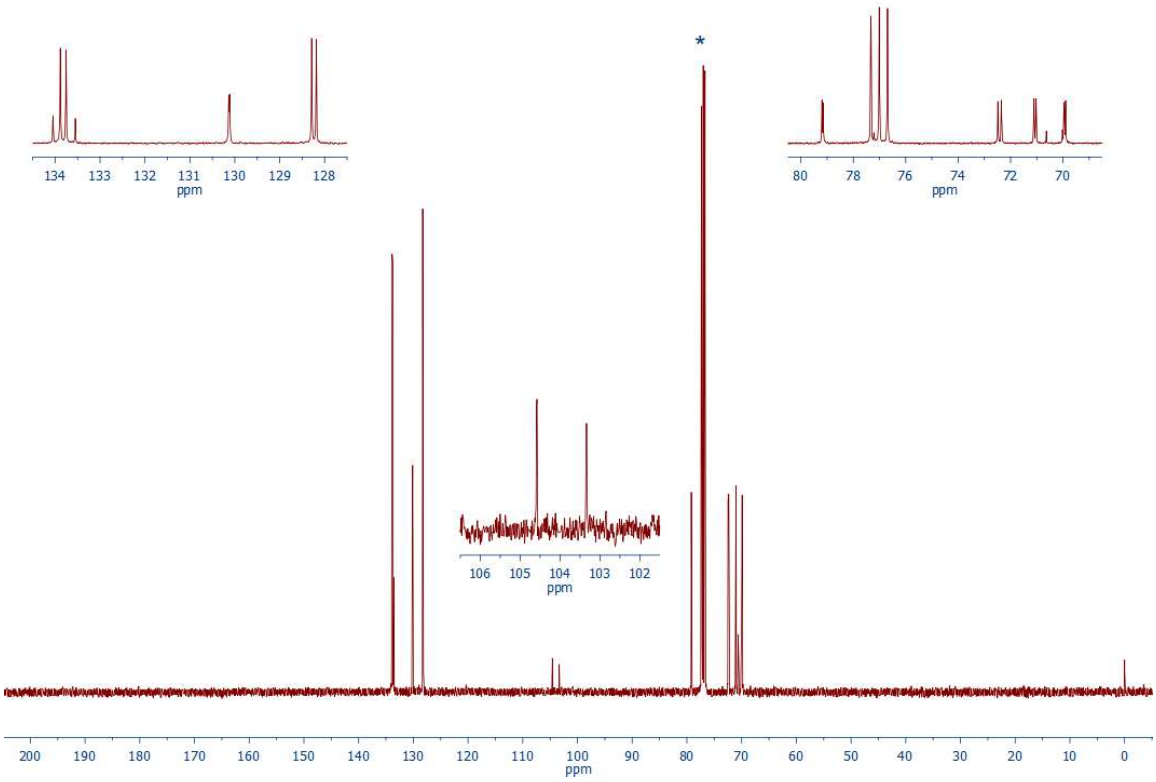

Figure S13. $^{13}C\{^{1}H\}$ NMR spectrum (100.58 MHz, $CDCl_3$) of **1**.

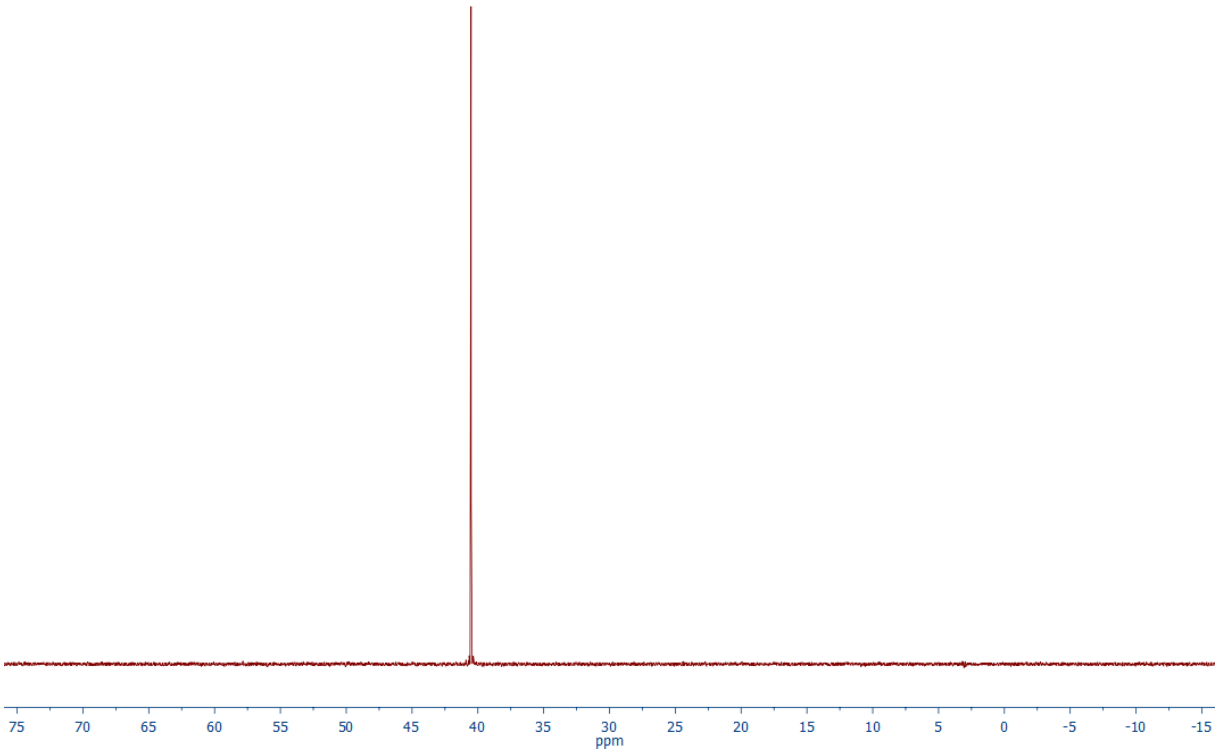

Figure S14. $^{31}P\{^{1}H\}$ NMR spectrum (161.90 MHz, $CDCl_3$) of **1**.

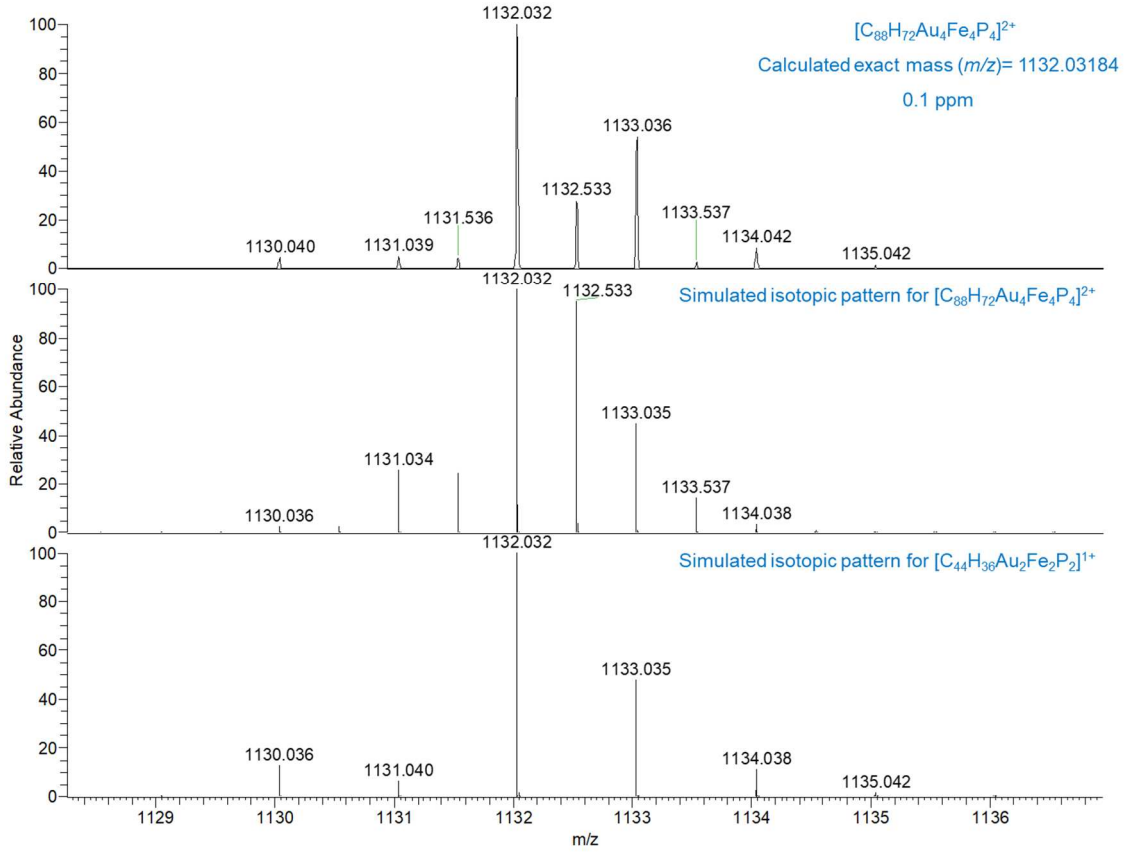

Figure S15. ESI+ HRMS spectrum of **1**.

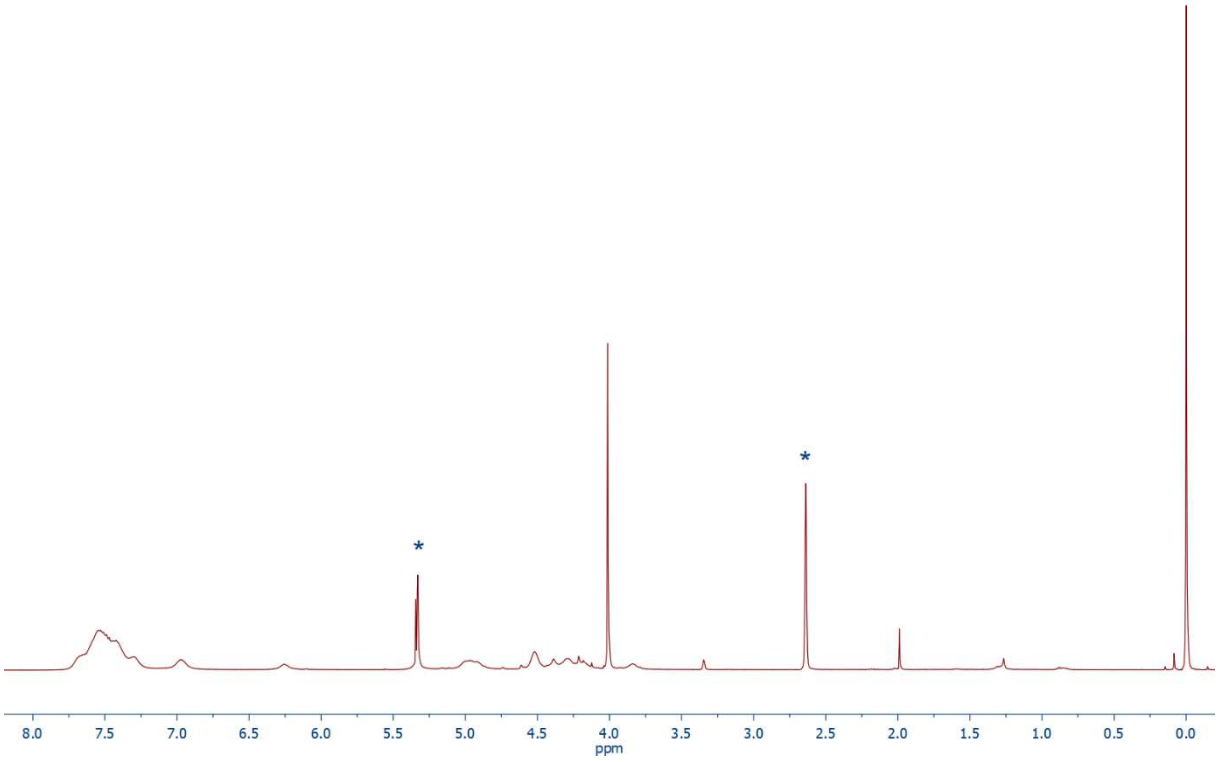

Figure S16. ^{1}H NMR spectrum (399.95 MHz, CD_2Cl_2) of **2**.

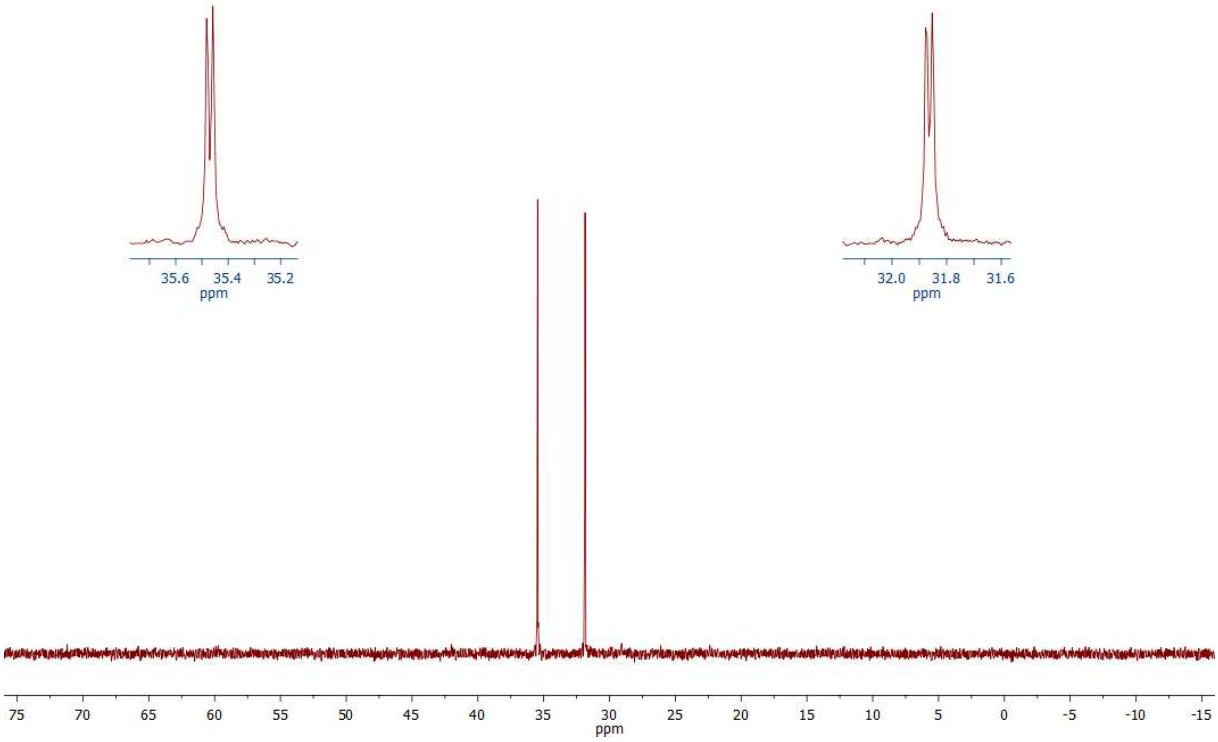

Figure S17. $^{31}P\{^{1}H\}$ NMR spectrum (161.97 MHz, CD_2Cl_2) of **2**.

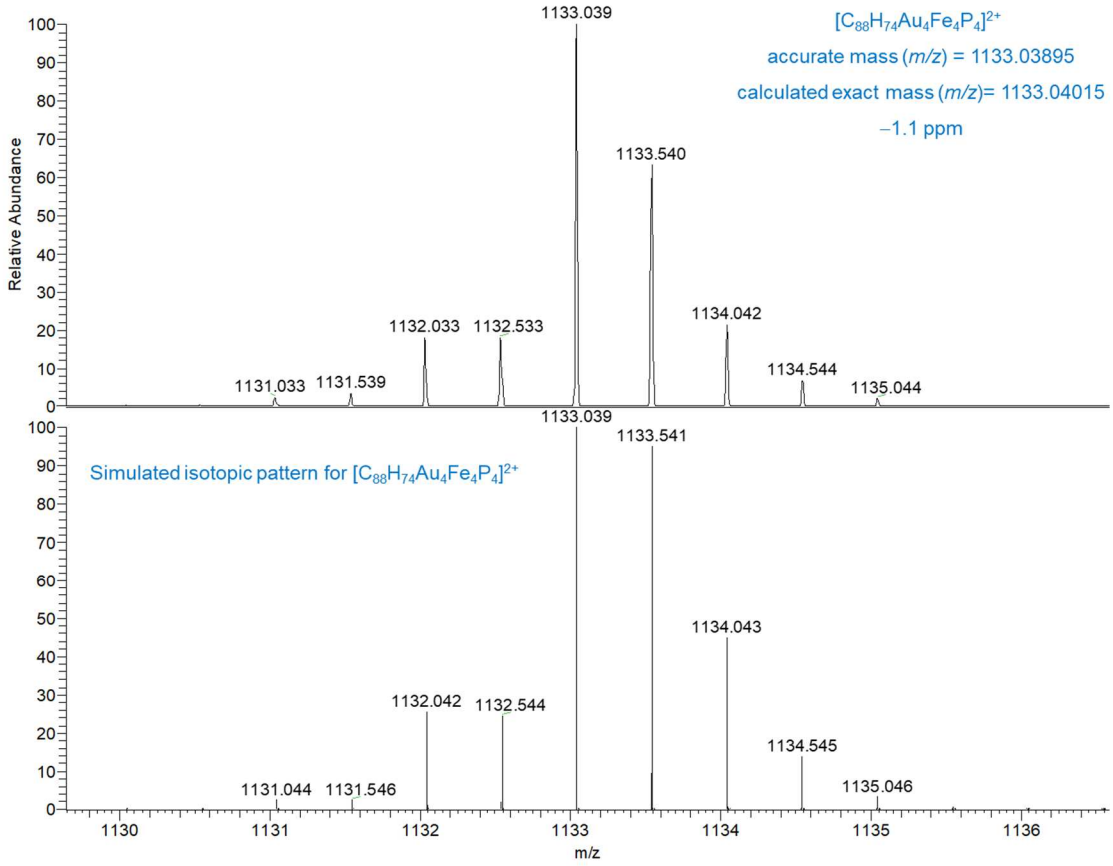

Figure S18. ESI+ HRMS spectrum of **2**.

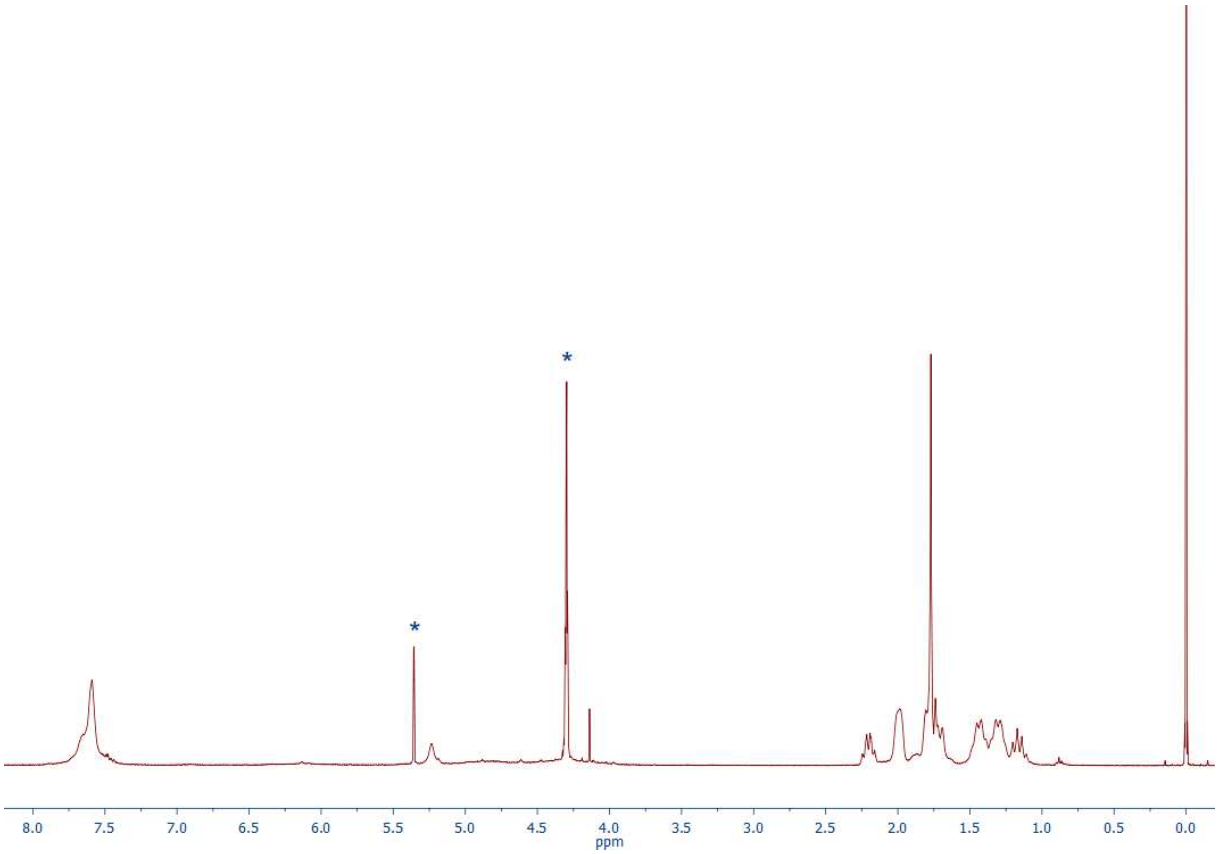

Figure S19. ^{1}H NMR spectrum (399.95 MHz, CD_2Cl_2+CD_3NO_2) of **3**.

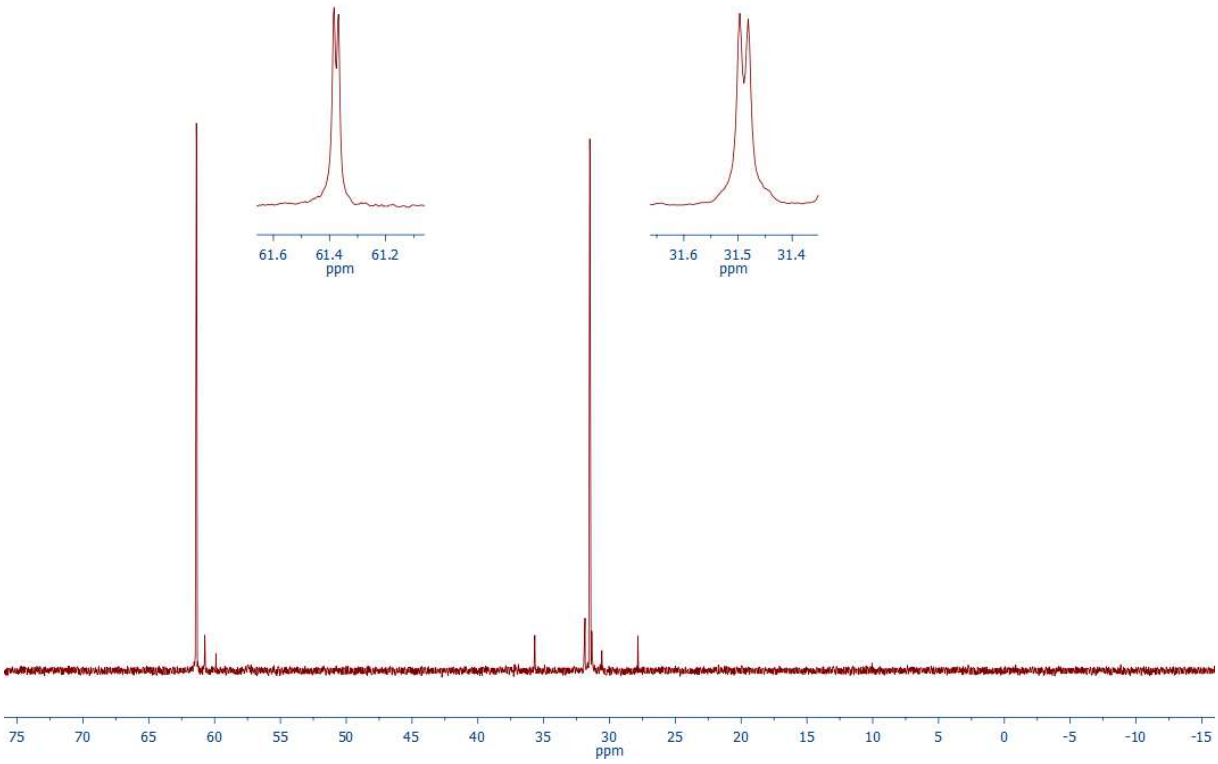

Figure S20. ^{31}P NMR spectrum (161.90 MHz, CD_2Cl_2+CD_3NO_2) of **3**.

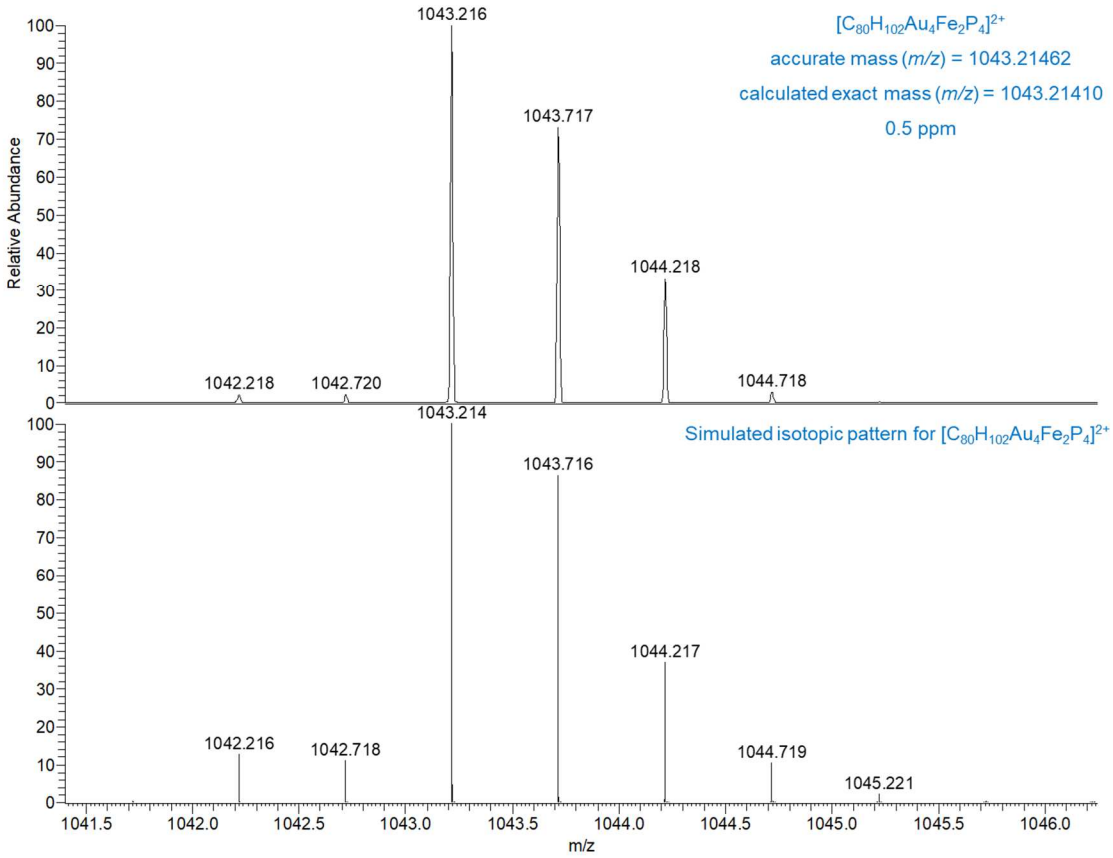

Figure S21. ESI+ HRMS spectrum of **3**.

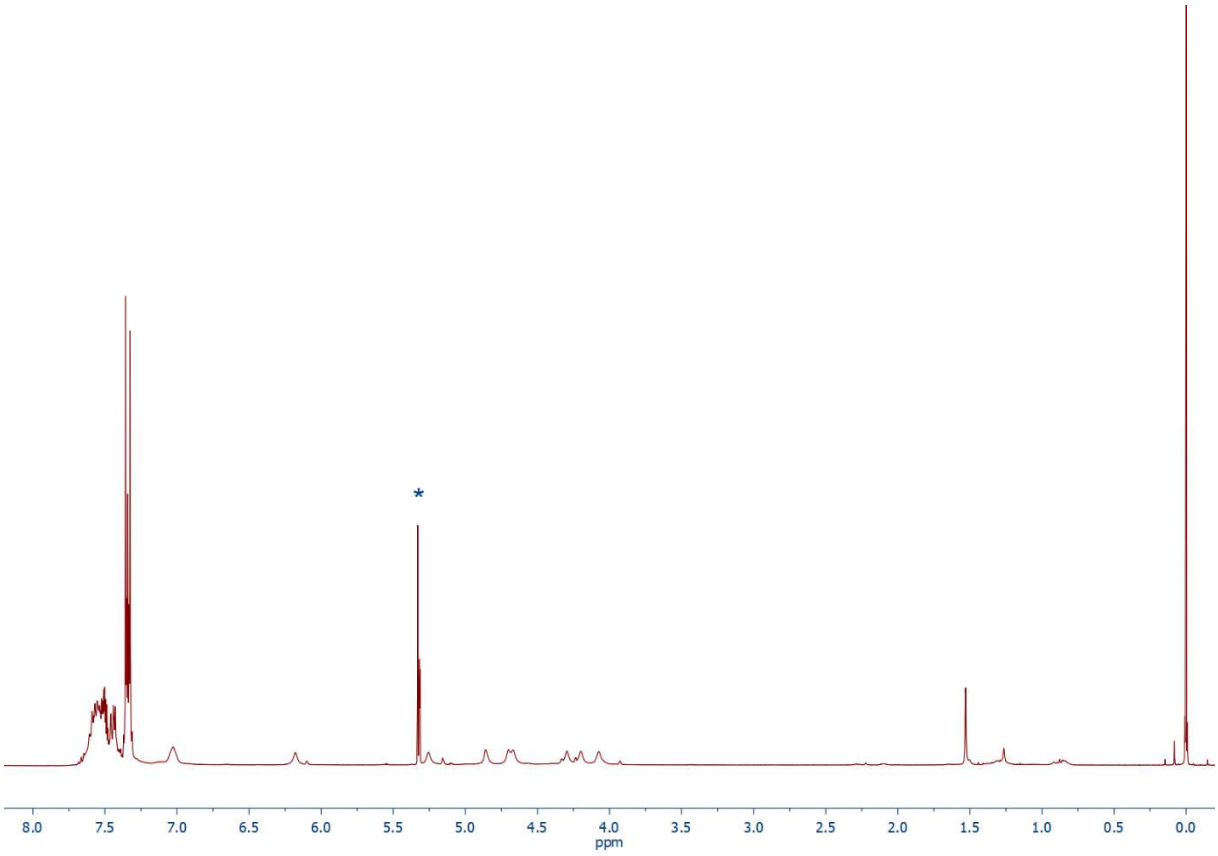

Figure S22. ^{1}H NMR spectrum (399.95 MHz, CD_2Cl_2) of **4**.

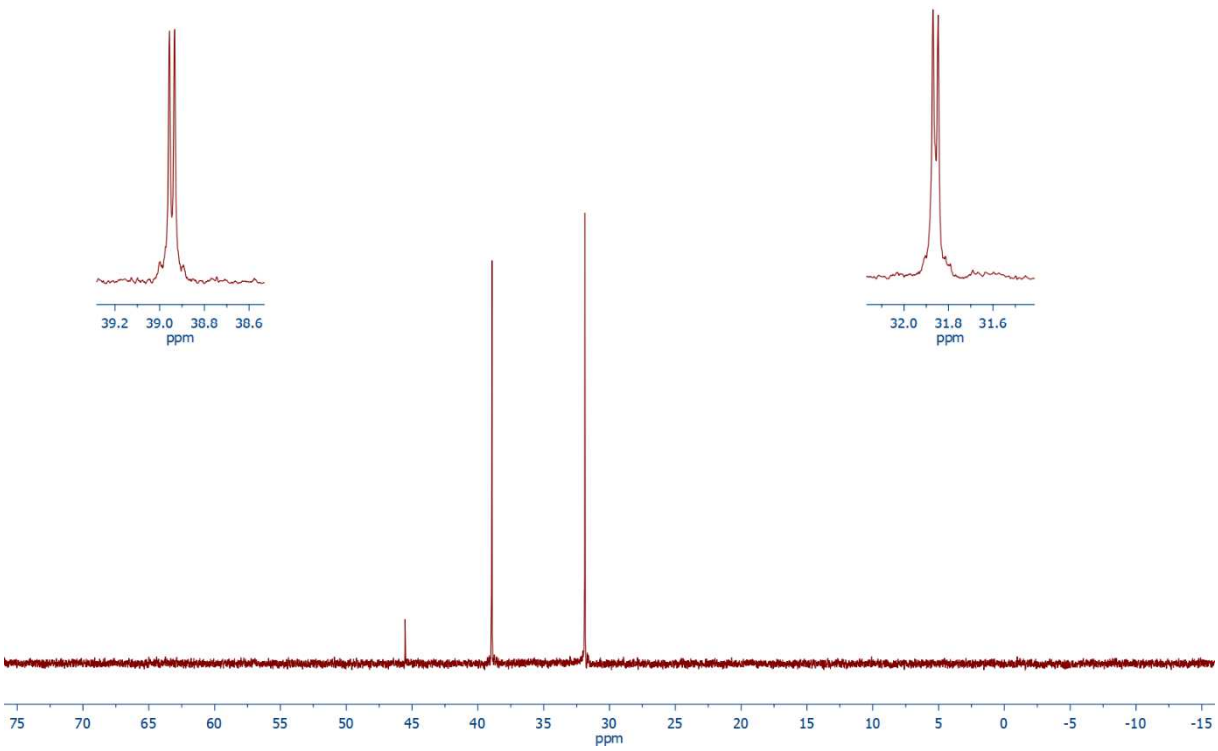

Figure S23 $^{31}P\{^{1}H\}$ NMR spectrum (161.90 MHz, CD_2Cl_2) of **4** (Note: the minor peak at $\delta_P \approx 45$ is due to the inherently present cation $[Au(PPh_3)_2]^+$).

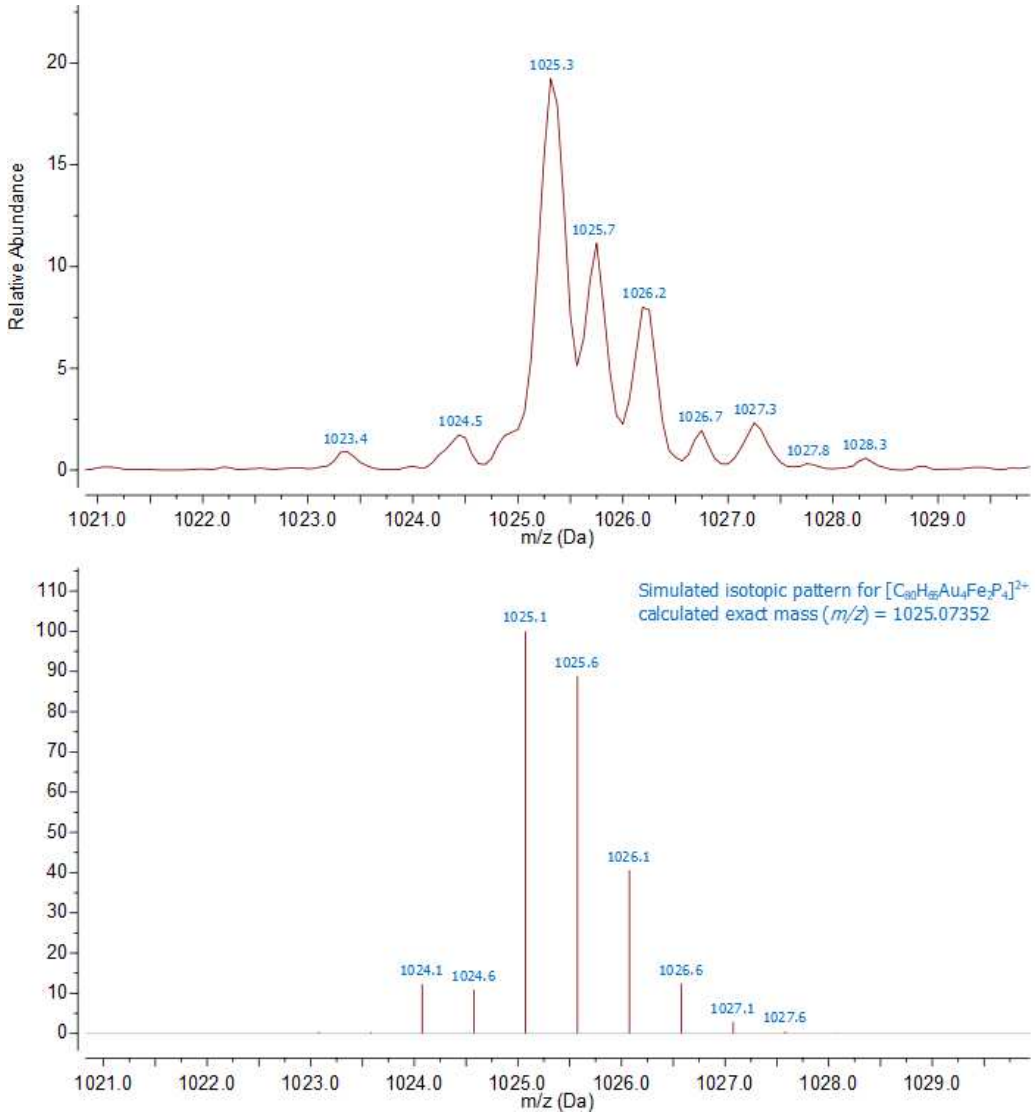

Figure S24. ESI+ MS spectrum of **4**.

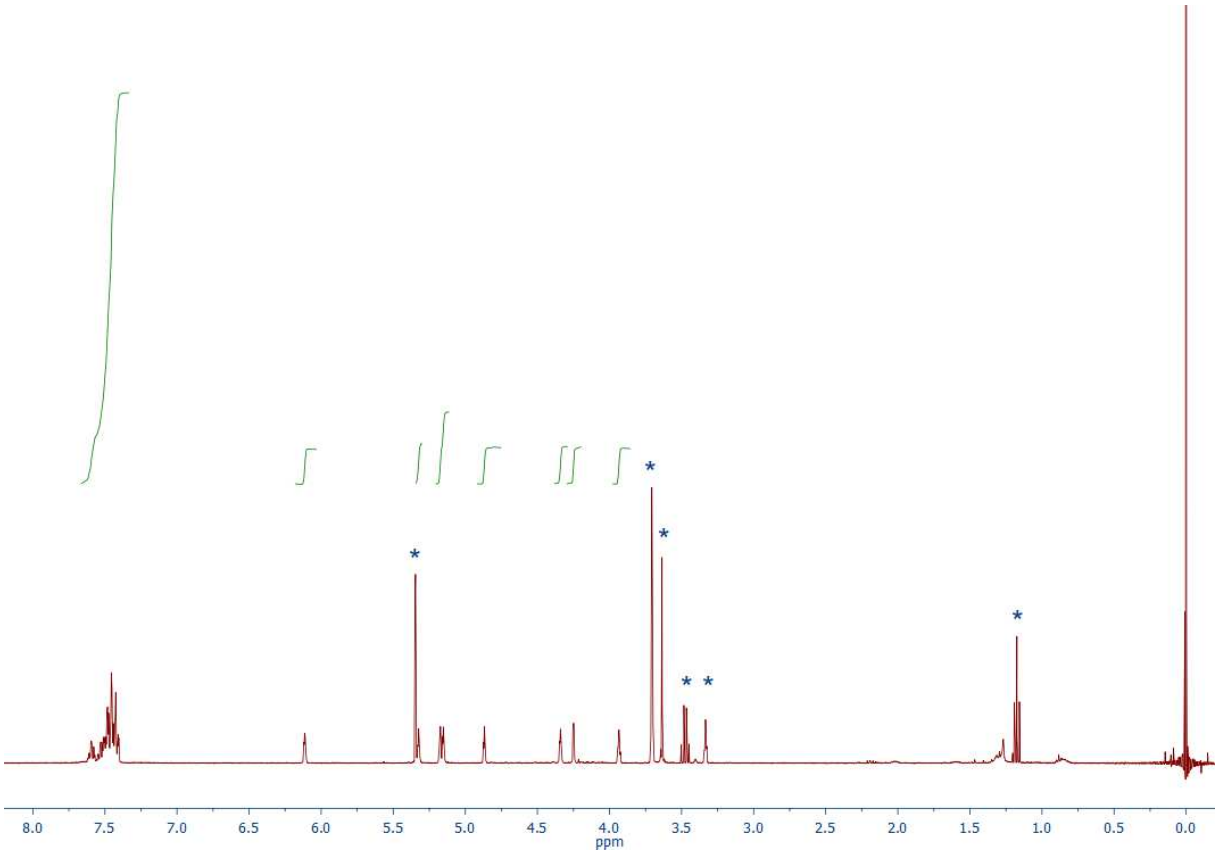

Figure S25. ^{1}H NMR spectrum (399.95 MHz, CD_2Cl_2+CD_3OD) of **5**.

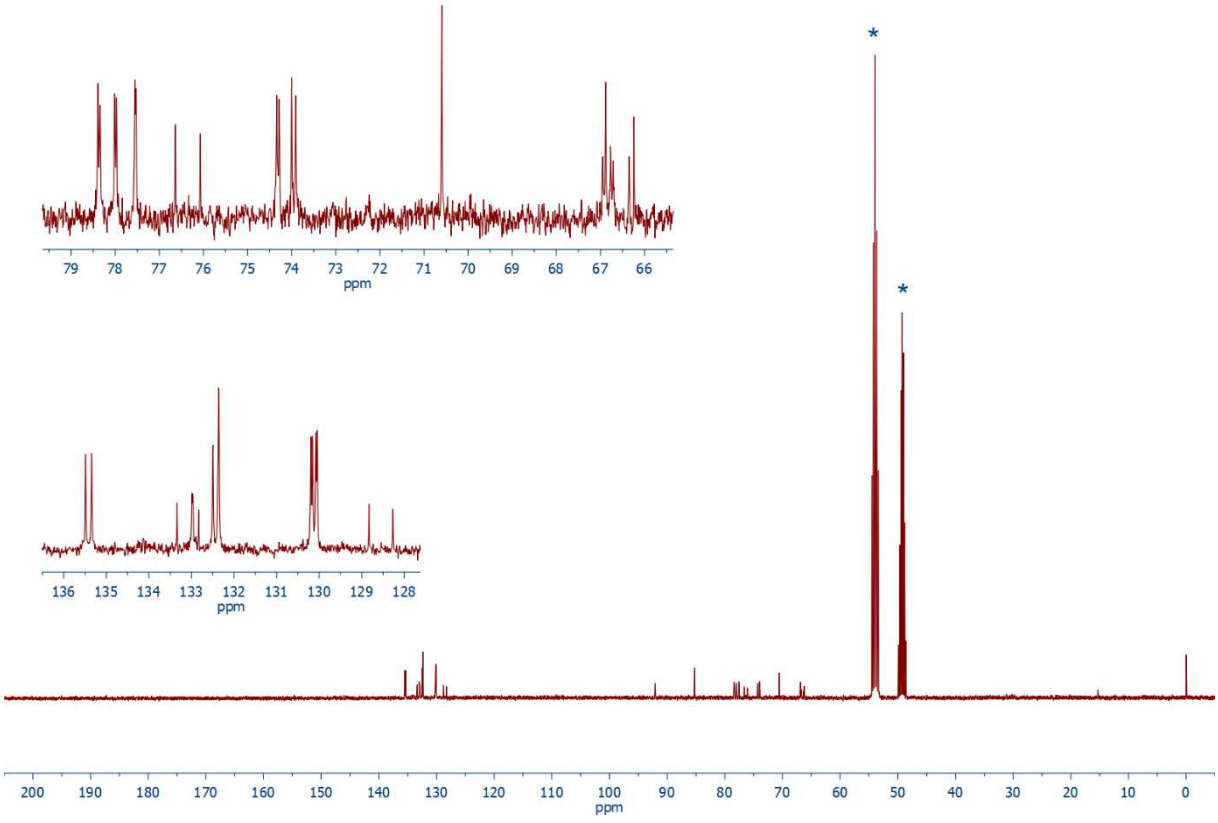

Figure S26. $^{13}C\{^{1}H\}$ NMR spectrum (100.58 MHz, CD_2Cl_2+CD_3OD) of **5**.

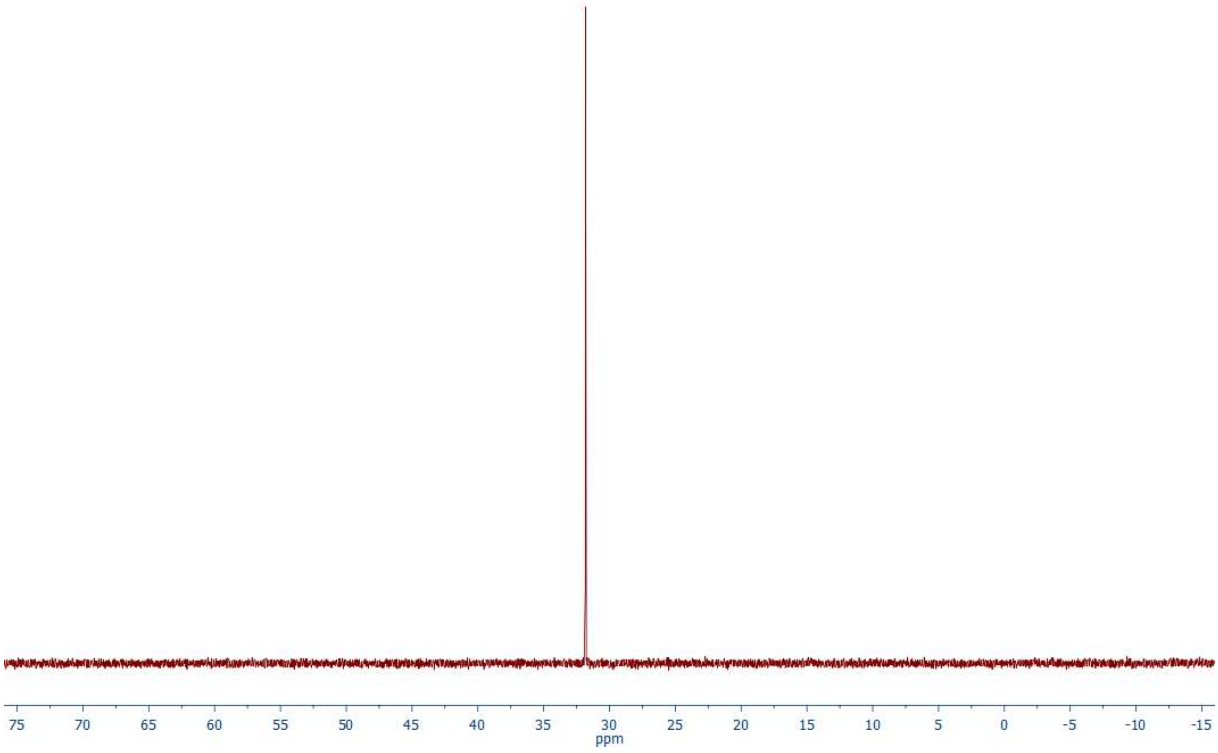

Figure S27. $^{31}P\{^{1}H\}$ NMR spectrum (161.90 MHz, CD_2Cl_2+CD_3OD) of **5**.

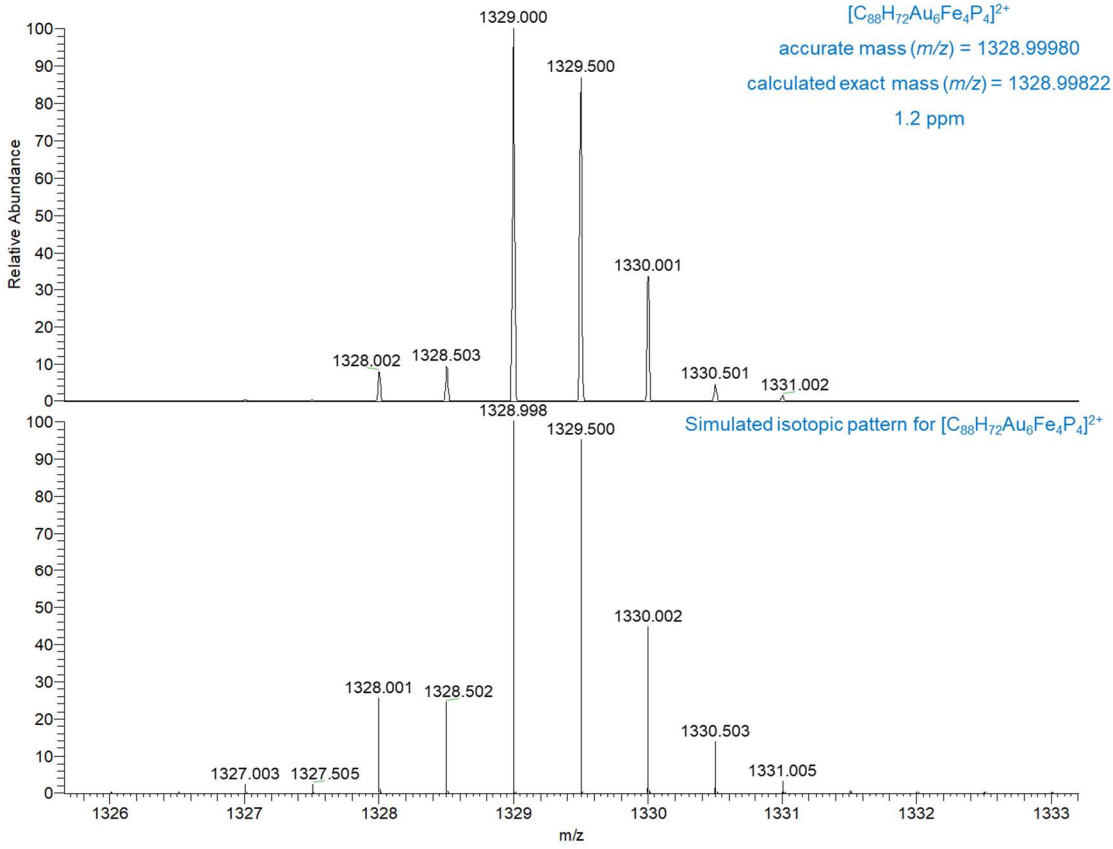

Figure S28. ESI+ HRMS spectrum of **5**.

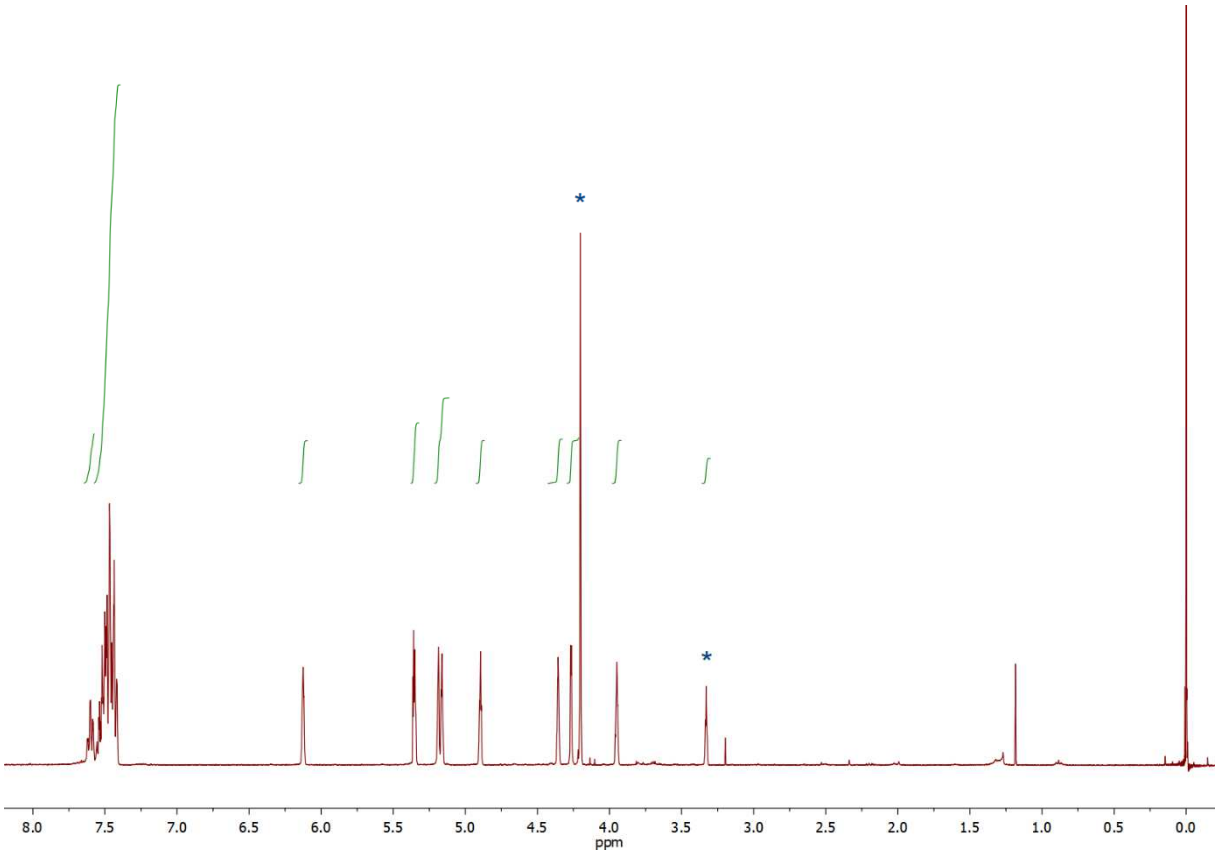

Figure S29. ^{1}H NMR spectrum (399.95 MHz, CD_2Cl_2+CD_3OD) of **5a**.

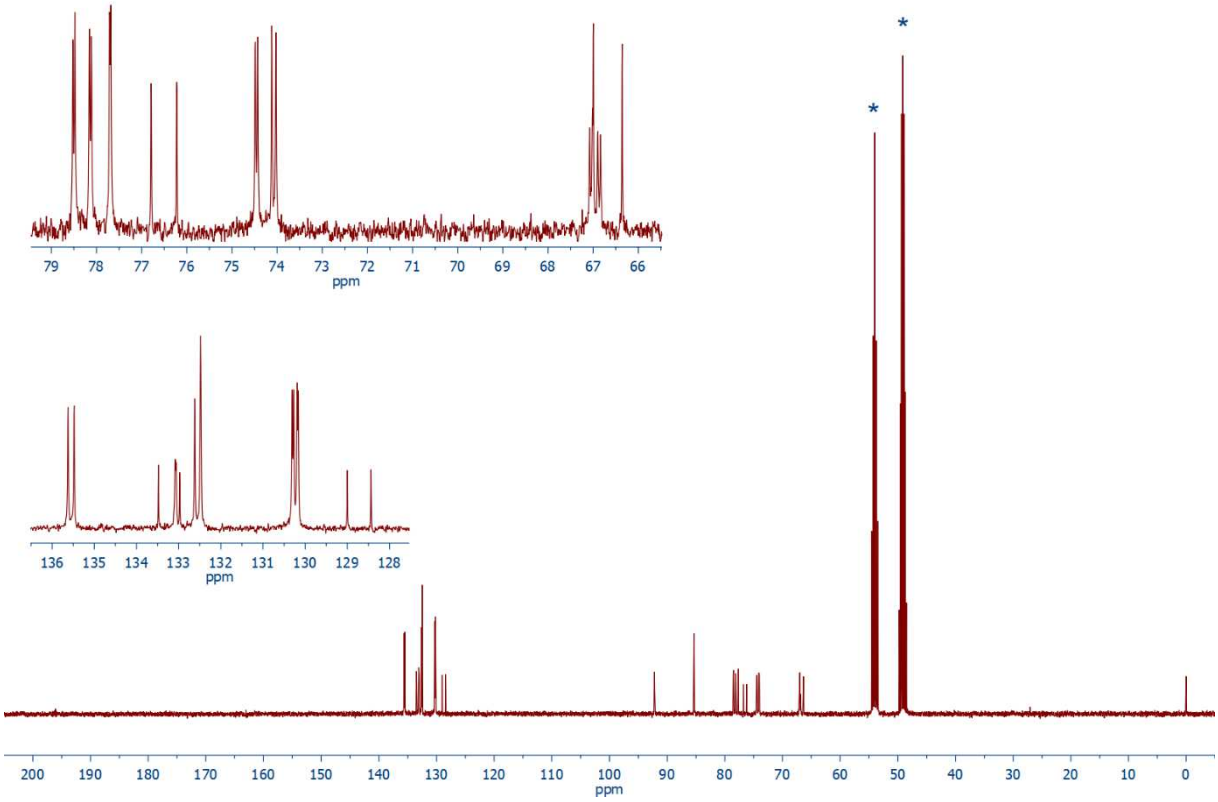

Figure S30. $^{13}C\{^{1}H\}$ NMR spectrum (100.58 MHz, CD_2Cl_2+CD_3OD) of **5a**.

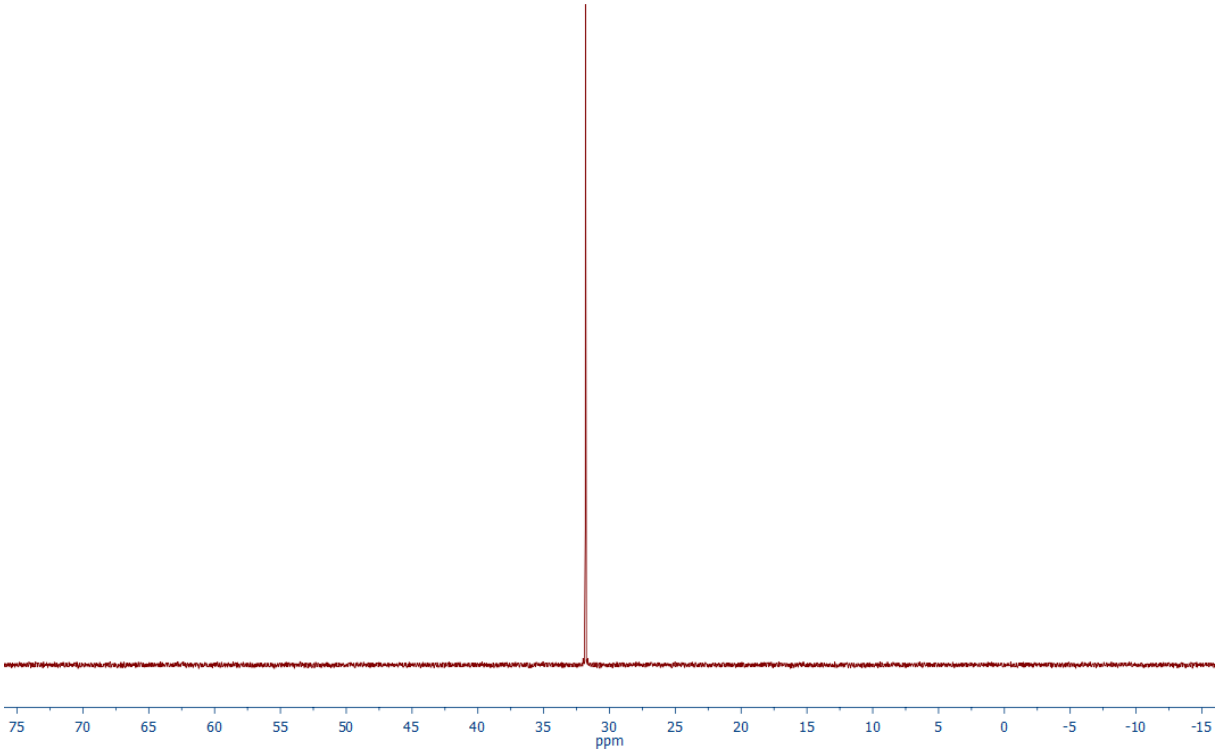

Figure S31. $^{31}P\{^{1}H\}$ NMR spectrum (161.90 MHz, CD_2Cl_2+CD_3OD) of **5a**.

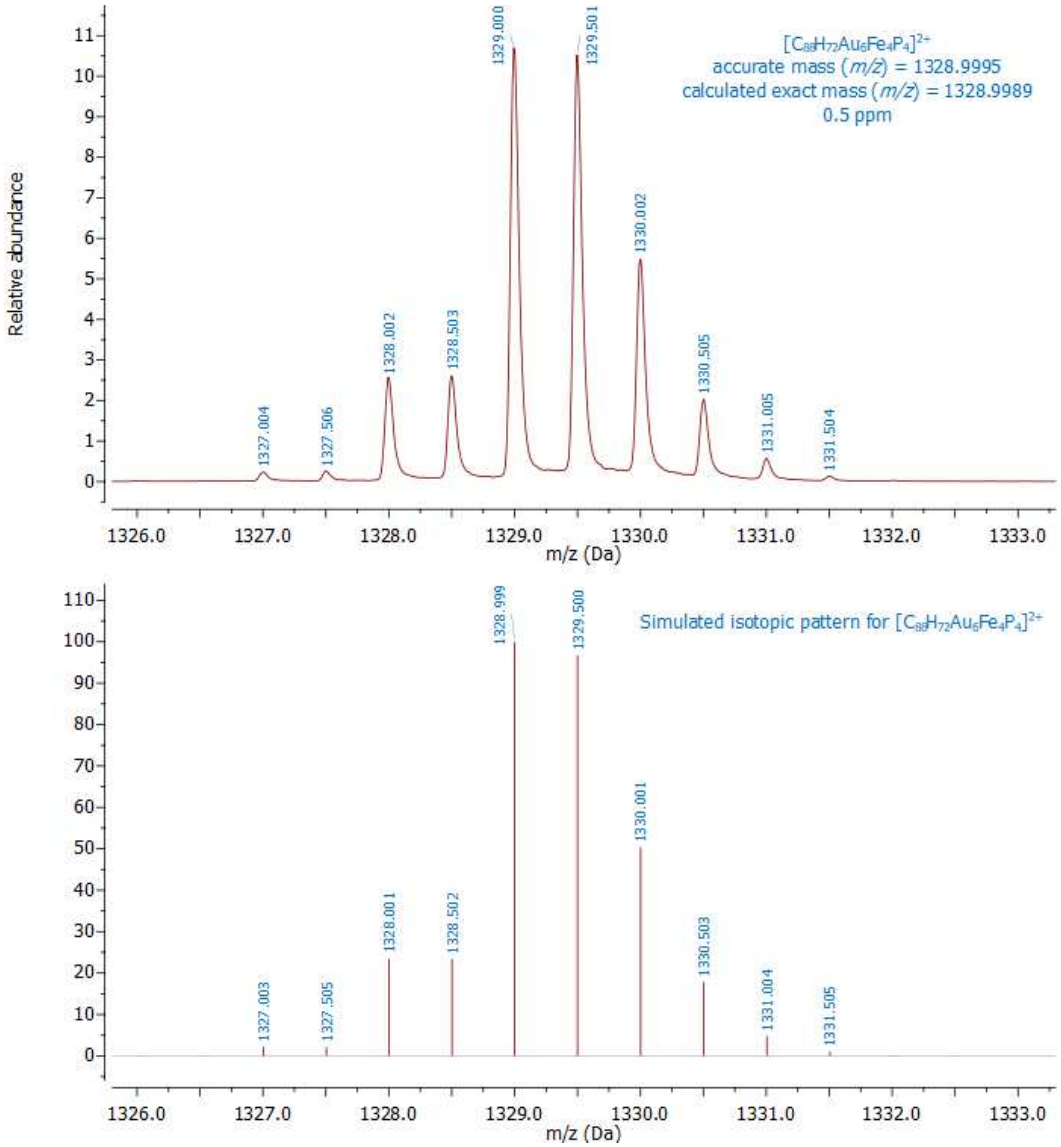

Figure S32. HR ESI+ MS spectrum of **5a**.

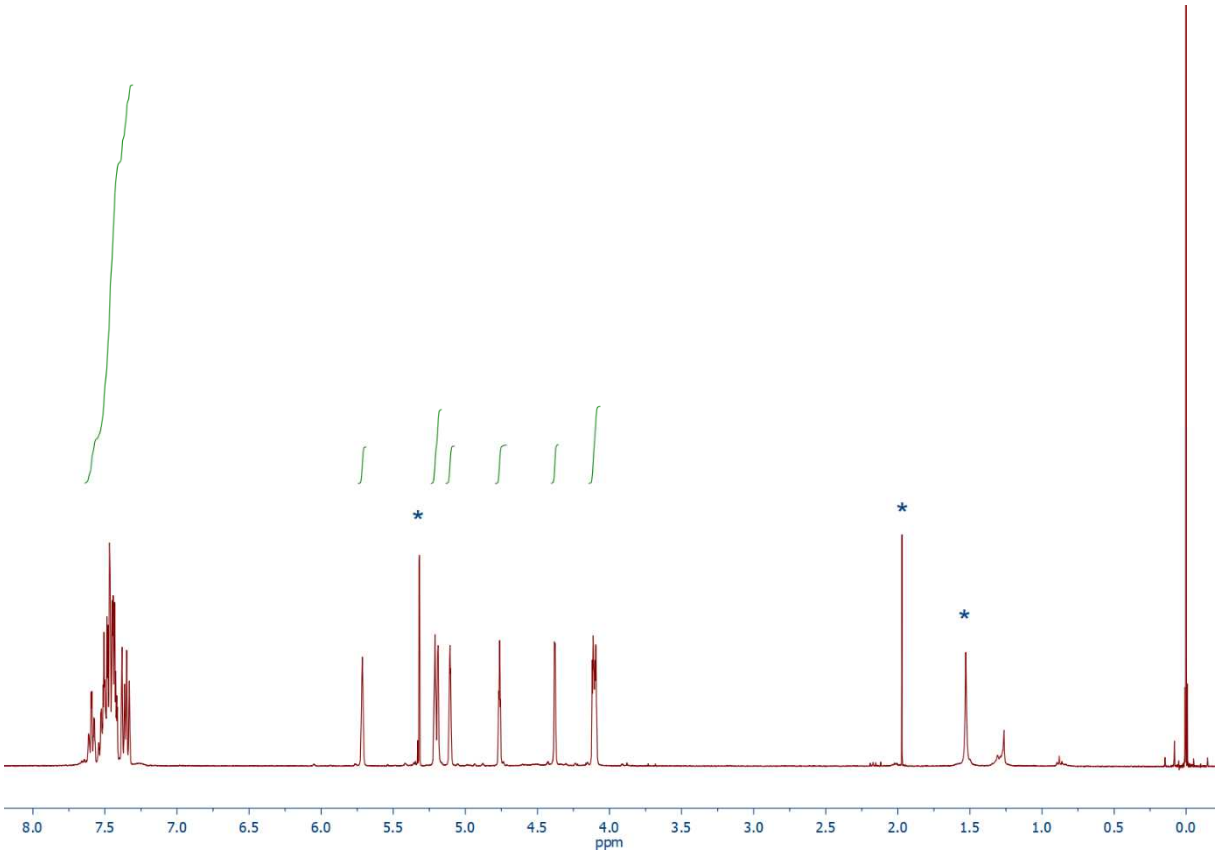

Figure S33. ^{1}H NMR spectrum (399.95 MHz, CD_2Cl_2+CD_3OD) of **6**.

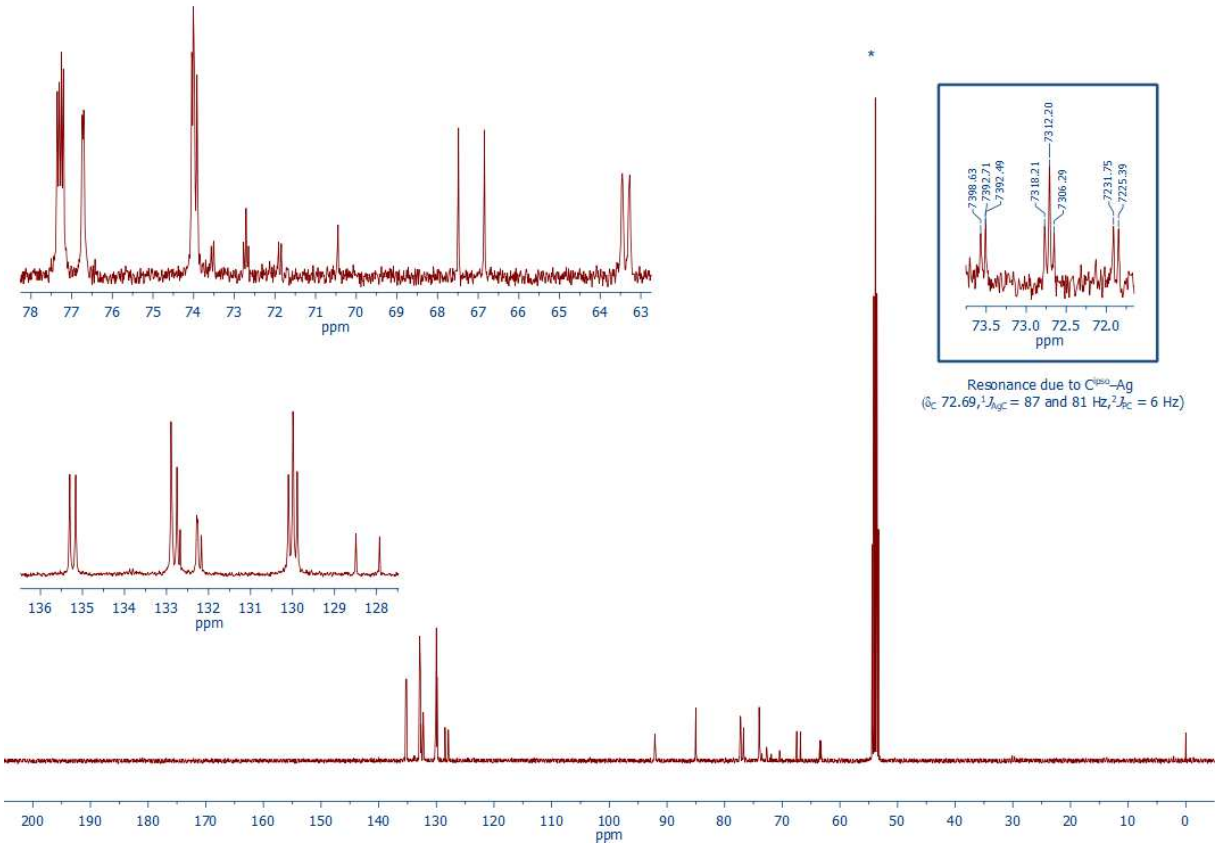

Figure S34. $^{13}C\{^{1}H\}$ NMR spectrum (100.58 MHz, CD_2Cl_2+CD_3OD) of **6**.

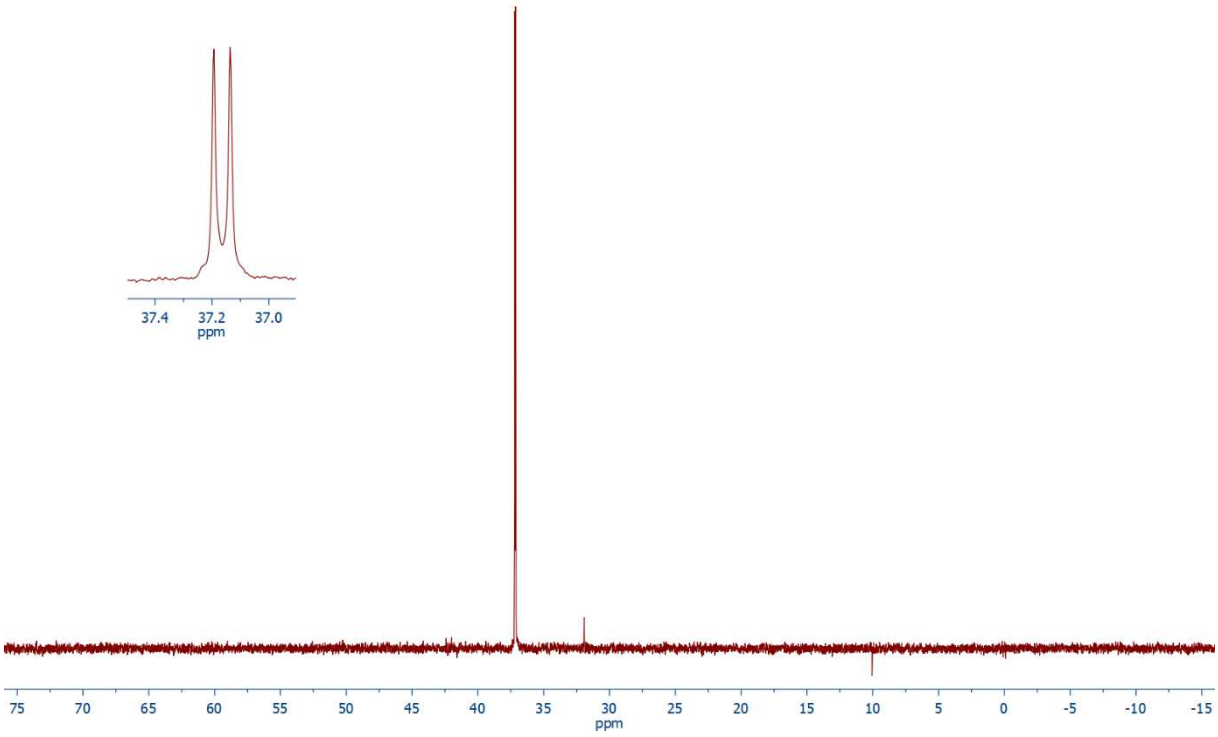

Figure S35. $^{31}P\{^{1}H\}$ NMR spectrum (161.90 MHz, CD_2Cl_2+CD_3OD) of **6**.

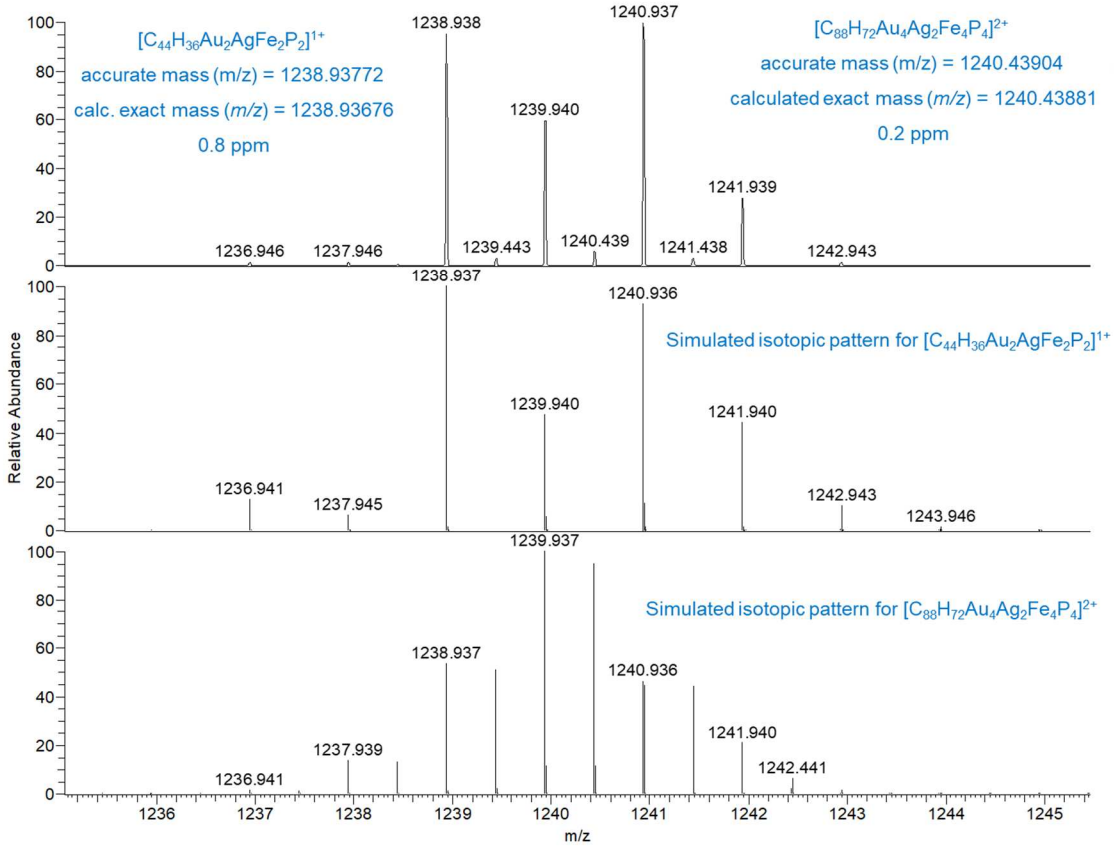

Figure S36. HR ESI+ MS spectrum of **6**.

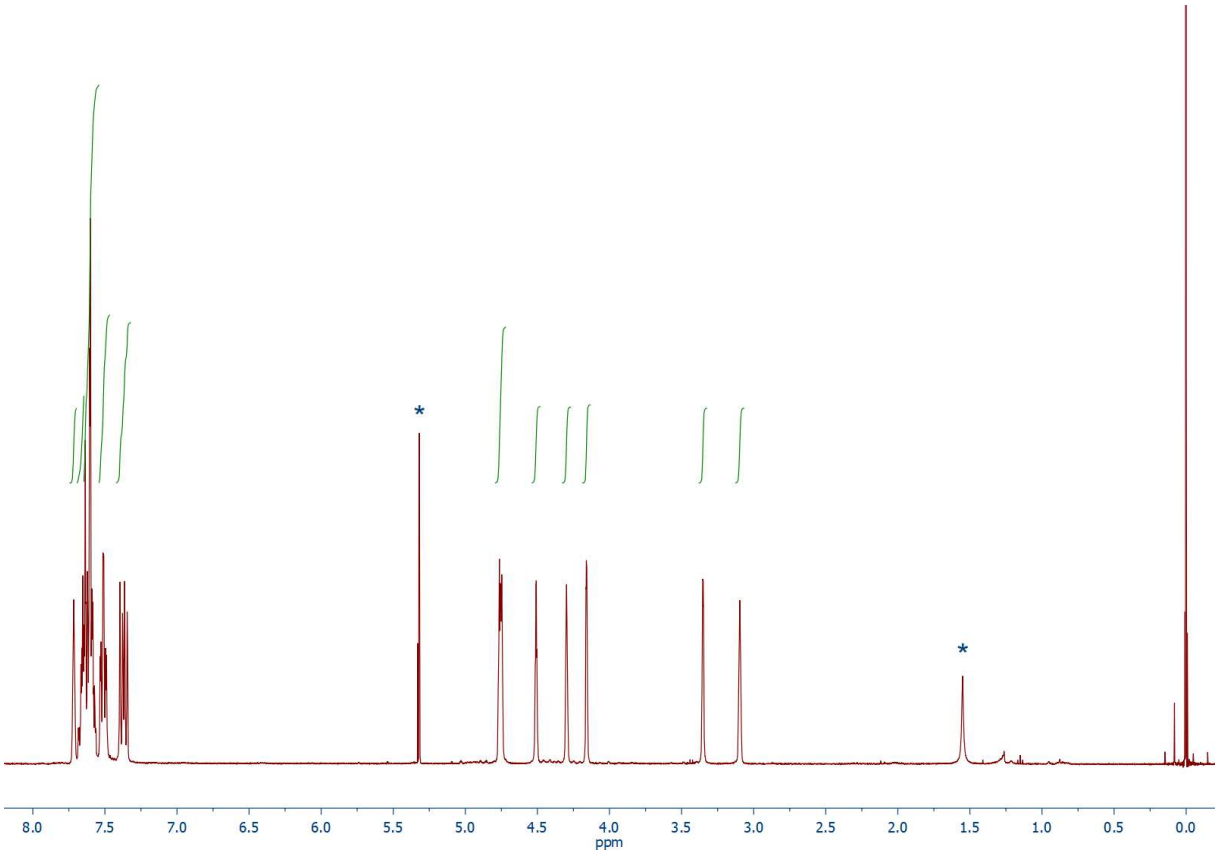

Figure S37. ^{1}H NMR spectrum (399.95 MHz, CD_2Cl_2) of **8**.

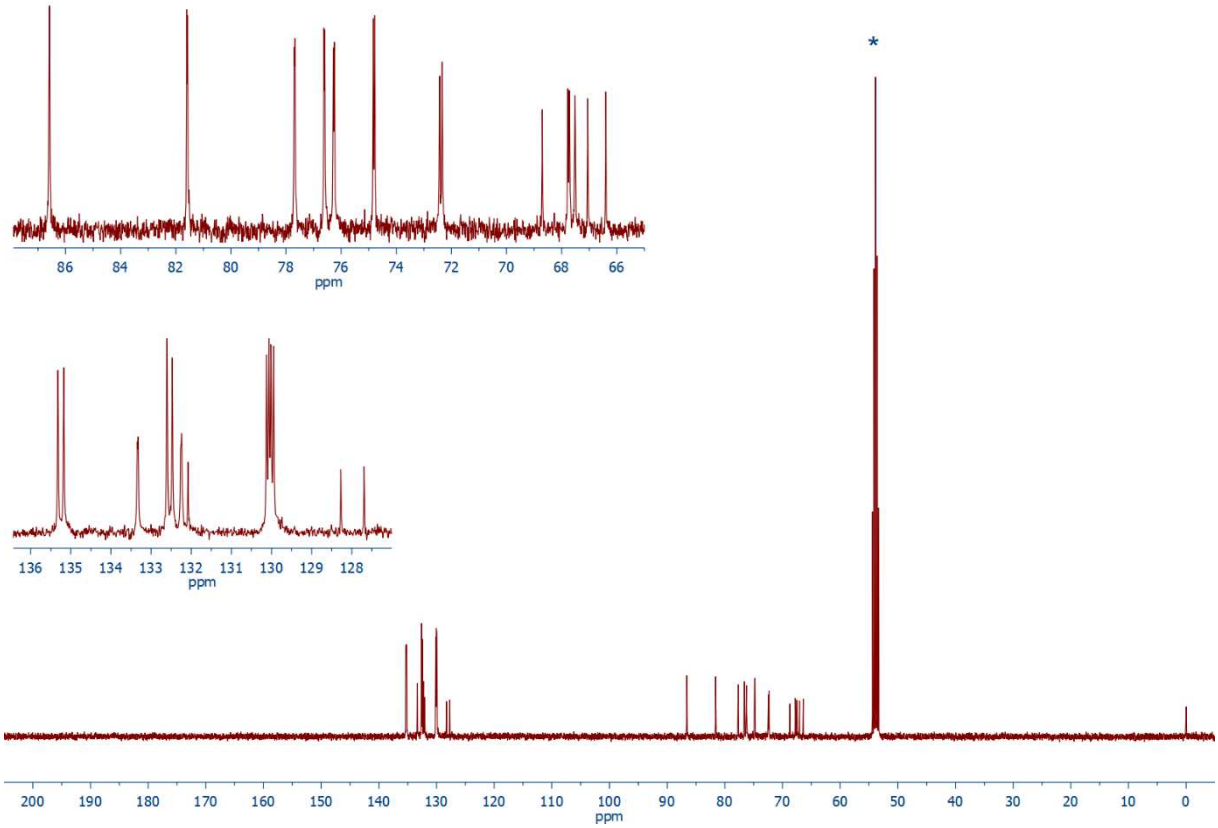

Figure S38. $^{13}C\{^{1}H\}$ NMR spectrum (100.58 MHz, CD_2Cl_2) of **8**.

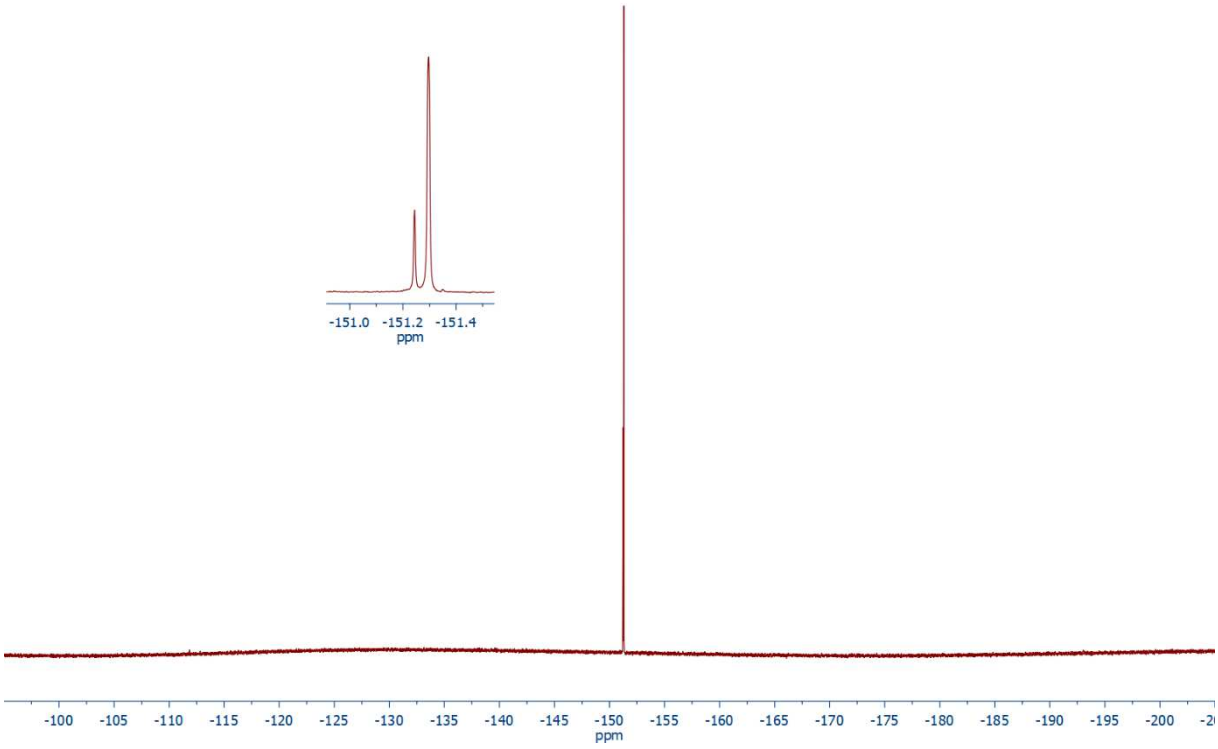

Figure S39. ^{19}F NMR spectrum (376.29 MHz, CD_2Cl_2) of **8**.

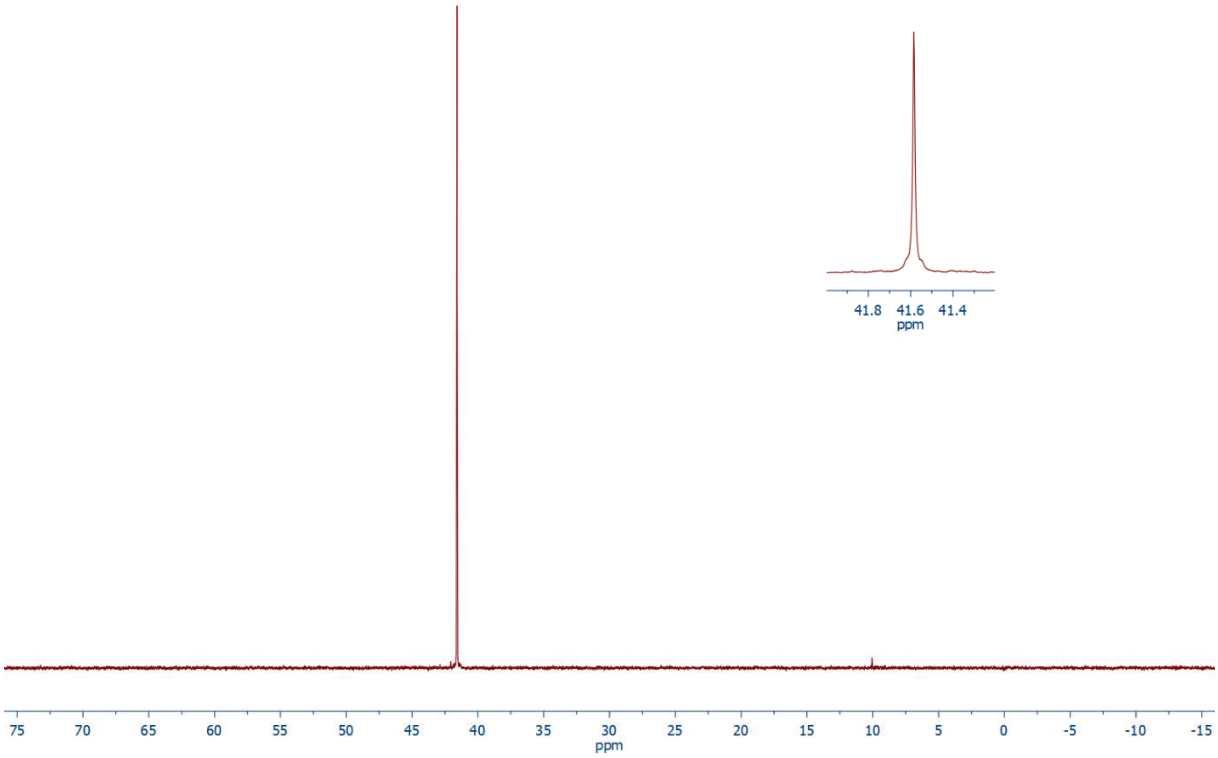

Figure S40. $^{31}P\{^1H\}$ NMR spectrum (161.90 MHz, CD_2Cl_2) of **8**.

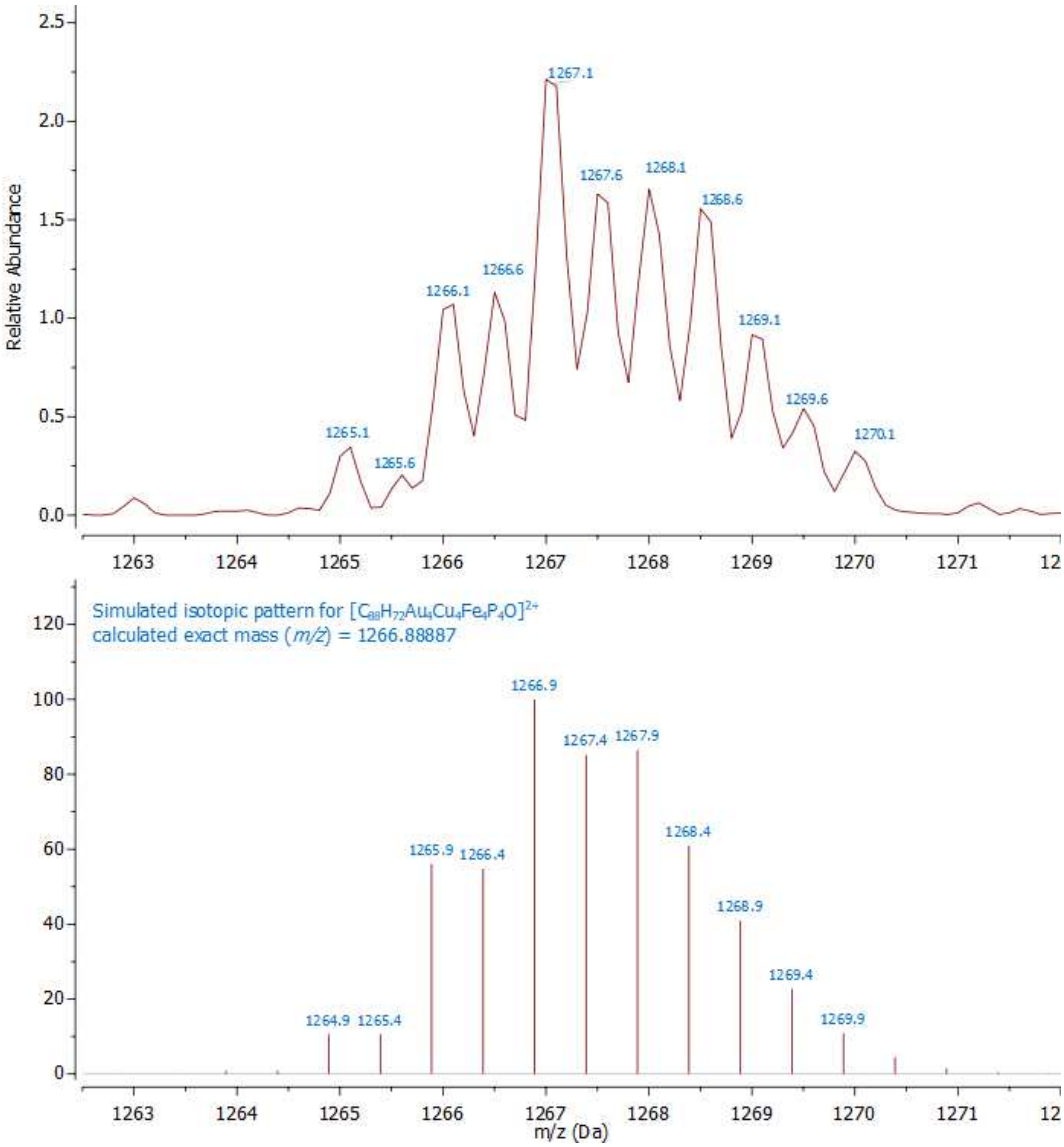

Figure S41. ESI+ HRMS spectrum of **8**.

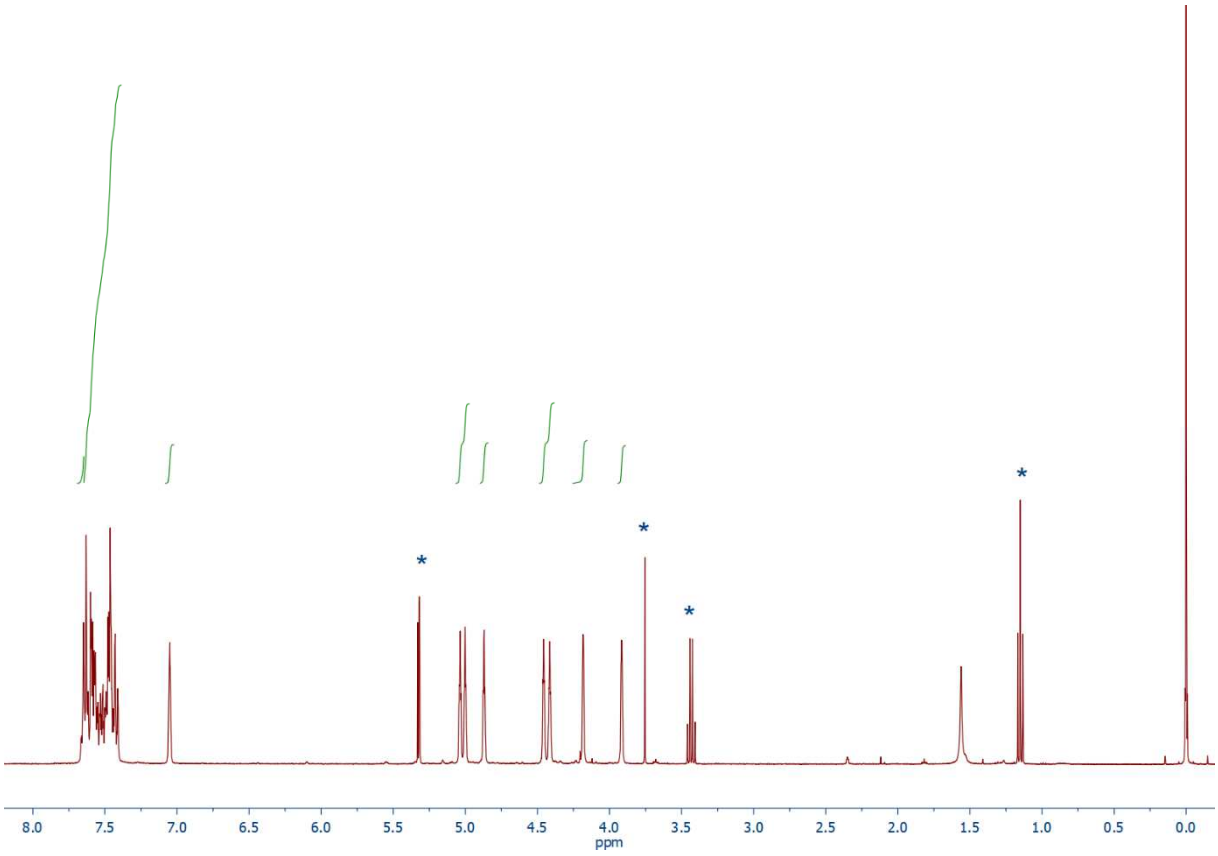

Figure S42. ^{1}H NMR spectrum (399.95 MHz, CD_2Cl_2) of **9**.

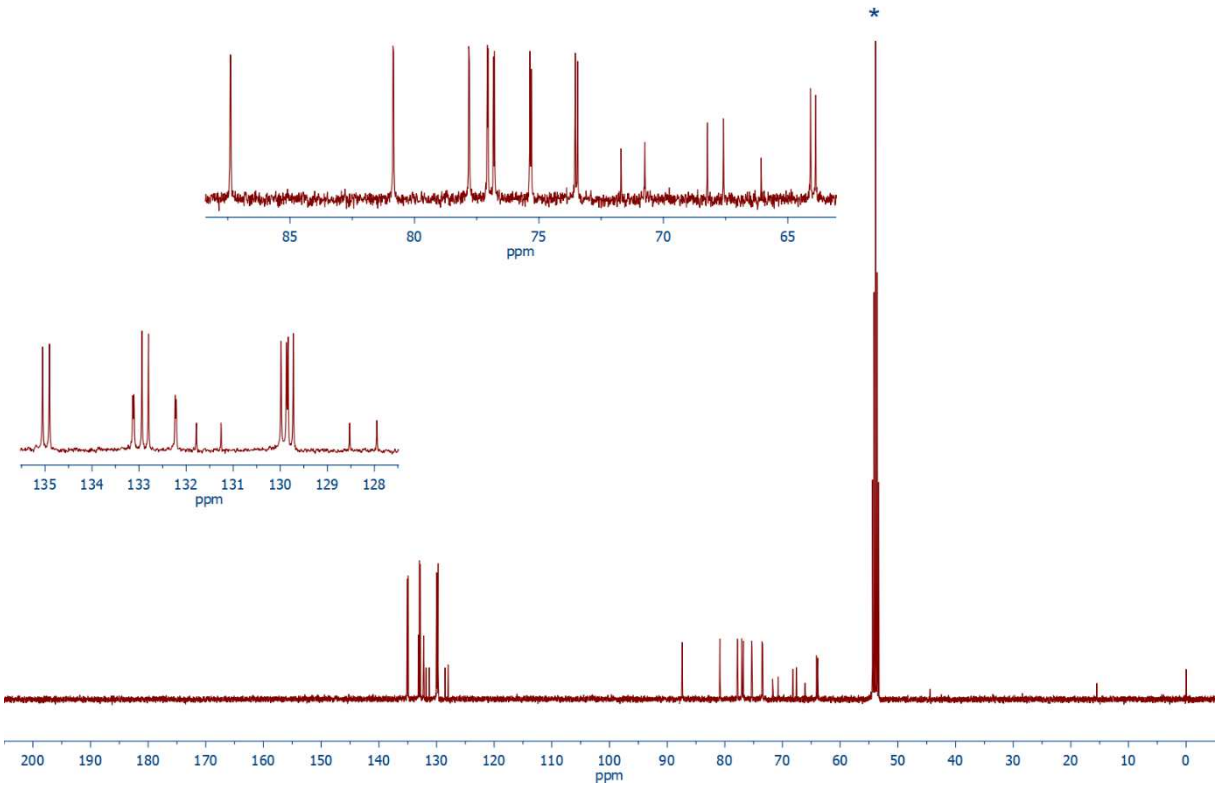

Figure S43. $^{13}C\{^{1}H\}$ NMR spectrum (100.58 MHz, CD_2Cl_2) of **9**.

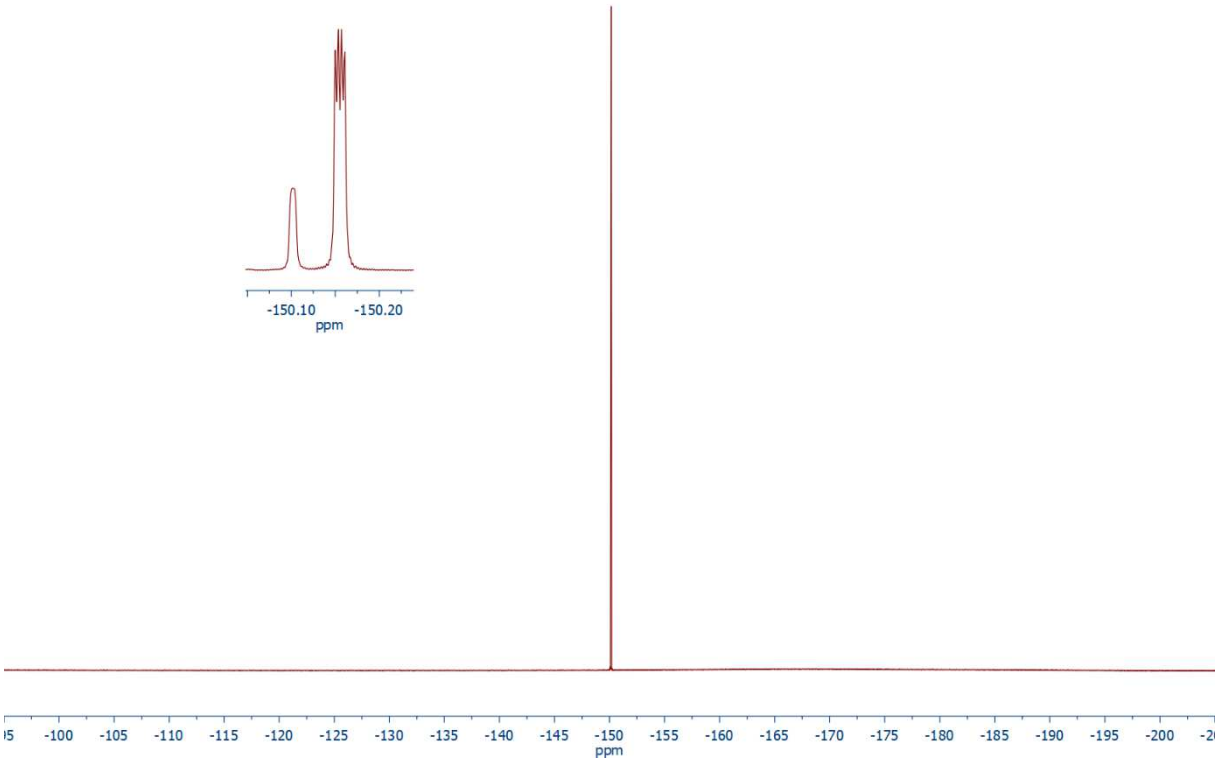

Figure S44. $^{19}F\{^{1}H\}$ NMR spectrum (376.46 MHz, CD_2Cl_2) of **9**.

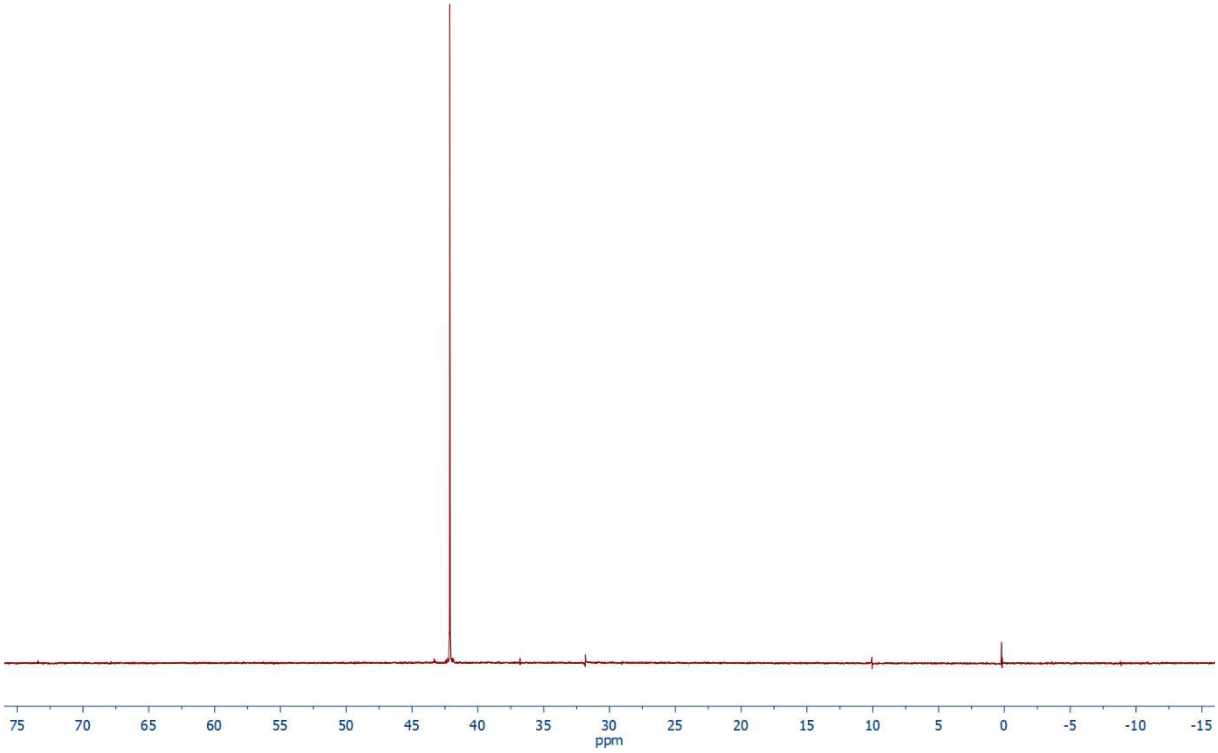

Figure S45. $^{31}P\{^{1}H\}$ NMR spectrum (161.90 MHz, CD_2Cl_2) of **9**.

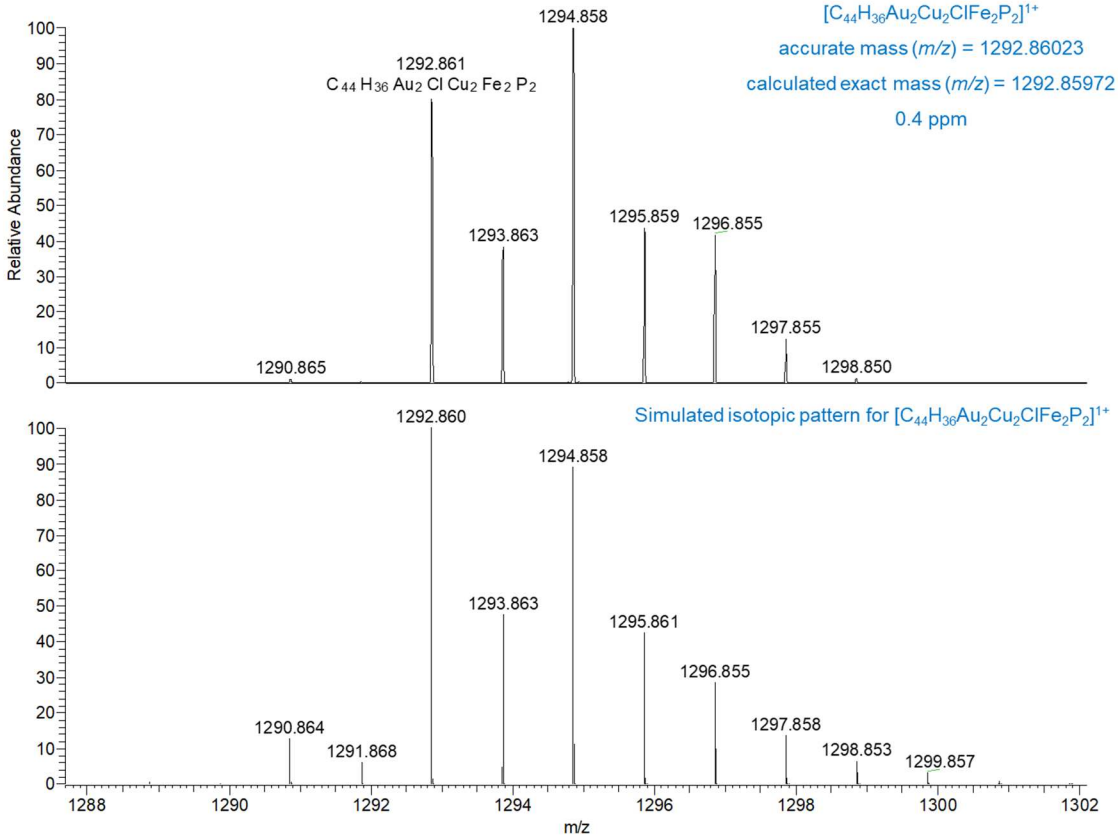

Figure S46. ESI+ HRMS spectrum of **9**.

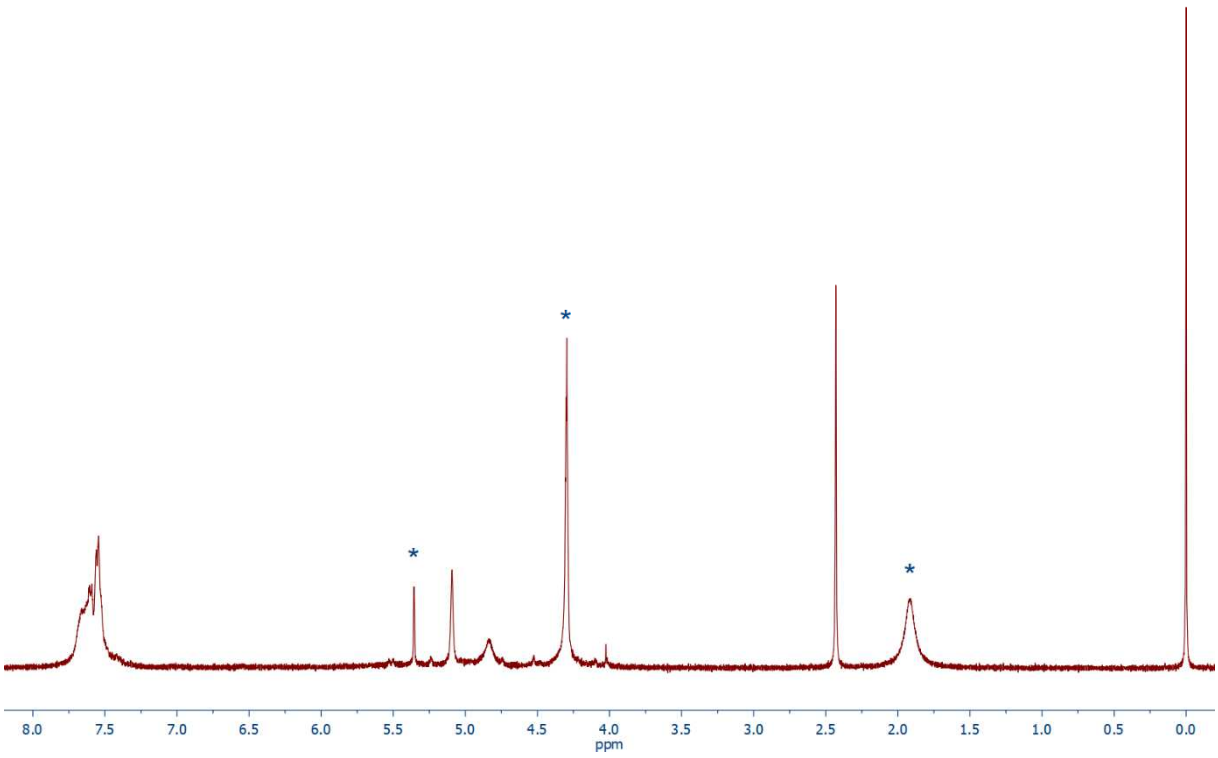

Figure S47. ^{1}H NMR spectrum (399.95 MHz, CD_2Cl_2-CD_3NO_2) of **10**.

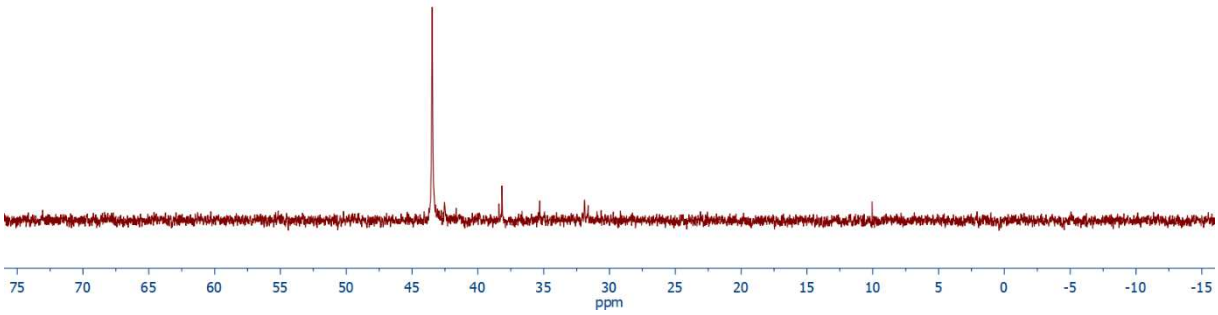

Figure S48. $^{31}P\{^{1}H\}$ NMR spectrum (161.90 MHz, CD_2Cl_2-CD_3NO_2) of **10**.

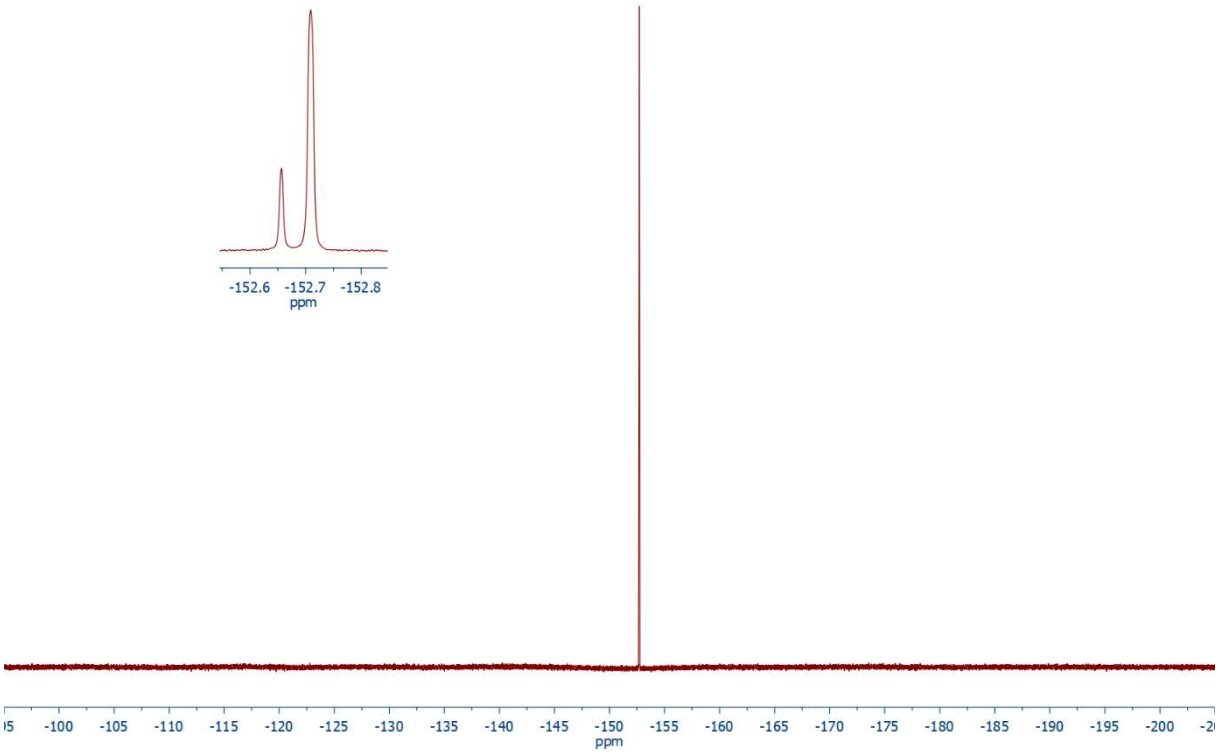

Figure S49. $^{19}F\{^{1}H\}$ NMR spectrum (282.19 MHz, CD_2Cl_2-CD_3NO_2) of **10**.

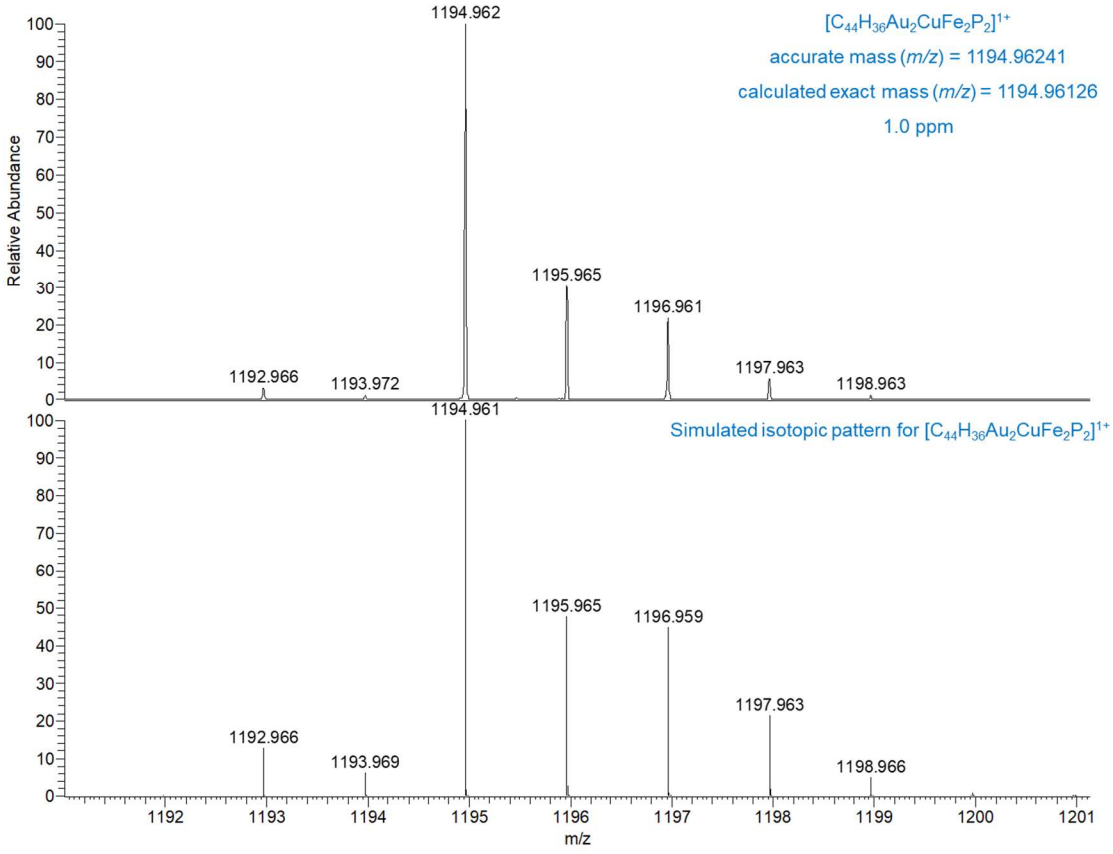

Figure S50. ESI+ HRMS spectrum of **10**.

REFERENCES

[1] K. Škoch, I. Císařová and P. Štěpnička, *Chem. Eur. J.,* 2015, **21**, 15998.

[2] K. Roessler, T. Rüffer, B. Walfort, R. Packheiser, R. Holze, M. Zharnikov and H. Lang, *J. Organomet. Chem.,* 2007, **692**, 1530.

[3] K. Kang, S. Liu, T. Xu, D. Wang, X. Leng, R. Bai, Y. Lan and Q. Shen, *Organometallics,* 2017, **36**, 4727.

[4] I. R. Butler and R. L. Davies, *Synthesis,* 1996, 1350.

[5] R. E. M. Brooner, T. J. Brown and R. A. Widenhoefer, *Chem. Eur. J.,* 2013, **19**, 8276.

[6] M. J. Frisch, G. W. Trucks, H. B. Schlegel, G. E. Scuseria, M. A. Robb, J. R. Cheeseman, G. Scalmani, V. Barone, G. A. Petersson, H. Nakatsuji, X. Li, M. Caricato, A. V. Marenich, J. Bloino, B. G. Janesko, R. Gomperts, B. Mennucci, H. P. Hratchian, J. V. Ort, A. F. Izmaylov, J. L. Sonnenberg, D. Williams-Young, F. Ding, F. Lipparini, F. Egidi, J. Goings, B. Peng, A. Petrone, T. Henderson, D. Ranasinghe, V. G. Zakrzewski, J. Gao, N. Rega, G. Zheng, W. Liang, M. Hada, M. Ehara, K. Toyota, R. Fukuda, J. Hasegawa, M. Ishida, T. Nakajima, Y. Honda, O. Kitao, H. Nakai, T. Vreven, K. Throssell, J. A. Montgomery, Jr., J. E. Peralta, F. Ogliaro, M. J. Bearpark, J. J. Heyd, E. N. Brothers, K. N. Kudin, V. N. Staroverov, T. A. Keith, R. Kobayashi, J. Normand, K. Raghavachari, A. P. Rendell, J. C. Burant, S. S. Iyengar, J. Tomasi, M. Cossi, J. M. Millam, M. Klene, C. Adamo, R. Cammi, J. W. Ochterski, R. L. Martin, K. Morokuma, O. Farkas, J. B. Foresman and D. J. Fox, Gaussian, Inc., Wallingford CT, 2019.

[7] Y. Zhao and D. G. Truhlar, *Theor. Chem. Acc.,* 2008, **120**, 215.

[8] P. Fuentealba, H. Preuss, H. Stoll and L. von Szentpály, *Chem. Phys. Lett.,* 1982, **89**, 418.

[9] S. Grimme, J. Antony, S. Ehrlich and H. Krieg, *J. Chem. Phys.,* 2010, **132**, 154104.

[10] E. D. Glendening, C. R. Landis and F. Weinhold, *J. Comput. Chem.,* 2013, **34**, 1429.

[11] F. London, *J. Phys. Radium,* 1937, **8**, 397.

[12] E. Clementi, D. L. Raimondi, *J. Chem. Phys*., 1963, **38**, 2686.

[13] G. M. Sheldrick, *Acta Crystallogr., Sect. A: Found. Adv.,* 2015, **71**, 3.

[14] G. M. Sheldrick, *Acta Crystallogr., Sect. C: Struct. Chem*., 2015, **71**, 3.

[15] A. L. Spek, *Acta Crystallogr., Sect. C: Struct. Chem*., 2015, **71**, 9.

[16] a) A. L. Spek, *J. Appl. Crystallogr*., 2003, **36**, 7; b) A. L. Spek, *Acta Crystallogr. D, Biol. Crystallogr*., 2009, **65**, 148.

[17] N. Meyer, H. Schucht, C. W. Lehmann, B. Weibert, R. F Winter and F. Mohr, *Eur. J. Inorg. Chem.,* 2017, 521.

[18] J. Schulz, I. Císařová, R. Gyepes and P. Štěpnička, *Angew. Chem. Int. Ed.,* 2021, **60**, 6992.

[19] V. G. Adrianov, Y. T. Struchkov and E. R. Rossinskaja, *J. Chem. Soc., Chem. Commun*., 1973, 338.

[20] B. Cordero, V. Gómez, A. E. Platero-Prats, M. Revés, J. Echeverría, E. Cremades, F. Barragána and S. Alvarez, *Dalton Trans*., 2008, 2832.

[21] E. J. Fernández, A. Laguna, J. M. López-de-Luzuriaga, M. Monge, M. Montiel, M. E. Olmos and M. Rodríguez-Castillo, *Organometallics,* 2006, **25**, 3639.